Transient Modeling of Borehole Temperature and Basal Melting in an Ice Sheet

Master Thesis

Faculty of Science
University of Bern

Adrien Michel

February 2016

Supervisors
Dr. Hubertus Fischer
University of Bern, Physics Institute, Climate and Environmental Physics and Oeschger Centre for Climate Change Research
&
Dr. Jakob Schwander
University of Bern, Physics Institute, Climate and Environmental Physics and Oeschger Centre for Climate Change Research

Contents

Abstract

Ice cores represent key archives to explore past climate. The recovery of a 1.5-million-year long ice core would significantly increase our understanding of the past climate dynamics, in particular the role of greenhouse gases in glacial cycles. The search of such an old ice core in Antarctica raises the question of how to predict the age of the bottom-most ice. A transient one dimensional thermo-mechanical model is developed in this thesis to infer the temperature profile, the basal melting, and age scale for ice domes. The output for the temperature profile and the age scale are compared with borehole temperature measurements and age scales existing in the literature.

This new model includes a firn layer and temperature and density dependent thermal parameters. The thermodynamics for the model is driven by the surface air temperature, the basal ground heat flux and by heat diffusion and advection processes taking place in the ice sheet along with a simple parameterization of the internal energy production and of the influence of the basal topography.

The usage of a transient model is shown to be a substantive improvement with respect to steady state models. Sensitivity tests show the influence of the firn density profile, of the thermal properties of firn, of the ice vertical velocity profile, and of the basal ground heat flux and topography on the temperature profile and melt rate.

The model produces a good temperature profile, age scale, and ground heat flux value when tested with Greenland (GRIP) conditions but underestimates the temperature profile at Dome C. To obtain a reasonable temperature profile for Dome C, some corrections on the past surface temperature are needed. These corrections are shown to be partially consistent with the uncertainty induced by the deuterium thermometry and several hypothesis are given to explain the remaining difference. Despite this temperature issue for Dome C, the results found for the thickness of an ideal 1.5-million-year old ice drill site are shown to be robust.

By using boundary conditions based on the Dome C ice core record and on benthic time series, as well as internal parameters defined with Dome C conditions, it is shown that 1.5-million-year old ice is very likely exist between 25 meters and 75 meters above bedrock for a site with the same climatic and mechanical conditions as Dome C but with an ice sheet thickness comprised between 2750 and 2950 meters. For such a site, today's ground ice temperature is between –8°C and the melting point.

Introduction

Ice cores are key proxies to explore past climate on Earth and can thus help us to gain a better understanding of the climate dynamics. The oldest ice core currently available has been retrieved at Dome Concordia in Antartica. The 3'190-meter-long core taken from Dome C has been analyzed and provides us with data covering the last 800'000 years [EPICA, Jou, M-D].

The International Partnerships in Ice Core Sciences (IPICS) is now seeking a site with ice older than at Dome C with the objective to find 1.5 million years old ice [Be, Fi]. Such an ice core would significantly increase our understanding of the Quaternary climate dynamics and, in particular, the role of greenhouse gases in glacial cycles [Fi]. This raises the question how to predict the age of the bottom-most ice.

A steady state age model [Fi] using constant values for the ice sheet thickness, the surface temperature and, the snow accumulation concludes that sites fulfilling the condition of having 1.5 Myr old ice in the bottom 100 m of the ice sheet most likely exist in the East Antarctic ice sheet. However, this steady-state model does not pretend to give a precise description of the requirements for an oldest ice site, but only to show what are the dependencies between ice age, ice sheet thickness, ground heat flux, and accumulation rate. The aim of this master thesis is to develop an accurate 1D transient thermo-mechanical ice sheet model to see if a more precise description of an oldest ice ideal site can be obtained.

The model will firstly be used to verify if the borehole temperature record [Catherine Ritz, personal communication] and age scale [Baz, Ve] at Dome C can be reproduced. Secondly, the model will test whether or not the conditions described in [Fi] for the oldest ice site produce a similar age scale when used in a transient model. The projected goal is to get a more accurate description of the necessary conditions (mainly ice sheet thickness) for a potential 1.5 Myr old ice age drill site. The model will also be used to explore the transient behavior of the ice sheet, notably the basal melting, under changing boundary conditions. To test the consistency of the model, it will be tested and confronted to measurements for a drill site in central Greenland called GRIP.

Importance of older ice cores

Ice cores are key proxies for understanding Earth's previous climates because it provides information about past environmental conditions as well as direct information on atmospheric composition from air bubbles. Moreover, ice cores offer a high temporal up to annual resolution.

In particular, ice core analysis allows the retrieval of past greenhouse gases concentrations [EPICA, Fi2], related to global climate [M-D], and more regional climate related proxies, such as dust and chemical aerosol species [EPICA].

Nowadays, the last 8 glacial cycles can be studied using ice cores [EPICA, Jou, M-D]. Finding a 1.5 Myr old core would allow the study of more cycles with an unprecedented amount of data. Such an ice core would permit the exploration of a time period marked by faster Milankovich cycles in global ice volume (41 kyr whereas more recent cycles are of order 100 kyr long [Fi, Im, L.R]), and the retrieval of accurate data on the transition between these two regimes. This so called *mid-Pleistocene transition* is not yet fully understood [El, Im].

Understanding past glacial cycles is also a key element to retrieve the link between greenhouse gas concentration, surface temperature and sea level and their feedback loops [Fi2, IPCC], which are crucial pieces of information for the anticipation of future climate changes and adaptation measures.

Moreover, ice sheets themselves have a great impact on terrestrial climate in general [Cl] and our understanding of the coupling between ice sheets and climate could also be improved by finding 1.5 Myr old ice.

Requirements for an oldest ice site

A naive approach would be to consider that the solution to retrieve old ice is to search for an ice dome as thick as possible. However, thicker ice increases the pressure at the bottom of the ice sheet which leads to a decrease in the ice melting temperature [C.P] and thus to more basal melting [Fi]. By the melting process, the old ice at the bottom of the ice sheet is lost. Inversely, if the ice sheet is too thin, the spatial resolution of the different proxies present in the ice core (i.e. the temporal resolution of the record) is too low for an accurate laboratory measurement and analysis.

Two different visions can be confronted for the ideal basal condition. It can be argued that some melting (as few as possible) to ensure an ice sheet flow (not frozen to bedrock) is ideal to avoid breaks, folding or general stratigraphic disturbances in the ice core column as observed in some existing cores [Al]. However, basal ice at the melting temperature is not ideal for gas retrieval because of the diffusion processes and the risk of higher melting in the past (thus smaller age) is hard to estimate. From this point of view, an ice sheet frozen to bedrock with a basal temperature at maximum $-10°C$ is recommended [Be, Po]. These two different basal conditions will be investigated with the model developed for this thesis.

The drill site should be situated over a Dome, or at least over an ice divide, to avoid lateral ice inflow in the ice core, even though domes and ice divides have probably migrated in the past [Ne].

In this study, the ideal ice sheet thickness for the retrieval of 1.5 Myr old ice will be defined for given ground heat flux and vertical velocity profile (form factor) range defined at Dome C and with boundary condition times series established by correlation between Dome C ice core analysis and benthic marine sediments records.

Dome Concordia and GRIP

Dome Concordia, also called Dome C or EDC (for EPICA Dome C), is a dome situated on the Antarctic Plateau at the position 75°06' S, 123°21' E, i.e. south of Australia. The dome summit is at $3'233$ m above sea level and the ice thickness is estimated at $3'309 \pm 22$ m [EPICA], meaning that the bedrock lies below the sea level. The research station and drill location is located ~ 6 km away of the geographic dome [Vit].

Back in the seventies, a first 950-meter-long core estimated to cover the last 32 kyr [Lo] had already been drilled at Dome C 56 km away of the new Dome C research station. The EPICA coring started in 1996 but got stuck at 788 m deep in 1999, thereby creating the EDC96 core. This ice core already lead to a high number of published studies covering the last 45 kyr [EPICA, Fi2, Jou2]. The second core, EDC99, covering depths between 772 m and 3260 m was finished in 2004 [EPICA, S.D-J.]. This drilling is estimated to have been stopped only 15 m above bedrock [S.D-J]. Several age scales exist for this core which all agree on the fact that the EDC99 core covers a time-period between 42 and $\sim$ 800 kyr BP. This means that the Dome C core is far older than the previously recovered oldest ice core from Vostok (which covers the last 420 kyr [Pe]).

GRIP, standing for Greenland Ice Core Project, is a $\sim$ 3000 m long ice core drilled in 1992 in central Greenland [D-J3, GRIP] covering about 100 kyr. Along with the American ice core GISP 2 this core allowed, among other things, for a better understanding of the stadial/interstadial transitions and identified a series of rapid (decadal scale) climate variations [Da, Ta].

Structure of the thesis

This thesis is composed of three chapters: in the first chapter, all the physical processes in ice and their mathematical formulation are described with special attention given to the density profile, the melting model, the internal heat production, and the lateral heat conduction, which are described differently and with more accuracy than in other models [Fi, Pa1]. A large part of the first chapter is dedicated to the establishment of the boundary condition time series at EDC and GRIP. The needed time series are surface temperature, accumulation rate and ice thickness. They are retrieved from ice core data [Baz, D-J3, Jou, Ve], models [Baz, D-J3, Joh, P.DC, Pa1, Pa3, Ve], and benthic time series [L.R]. In addition, borehole temperature records and age scales are discussed. At the end of the first chapter, different algorithms to solve the heat equation are presented and the computational performances of the model are given.

The second chapter is composed of different tests of the model: Necessary spin up time, sensitivity tests to free and internal parameters values, comparison of the different solving algorithms and comparison with other models. All of these tests are performed to ensure that the model output reacts as it should when changing the parameters and to ensure that it is coherent with other models.

In the last chapter, the model is tested for GRIP and Dome C to infer if it is able to reproduce the observed borehole temperature and age profile. For the purpose of defining the ideal conditions for an *oldest ice* drill site, free parameters obtained for Dome C are used for a run of the model with the same boundary condition time series but with different thickness in order to infer the influence of ice sheet thickness on basal ice age and melt rate.

Chapter 1

Description of the model

This first chapter describes the model developed for this master's thesis. Firstly, a mathematical description of the properties and processes in polar ice are given. The second section discusses the boundary condition at Dome C and GRIP in the past. The third section presents the discretization of the physical processes as well as the numerical algorithm used to solve them. Finally, technical details are given.

1.1   Processes in ice

1.1.1   Equation of heat transfer

Three effects dominate heat transfer and temperature change in ice: heat diffusion, which is proportional to the second spatial derivative of temperature, advection (the physical ice movement) and to a lesser degree internal heat production (due to friction during deformation). When considering the thermal conductivity of ice as temperature dependent (Section 1.1.4), a term proportional to the product of the spatial derivative of thermal conductivity and temperature is added to the diffusion process. This model being only one dimensional, no lateral advection is considered. However, some lateral diffusion is taken into account (see Section 1.1.7).

These contributions can be summarized in the following heat transfer equation [C.P, Fi]:

$$\frac{\partial T(z,t)}{\partial t} = \frac{K(z,t)}{\rho(z,t)c(z,t)}\frac{\partial^2 T(z,t)}{\partial z^2} + \left(\frac{1}{\rho(z,t)c(z,t)}\frac{\partial K(z,t)}{\partial z} - w(z,t)\right)\frac{\partial T(z,t)}{\partial z} + \frac{\dot{E}_I(z,t)}{\rho(z,t)c(z,t)} \quad (1.1)$$

Where T is the temperature (in K), K the thermal conductivity (in $Wm^{-2}K^{-1}$), ρ the density (in $kg\,m^{-3}$), c the specific heat capacity (in $J\,kg^{-1}K^{-1}$), and w the vertical ice velocity (in $m\,s^{-1}$). $\dot{E}_I$ is used to parametrize the internal heat production density and the lateral influx of heat by horizontal diffusion (in $W\,m^{-3}$). The reference system used throughout this work is the following: the time t is running from 0 (starting time, usually 1 million or 4 millions years ago in the model) to today (corresponding to 2000), the position z is running from 0 at bedrock to H on the top of the ice sheet.

1.1.2 Vertical velocity profile

The velocity profile (in ms^{-1}) in an ice dome takes the form [Fi, Pa, Bo]:

$$w(z, t) = -\left(A(t) - \frac{\partial H(t)}{\partial t} - M(t)\right)\omega(\zeta) - M(t) \tag{1.2}$$

With $A(t)$ the accumulation rate (in m ice-eq s^{-1}), $H(t)$ the ice sheet thickness (in m), $M(t)$ the basal melt rate (in m s^{-1}), ω the flux shape function [Pa2], and ζ the reduced height z/H.

In a simple model, the flux shape function can be approximated by the form [Fi]:

$$\omega(\zeta) = \zeta^{m+1} \tag{1.3}$$

With m being the form factor, supposed to be around 0.5 at Dome C [Fi] and considered as a free parameter in this model. A more complicated version of the flux shape function [Pa1] assumes:

$$\omega(\zeta) = 1 - \frac{p+2}{p+1}(1-\zeta) + \frac{1}{p+1}(1-\zeta)^{p+2} \tag{1.4}$$

With $p = n - 1 + kG_0H$ and $k = \frac{Q}{RT_G^2}$, n being the Glen's law exponent (usually 3 is used [C.P, Pa1]), G_0 the vertical temperature gradient approximated by $2.162 \cdot 10^{-2}$ K m^{-1} [Pa1], Q the creep activation energy (between 60 and 120 kJmol^{-1} [Pa1, L.D]), R the ideal gas constant (8.314 J mol^{-1}K^{-1}), T_G the bedrock temperature (in K). However, since Q is not well constrained and the basal topography is not well known, this theoretical relationship may not hold for Dome C and p will be set as a free parameter (see [Pa1], which finds $p \sim 2$ for Dome C).

These 2 models can be extended to take into account basal sliding by redefining ω as [Pa]:

$$\omega(\zeta) = s\zeta + (1 - s)\omega'(\zeta) \tag{1.5}$$

where s is the ratio of the basal horizontal velocity to the vertically averaged horizontal velocity (between 0 and 1) and ω' the function defined by (1.3) or (1.4).

In [Bo], two models are proposed, one reducing to $\omega(\zeta) = \zeta^m$ with a proposed m = 1.5 and one reducing to $\omega(\zeta) = 1 - (1 - \zeta)^{m+1}$, since these two models are very similar to [Fi] and [Pa1], they will not be considered in this thesis.

The difference between (1.3) and (1.4) as well as the effect of basal sliding on the flux shape function are shown in Figure 1.1. It shows that [Fi] and [Pa1] are quite similar for the couple m = 0.5, p = 2 and m = 0.7, p = 1. Regarding basal sliding, the effect on the velocity profile is really small. As it will be discussed in Section 1.1.6, there is a second effect of basal sliding: the heat production by basal friction. However, basal friction heat production is indistinguishable from ground heat flux, and since ground heat flux will be set as a free parameter, there is no possibility to retrieve an hypothetical basal sliding ratio s with this model. Basal sliding will, as a consequence, be set to zero.

The effect of the melt rate and the accumulation rate on the velocity is shown in Figure 1.2. Accumulation rate values used on the right panel are typical values that can expected during glacial periods (blue line) or during interglacial periods (red line), which shows a huge difference in the ice sheet dynamics between these two climatic conditions (see Section 1.2.1.3).

These different models are tested in Section 2.2.
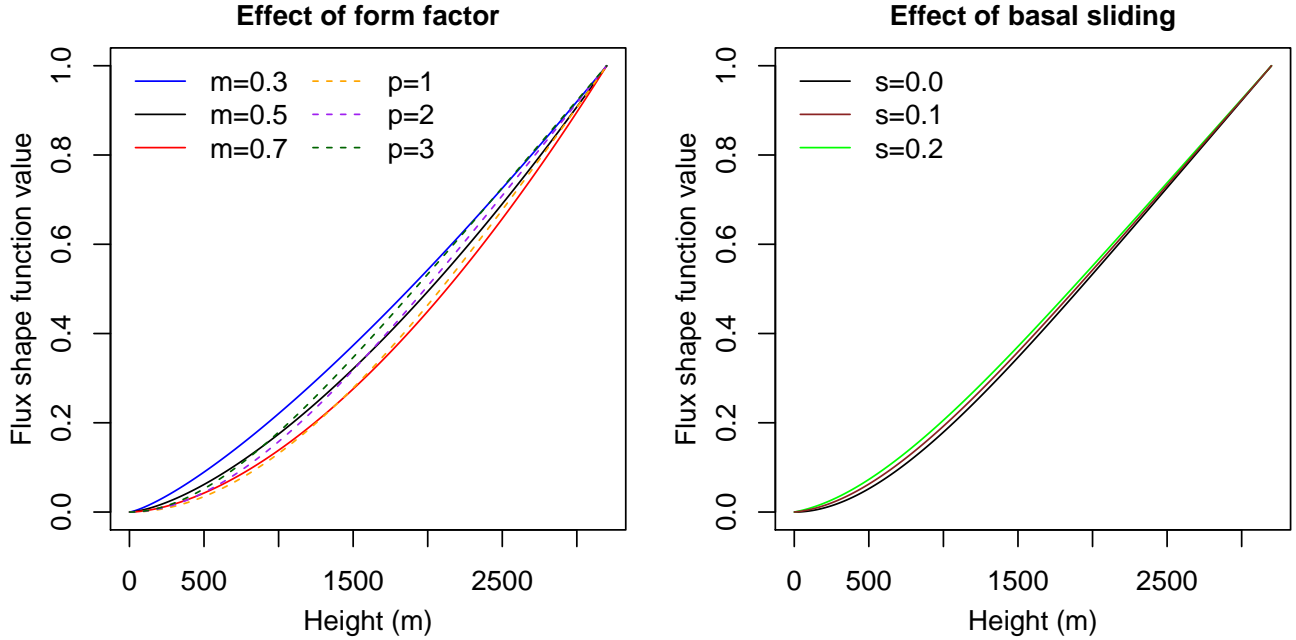
Figure 1.1: Left: Comparison of [Fi] (derived from (1.3), solid lines) and [Pa1] (derived (1.4), dashed lines) flux shape function for different values of m and p. Right: Effect of basal sliding on [Pa1] flux shape function, derived from (1.5) using (1.4) with p=2.

1.1.3   Firn and ice density

The density of the firn layer is approximated by an improved Herron-Langway model [H.L], where instead of being constant as in [H.L], the pure ice density is taken temperature and pressure dependent. This model reads:

$$\rho(z, t) = \rho_i(T(z, t)) \frac{\mathcal{Z}(z, t)}{\mathcal{Z}(z, t) + 1} \tag{1.6}$$

With ρ_i being the pure ice density and $\mathcal{Z}$ a function taking a different form above and below $\rho = 550 \text{ kg m}^{-3}$.

The height corresponding to a density of 550 kg m^{-3} is given by:

$$h_{550}(t) = H(t) - \frac{1000}{\rho_i k_0(t)} \left[\ln \left(\frac{550}{\rho_i(H(t)) - 550} \right) - \ln \left(\frac{\rho_s}{\rho_i(H(t)) - \rho_s} \right) \right]$$

Where ρ_s is the surface snow density (taken as 350kg/m^3), $k_0(t) = 11 \exp \left(-\frac{10160}{R T_S(t)} \right)$, with T_S the
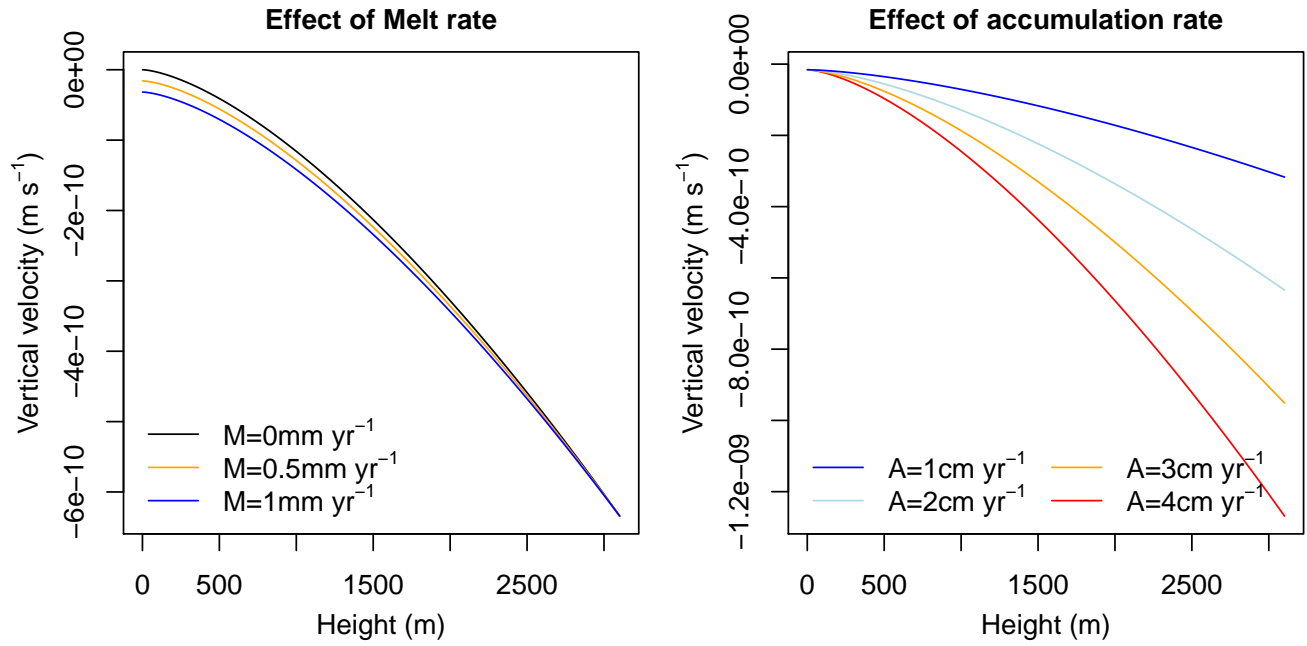
Figure 1.2: Left: Vertical velocity profile for various melt rate values, derived from (1.2) and (1.3) with $A = 2\,\mathrm{cm\,yr^{-1}}$ and H constant. Right: Same as left panel, but with various values of accumulation rate A (and with $M = 5\,\mathrm{mm\,yr^{-1}}$).

surface temperature (in K), and ρ_i the pure ice density (see definition below)[1].

Above h_{550}, $\mathcal{Z}(z, t)$ corresponds to:

$$\mathcal{Z}(z, t) = \exp[\rho_i(z, t)k_0(t)(H(t) - z) + \ln(\rho_s / (\rho_i(z, t) - \rho_s))]$$

And below h_{550}:

$$\mathcal{Z}(z, t) = \exp\left[\rho_i(z, t)k_1(t)\frac{H(t) - z - h_{550}(t)}{\sqrt{A(t)}} + \ln(\rho_s / (\rho_i(z, t) - \rho_s))\right]$$

With $k_1(t) = 575 \exp\left(-\frac{21400}{RT_S(t)}\right)$.

The pure ice density is related to temperature by [Sc]:

$$\rho_i(z, t) = 916.5 - 0.14438(T(z, t) - 273.16) - 1.5175 \cdot 10^{-4}(T(z, t) - 273.16)^2$$

and related to pressure by [C.P]:

$$\frac{\partial \rho_i(P(z, t))}{\partial P} = 1.1 \cdot 10^{-7} \frac{\mathrm{kg}}{\mathrm{m^3 Pa}}$$

---

[1] Note that in the improved version of the model, ρ_i should be taken at h_{550}, i.e. the density that pure ice would have with temperature and pressure at depth h_{550}. But since value of h_{550} not known yet, ρ_i is approximated with the surface value, i.e. $\rho_i(H(T))$.

Where $P(z, t) = \int_z^{H(t)} \rho(z, t) g \, dz$ and g being the earth gravitational acceleration ($9.81 \, \mathrm{m\,s^{-2}}$).

Assuming that pressure and temperature contributions are independent, the pure ice density can be written as:

$$\rho_i(z, t) = 916.5 - 0.14438(T(z, 7) - 273.16) - 1.5175 \cdot 10^{-4}(T(z, t) - 273.16)^2 + 1.1 \cdot 10^{-7}P(z, t) \quad (1.7)$$

Note that there is a circular relationship between ρ and ρ_i when including pressure. To avoid this issue, an iterative approach is used. A first density profile ignoring pressure is computed and used to compute the pressure, allowing to get a pure ice density profile using (1.7). The final density is then obtained by a second pass of the Herron-Langway model using the pure ice density profile obtained at the previous step. This could be iterated until reaching an equilibrium, but tests show that one iteration is enough to be only $\sim 5 \cdot 10^{-3} \, \mathrm{kg\,m^{-3}}$ away from the equilibrium value. A typical Dome C density profile obtained with this model is shown in Figure 1.3, left panel. This is obtained using today's surface temperature, thickness, and accumulation rate (see Section 1.2), and a temperature profile obtained from a transient run with constant density (see Section 1.3).

The inclusion of the pressure correction leads to a correction of order $3 \, \mathrm{kg\,m^{-3}}$ for the ice density (see Figure 1.3, right panel). The profile obtained with this model exhibits a behavior consistent with measurements [Go]. By including pressure and temperature, the mean density for the pure ice part (below 200m depth) is about $922 \, \mathrm{kg\,m^{-3}}$.
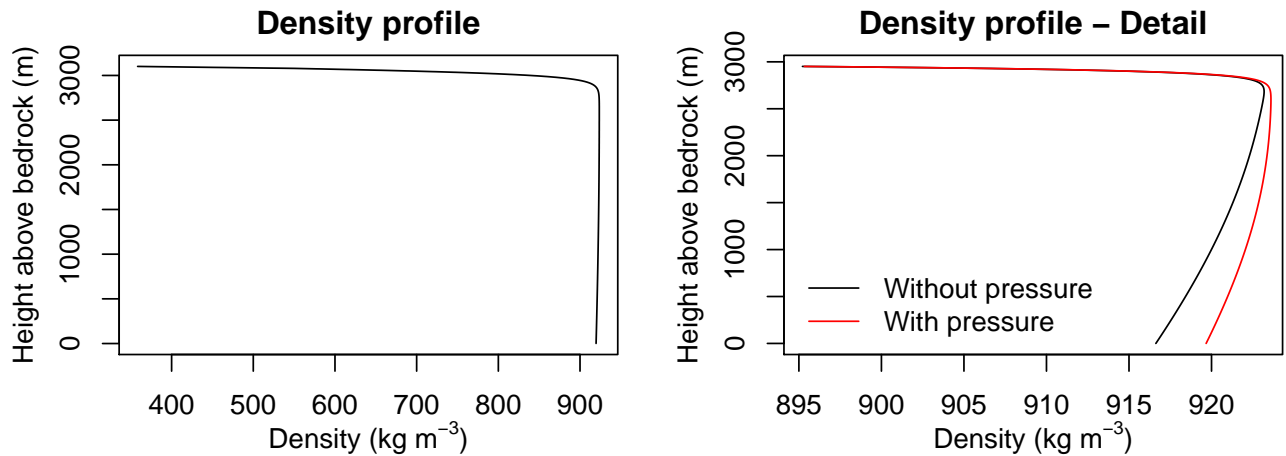
Figure 1.3: Left: Density profile obtained with typical Dome C contemporaneous conditions and temperature profile. Right: Lower part of the density profile with and without pressure term included in (1.7).

This formulation assumes that the density is in a steady state, which is obviously not the case because surface temperature and accumulation rate change with time. However, the firn densification process it not sufficiently understood to have a simple and robust theoretical model of the density evolution over time. Some models are a bit more sophisticated than Herron-Langway to describe the time evolution of density [Bar, Sp], but they exhibit some discontinuities and fail to really fit the measurements [Sp]. Moreover, typical values for the time derivative of ρ given by dynamical models [H.L, Bar, Sp] show that with the time step (100 yr) and boundary condition used in this work (Sections 1.2 and 1.4), the equilibrium is reached within the time of one time step (except for the first dozens of meters) and that steady state is a reasonable approximation.

1.1.4   Thermal conductivity and heat capacity

For pure ice, at density $\rho = 917 \, \mathrm{kg \, m^{-3}}$, the thermal conductivity is given by [C.P]:

$$K_i(z, t) = 9.838 \cdot \exp(-5.7 \cdot 10^{-3} \cdot T(z, t)) \tag{1.8}$$

The effect of the density on the thermal conductivity (e.g for the firn layer) is not very well known. An upper limit is given in [C.P]:

$$K(z, t) = \frac{2K_i(T(z, t))\rho(z, t)}{3 \cdot 917 - \rho(z, t)} \tag{1.9}$$

Another formulation for the density influence on thermal conductivity is given in [Sc]:

$$K(z, t) = K_i(T(z, t)) \left(\frac{\rho(z, t)}{917} \right)^{2 - 0.5 \frac{\rho(z,t)}{917}} \tag{1.10}$$

Both formulations are purely empirical.

The specific heat capacity of ice is empirically given by [C.P]:

$$c(z, t) = 152.5 + 7.122 \cdot T(z, t) \tag{1.11}$$

If the heat needed to warm the air and water vapour in snow is neglected, this formulation can be applied also to the firn layer along with the corresponding density.

1.1.5   Melt rate

At the interface between bedrock and ice, there are two heat fluxes: one flux from the ground Q_G and one from the ice Q_{ice}. The geothermal heat flux Q_G mentioned in this section effectively includes heat production by basal sliding since they are not distinguishable (see Secion 1.1.6). The flux from the ice is governed by the temperature gradient at the bottom and the advection due to vertical velocity:

$$Q_{ice}(t) = K(0, t) \frac{dT(z, t)}{dz} \Big|_{z=0} - \rho(0, t)c(0, t)w(0, t)\Delta T$$

The first term being the diffusion precess and the second term the advection process. ΔT is the temperature difference between the bedrock temperature and the mean temperature of the ice advected by vertical velocity.

In equilibrium, the addition of these two fluxes must be equal to zero. If the result is positive, the extra energy is used to melt some ice. The equilibrium equation then becomes:

$$Q_G + K \frac{\partial T(z, t)}{\partial z} \Big|_{z=0} - \rho(0, t)c(0, t)w(0, t)\Delta T - \rho(0, t)M(t)L = 0$$

Since from (1.2), $w(0, t) = -M(t)$:

$$Q_G + K\frac{\partial T(z,t)}{\partial z}\bigg|_{z=0} - \rho(0,t)M(t)(L + c(0,t)\Delta T) = 0$$

The melting point of ice T_M as function of pressure is given by [C.P.]:

$$T_M(t) = 273.16 - 7.2 \cdot 10^{-8} \cdot P(0,t) \tag{1.12}$$

Note that if the water is air saturated, the melting point becomes [C.P.]:

$$T_M(t) = 273.16 - 9.8 \cdot 10^{-8} \cdot P(0,t) \tag{1.13}$$

Where $P(0,t)$ is the pressure (in Pa) at bedrock which can be obtained by integrating the density over height.

Lab measurements performed at the Division for Climate and Environmental Physics (CEP) in Bern [Jakob Schwander, personal communication] show that water is far from saturation because there is not enough air available to saturate the melt water, meaning that (1.12) should be used.

If some melting occurs, the basal temperature will be T_M and thus:

$$Q_G + K\frac{\partial T(z,t)}{\partial z}\bigg|_{z=0, T(0,t)=T_M} - \rho(T_M)M(t)(L + c(0,t)\Delta T) = 0 \tag{1.14}$$

This equation can then be solved for $M(t)$.

If the calculated melting is negative (i.e. $Q_G + K\frac{\partial T(z,t)}{\partial z}\big|_{z=0, T(0,t)=T_M} < 0$), this implies that the cold flux from the top is bigger than the warm flux from the ground. In this case there are several possibilities: if some water is available, it will freeze and the bottom temperature will stay at T_M, or, if no water is available, the bottom ice will cool down to a temperature smaller than T_M and, in addition, some cooling of the bedrock itself can be considered. In this model, it will be considered that there is no available water and thus no refreezing processes, nor cooling of the bedrock. The ground heat flux is considered as constant over time and independent of the basal ice temperature.

This description holds for an equilibrium situation, but considering that the boundary conditions changes are in discrete steps, the value of T_M will jump from one time step to the next one (especially because of ice sheet thickness H changes). This implies that in most cases the situation is not in equilibrium when the timestep begins. A quantity of energy E_{eq} (in $J\,m^{-2}$) will then be used (or be released if the ice is warmer than the melting temperature[2]) to reach the equilibrium before the melting process starts.

Since the timing of the process is not relevant here, it can be averaged over the time step with $Q_{eq} = \frac{E_{eq}}{\Delta t}$. The mean melt rate is then:

$$Q_G + Q_{eq} + K\frac{\partial T(z,t)}{\partial z}\bigg|_{z=0, T(0,t)=T_M} - \rho(T_M)M(t)(L - c(0,t)\Delta T) = 0 \tag{1.15}$$

Note that the usual approach for this kind of Stefan problem[3] [Ja, Sh] can not be used here since the grid size is fixed in this model.

---

[2]Indeed, if the ice thickness increases between two time steps, T_M will decrease and the bottom temperature can then be bigger than T_M. In this case the ice will use this extra energy ($E_{EQ} = \rho c(T - T_M)$) as latent heat to melt, which can be interpreted as an energy input in the system.

[3]In phase transition physics, Stefan problems are problems where the boundary between the two phases is moving. The resolution on this kind of problem requires to compute the boundary position as part a of the solution [Ja].

1.1.6 Internal heat production

Three major terms contribute to internal heat production for Dome C conditions [C.P]: Ice deformation, firn compaction and basal sliding friction, given respectively by:

$$\dot{E}_I^{def}(z, t) = \dot{\epsilon}_{xx}\sigma_{xx} + \dot{\epsilon}_{yy}\sigma_{yy} + \dot{\epsilon}_{zz}\sigma_{zz} + 2(\dot{\epsilon}_{xy}\sigma_{xy} + \dot{\epsilon}_{xz}\sigma_{xz} + \dot{\epsilon}_{yz}\sigma_{yz}) \tag{1.16}$$

$$\dot{E}_I^{comp}(z, t) = \frac{w(z, t)P(z, t)}{\rho(z, t)} \frac{\partial \rho(z, t)}{\partial z} \tag{1.17}$$

$$\dot{E}_I^{slide}(0, t) = u_G \tau_G \tag{1.18}$$

Where $\dot{\epsilon}_{ij}(z, t)$ are the components of the deformation rate tensor, the $\sigma_{ij}(z, t)$ the components of the stress tensor[4], u_G the basal sliding velocity (in $m\,s^{-1}$) and τ_G the basal shear stress (in Pa).

Note that if the geothermal heat flux is used as a free parameter (see Sections 1.1.5 and 1.2.4) the contribution of basal sliding to the apparent geothermal heat flux is not distinguishable. However, basal sliding at Dome C obtained by [Pa1] suggests that this term would be substantially lower than the physical geothermal heat flux and can be neglected.

To solve (1.16) the stress tensor has to be retrieved; this is done by using the model described in [D-J]. This model describes an ice divide by a 2 dimensional flow, which is *a priori* different from the radial flow taking place around an ice Dome. However, the existing knowledge of Dome C surface velocity distribution suggest that the flow is not radial but strongly elliptical, with the flow at the Dome C pointing in the direction of the small axis of the ellipse [Vit]. In other words, the situation at Dome C drill site can be compared to an ice divide as a rough approximation. The lateral movements are thus considered only in one direction ($v = 0$) and the flow direction and dynamics are considered as constant when moving perpendicularly to the flow direction at Dome C ($\frac{\partial v}{\partial y} = \frac{\partial u}{\partial y} = \frac{\partial w}{\partial y} = 0$). Moreover, from [D-J] result it can be considered that $\frac{\partial w}{\partial x} = 0$ (and thus $\dot{\epsilon}_{xz} = \frac{\partial u}{\partial z}$) because the drill site is at a distance from the (virtual) divide position corresponding to more or less one or two ice sheet thickness [Vit] (the ice sheet thickness is used as distance unit in [D-J]).

Using all these considerations, equation (1.16) can then be reduced to:

$$\dot{E}_I^{def}(z, t) = \dot{\epsilon}_{xx}\sigma_{xx} + \dot{\epsilon}_{zz}\sigma_{zz} + 2\dot{\epsilon}_{xz}\sigma_{xz} \tag{1.19}$$

Using Glen's flaw law $\dot{\epsilon}_{ij} = A(T)\tau_E^{n-1}\tau_{ij}$ [C.P] with n = 3 (where A is the creep factor in $Pa^{-1}\,s^{-1}$, τ_{ij} the components of the deviatoric stress tensor, and $\tau_E^2 \equiv \frac{1}{2}\left[\tau_{xx}^2 + \dot{\tau}_{yy}^2 + \tau_{zz}^2\right] + \tau_{xy}^2 + \tau_{xz}^2 + \tau_{yz}^2$), as well as the fact that only $\dot{\epsilon}_{xx}$, $\dot{\epsilon}_{xz}$, and $\dot{\epsilon}_{zz}$ are non-zero (by symmetry of the problem), and also that $\tau_{xx} = -\tau_{zz}$ (because τ_{yy} is zero for an ice divide like flow), the different component of the deviatoric tensor can be retrieved.

From $\dot{\epsilon}_{ij} = A(T)\tau_E^{n-1}\tau_{ij}$ and the fact that only $\dot{\epsilon}_{xx}$, $\dot{\epsilon}_{xz}$, and $\dot{\epsilon}_{zz}$ are non-zero:

$$\tau_{yy} = \tau_{xy} = \tau_{yz} = 0$$

Then using $\tau_{xx} = -\tau_{zz}$:

$$\tau_E^2 = \tau_{xx}^2 + \tau_{xz}^2$$

---

[4]In (1.16) the time and depth dependence "(z,t)" of $\dot{\epsilon}_{ij}$ and σ_{ij} have been omitted for readability.

Inserting this result into $\dot{\epsilon}_{ij} = A(T)\tau_E^{n-1}\tau_{ij}$ gives the following equation system:

$$(1) \quad \dot{\epsilon}_{xx} \;=\; A(T)\left(\tau_{xx}^2 + \tau_{xz}^2\right)\tau_{xx}$$

$$(2) \quad \dot{\epsilon}_{xz} \;=\; A(T)\left(\tau_{xx}^2 + \tau_{xz}^2\right)\tau_{xz}$$

That can be solved to find:

$$\tau_{xz} \;=\; \dot{\epsilon}_{xz}\left[\frac{1}{A(T)\left(\dot{\epsilon}_{xx}^2 + \dot{\epsilon}_{xz}^2\right)}\right]^{\frac{1}{3}}$$

$$\tau_{xx} \;=\; \dot{\epsilon}_{xx}\left[\frac{1}{A(T)\left(\dot{\epsilon}_{xx}^2 + \dot{\epsilon}_{xz}^2\right)}\right]^{\frac{1}{3}}$$

(1.20)

From $\tau_{xx} = -\tau_{zz}$ and the above equation, it can be deduced that $\dot{\epsilon}_{xx} = -\dot{\epsilon}_{zz}$.

Using the definitions $\tau_{ii} = \sigma_{ii} - \sigma_M$ with $\sigma_M = \frac{1}{3}[\sigma_{xx} + \sigma_{yy} + \sigma_{zz}]$ and $\tau_{ij} = \sigma_{ij}$ for $i \neq j$:

$$\begin{aligned}
\sigma_{xx} &= \tau_{xx} \\
\sigma_{xz} &= \tau_{xz} \\
\sigma_{zz} &= \tau_{zz}
\end{aligned}$$

(1.21)

Finally, inserting (1.20) and (1.21) into (1.19) gives :

$$\dot{E}_I^{def}(z,t) = 2\left[\left(\frac{\partial w}{\partial z}\right)^2 + \left(\frac{\partial u}{\partial z}\right)^2\right]^{\frac{2}{3}} A(T)^{-\frac{1}{3}}$$

(1.22)

The term $\frac{\partial w}{\partial z}$ can easily be computed from (1.3), (1.4) or (1.5). The term $\frac{\partial u}{\partial z}$ is taken from [D-J] using a value of $0.015\,\mathrm{m\,yr^{-1}}$ for u_S [Vit] (considered as constant over time). Typical values for $A(T)$ are given in [C.P]. Technical details on the implementation of $\dot{E}_I^{def}$ are given in Appendix B.

Figure 1.4 shows typical values for $\dot{E}_I^{def}$ and $\dot{E}_I^{comp}$ obtained for contemporaneous Dome C conditions. Note that the small discontinuities on the right panel are due to the piecewise linear approximation of $A(T)$ and $\dot{\epsilon}_{xz}$ (see Appendix B) and the discontinuity in the middle panel is due to the discontinuous density derivative at h_{550} in the Herron-Langway model (see Section 1.1.3). A huge peak due to compaction is present on the top, whereas the compaction has a (negligible) negative energy production on the bottom (due to thermal expansion of ice, see Section 1.1.3) explaining the negative value seen on the bottom of the right panel for the compaction. The deformation component is slowly increasing toward the top of the ice sheet (mainly because $A^{-1/3}$ is 4 times bigger on the top than at ground level, whereas the sum of the velocity derivatives in (1.22) results in an almost symmetric *u shaped* curve).

1.1.7   Valley effect at Dome C

The drill location of Dome C [Vit] is above a depression in the bedrock [Fo]. This depression is approximated in the model by an infinite-long valley parametrized with a depth of $\Delta H \sim 100$ m and a width of $L \sim 5$ km [Fo]. Since the bedrock ice is always at melting temperature around Dome C, the location of the core in a hole will lead to a lateral influx of heat.
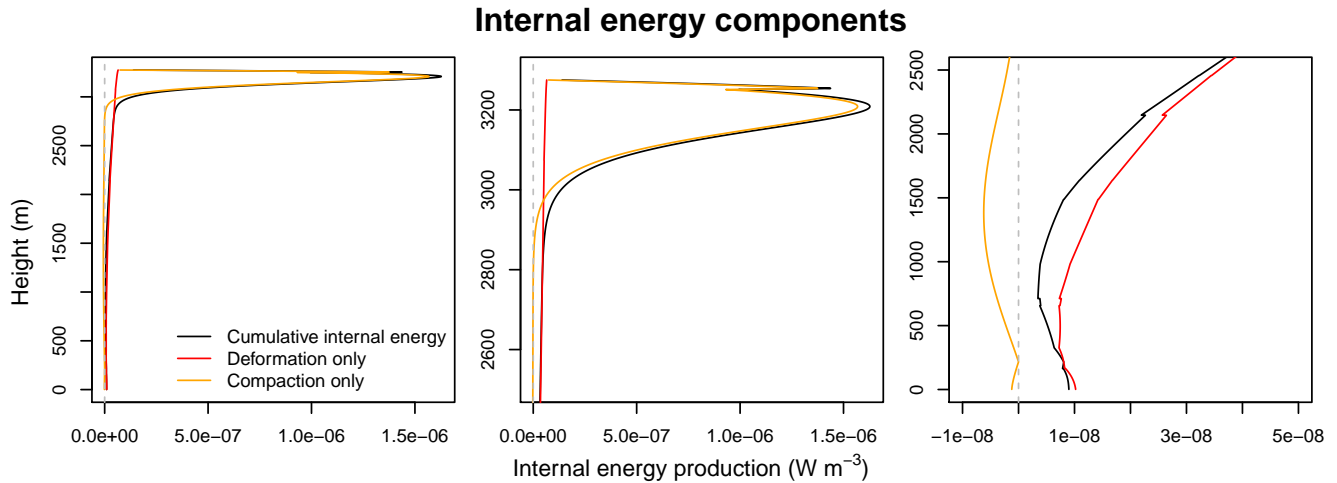
Internal energy components

Figure 1.4: Internal energy production due to deformation only (1.22) (red line), due to compaction only (1.17) (orange line), and T total internal energy production (black line). Left panel shows the full profile whereas middle and right panels show respectively the upper and lower parts of the profile. The discontinuity in the middle panel is due to the discontinuity of the density derivative in the model used (see Section 1.1.3) and the discontinuities in the right panel are due to the piecewise linear approximation of $A(T)$ and $\dot{\epsilon}_{xz}$ (see Appendix B)

For $z > \Delta H$ the heat flux is parametrized as follow:

$$\dot{E}_I^{hole}(z, t) = 2K(T(z, t))\frac{T_b(z, t) - T(z, t)}{(L/2)^2}$$

Where T_b is the temperature at the border of the hole obtained by a run of the model using $\tilde{H}(t) = H(t) - \Delta T$.

For $z < \Delta H$, the valley is parameterized by a flat background of width f followed by a parabola of height ΔH on both site between the points $x = \pm f/2$ and $x = \pm L/2$, see diagram shown in Figure 1.5. The distance between the center of the valley and the border for a given height z is thus $f/2 + (z/\Delta H)^2(L - f)/2$. The temperature on the valley border is considered to be at the melting temperature (given by the temperature of the valley bottom minus the vertical derivative of the melting temperature multiplied with the border height). From (1.12) and using $\partial P(z)/\partial z(z) = -9.81 \cdot 921$, the border temperature for $z < \Delta H$ is then $T(0, t) + 6.697 \cdot 10^{-4}z$ and the heat flux is given by:

$$\dot{E}_I^{hole}(z, t) = 2K(T(z, t))\frac{T(0, t) + 8.6.6974 \cdot 10^{-4}z - T(z, t)}{(f/2 + (z/\Delta H)^2(L - f)/2)^2}$$

This formulation leads to an exaggerated effect of the topography. Indeed, the border temperature profile T_b should be cooled since it is releasing heat to the middle of the valley. However, computing a more accurate border temperature profile would require a full 2D model that is not within the scope of this work. The value indicated here for L must then be interpreted as a mathematical valley width a corresponding real valley being narrower. By a rough approximation, it can be considered that taking into account the colling of the lateral temperature profile would divide the heat flux by a factor of 2, and thus that the real width of the valley is $L/\sqrt{2} \simeq 0.7L$).

Valley effect diagram
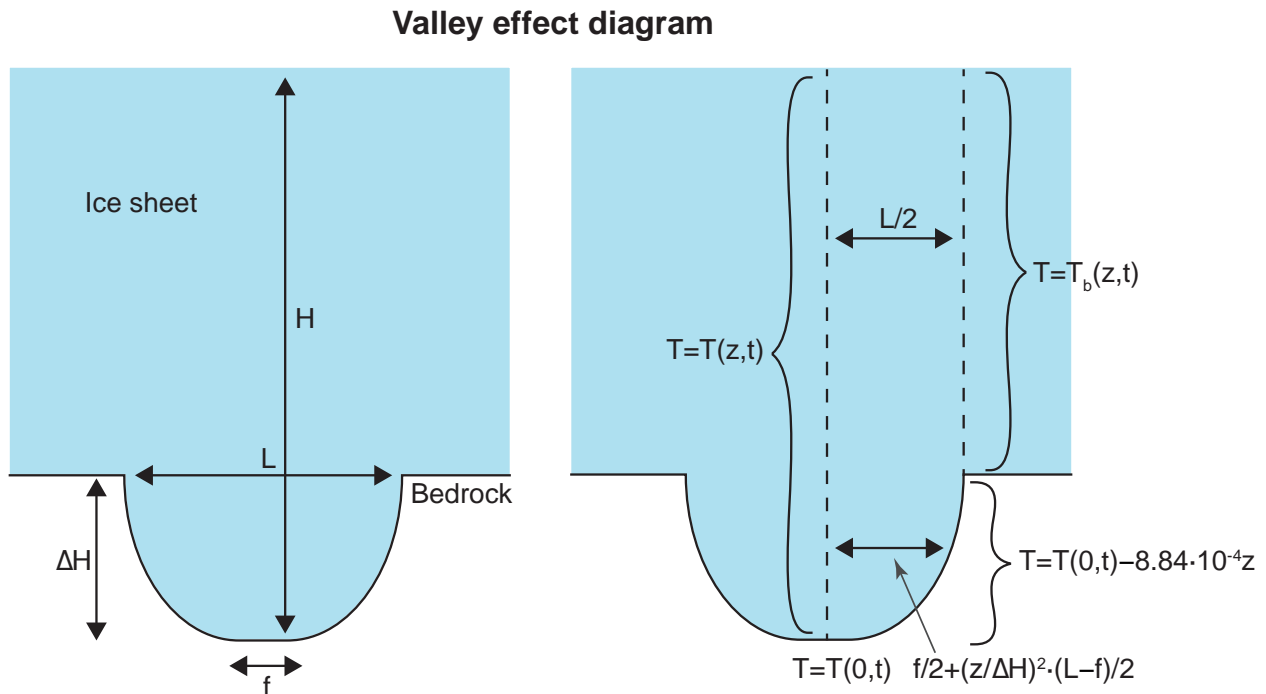
Figure 1.5:   Diagram of the situation at the drill location.

The fact the no cooling of the valley border is taken into account makes necessary the flat area at the center of the valley (i.e. where the model is ran). Without a flat area, $\Delta x = (z/\Delta H)^2 (L - f)/2$ goes to zero faster than the temperature difference (because the border is not cooled) leading to model divergence.

For implementation in the model, ΔH, f, and L are set as free parameters.

1.1.8   Age depth profile

The age-depth profile can, in general, be obtained by:

$$\text{Age(z)} = \int_{z}^{H(\text{age})} \frac{1}{w(z)} dz \tag{1.23}$$

But since w is not constant over time, this leads to a circular relationship. An iterative approach is sometimes used [Pa1]. Here a numerical integration is used. Starting at a given depth and today's vertical velocity for this depth, a new depth is obtained by subtracting the velocity multiplied with the length of the time step. This gives the height for this ice at the previous time step. Using now the velocity at this previous time step, the height at the time step before can be determined. This process is iterated until reaching the surface (taken as H at the time corresponding to the actual time step). The number of iterations needed to reach the surface gives the ice age corresponding to the initial depth. This process is done for various starting depth to obtain the ice-depth profile.

Note that age-depth profiles already existing for Dome C (see [Baz, Jou, Pa3, Ve] and Section 1.2) are a mix between numerical integration from models and various time markers found in ice cores.

1.2   Boundary conditions

In the previous sections it was implicitly assumed that the accumulation rate, surface temperature and ice thickness at a given location are known back in time. In this section the existing time series based on ice core measurement and models are presented and a simple parametrization is used to define these boundary conditions back in time.

1.2.1   EDC

The boundary conditions for temporal changes in ice thickness H, surface temperature T_S and accumulation rate A for Dome C are parametrized using the Lisiecki and Raymo LR04 benthic $\delta^{18}O$ time series [L.R], the AICC2012 time scale [Baz, Ve], and the EDC2007 times series [Jou, Pa3].

The goal is to establish a 4Myr time series for surface temperature, accumulation rate and ice thickness. This is done by using the 800'000 kyr long temperature record in EDC2007 and correlate it to the LR04 time series, allowing us to extrapolate this correlation backward in time to the full LR04 time series.

In a second step, an empirical model is developed to correlate the EDC2007 temperature with the AICC2012 accumulation rate and the EDC2007 ice thickness. This model is then used with the 4 Myr temperature time series retrieved from LR04.

The aim is to obtain a "realistic" time series, allowing to perform different sensitivity tests and to infer the basal melting behaviour in the last few millions of years. The time series with empirical models described below do not pretend to be a real representation of the past condition as one could obtain by using an ice core.

The R code used to establish the time series is presented in Appendix A.1.

1.2.1.1   Time scale correction

The EDC2007 time series are first adjusted to the AICC2012 time scale. To do so, an interpolation with linear spline is used to get one point every meter for all the EDC2007 parameters and the corresponding age. The same is done for the AICC2012 age scale (i.e. one point every meter and the corresponding age). Finally the AICC2012 age depth relation is simply transferred to the EDC2007 time series. The difference between the two age-scales along with the effect of using one or the other for EDC2007 temperature are shown in Figure 1.6.

The LR04 times series is recognized to have a good inverse correlation with Dome C temperature for glacial-interglacial events [Jou]. This correlation is used to correct the LR04 time scale. Indeed, without correction, the time seems to run faster in the LR04 time series (see Figure 1.7 top panel). The corrected LR04 time takes the form $t_{cor} = a \cdot t_{original} + S$. The scale factor a is incremented in a loop (with a 0.01 increment per loop), and a cross-correlation function is applied at each step of the loop to determine the lag S corresponding to the highest correlation between the standardized value of LR04 and the time-corrected EDC2007 standardized temperature. The pair $a - S$ leading to the best correlation is a $=1.097$ and $S = -1900yr$ with a correlation of -0.847. The corrected LR04 is shown in Figure 1.7 bottom panel with Dome C temperature. A ~ 2 kyr lag between

EDC2007 minus AICC 2012 time scale

EDC2007 temperature with EDC2007 and AICC 2012 timescale
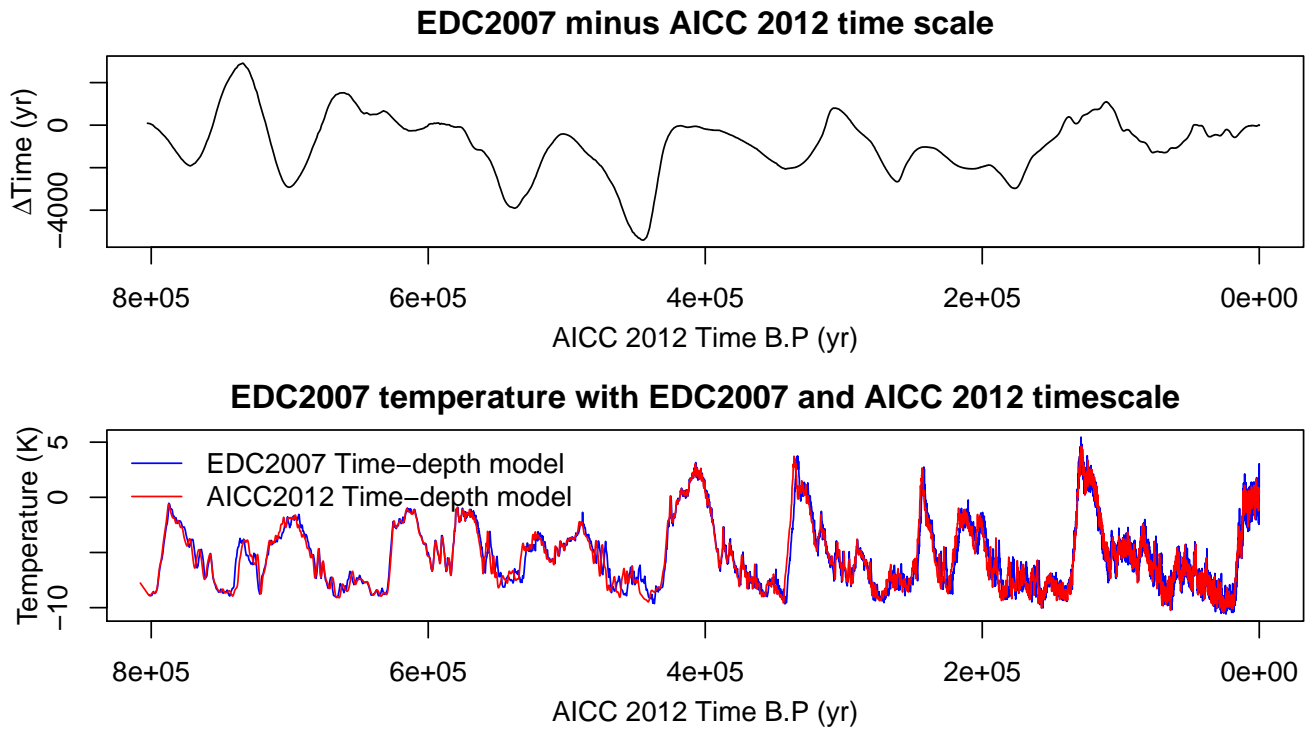
Figure 1.6: Top: Difference between the EDC2007 and AICC2012 age-depth model. Bottom: EDC2007 temperature plotted using the EDC2007 age-depth model (blue) and the AICC2012 age-depth model (red).

LR04 time corrected and uncorrected standardized inverse value

LR04 inverse time corrected and EDC2007 time corrected standardized value

Figure 1.7: Top: Time corrected (black) and uncorrected (blue) standardized inverse LR04 values. Bottom: Standardized EDC2007 temperature (with AICC2012 age-depth model) (red) and time corrected standardized inverse LR04 values (black). Since standardized values are used, no units apply.

benthic δ^{18}O and Dome C temperatures is fairly acceptable as sea level changes are expected to lag temperature changes on the ice sheet. Figure 1.7 bottom panel shows the good correlation between the scaled LR04 and EDC2007 values, even if some discrepancies exist, e.g. at 750 kyr B.P.

1.2.1.2   Surface temperature

The EDC2007 time series gives the relative temperature difference with respect to the last millennial mean value. This value is indicated to be -54.5°C [EPICA], but to fit the top of the temperature record with borehole measurement, a value of -55°C has to be used (see Section 3.2).

The LR04 δ^{18}O values are scaled in the following way to reproduce surface temperature:

$$\text{LR04}_\text{T} = -(\text{LR04} - \overline{\text{LR04}_{810}})\frac{\sigma(\text{EDC2007})}{\sigma(\text{LR04}_{810})} + \overline{\text{EDC2007}} - 55$$

Where LR04_T denotes the new temperature time series, LR04_{810} the LR04 δ^{18}O values for the last 810kyr, σ the square root of the variance, and the overline is used to denote the mean value. Since the δ^{18}O values are anti-correlated with temperature, their inverse values are used in the model. In other words, the LR04 mean is adjusted to match the EDC2007 mean temperature over the last 810 kyr, and the LR04 variance is scaled to match the EDC2007 temperature variance over the last 810 kyr.

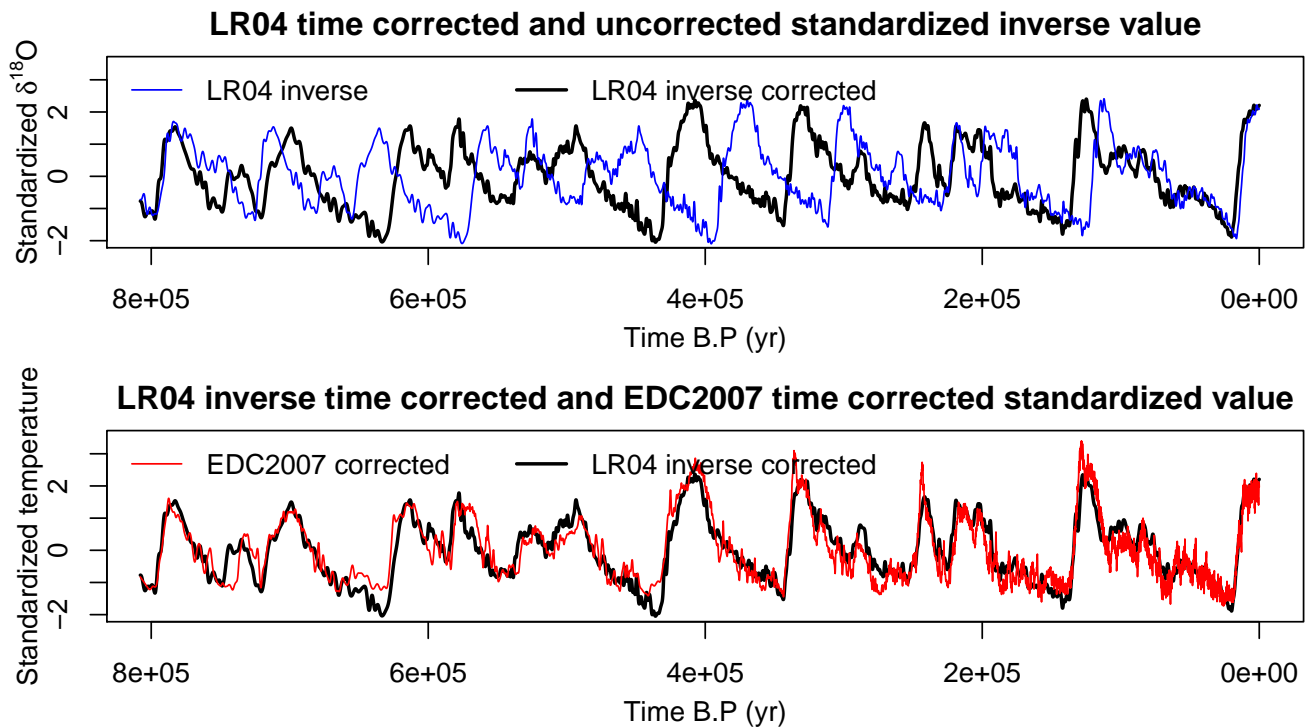Figure 1.8 shows the obtained temperature, compared to the EDC2007 values. The correlation is quite good but LR04_T fails to precisely reproduce today's and LGM temperature and clearly underestimates temperatures of the last 4 interglacials. Note that EDC2007 may already underestimate the last interglacial temperature [Sime].

Note that the altitude change of Dome C ($\sim$ 150 m between glacial and interglacial periods [P.DC, Pa1, Pa3]) should have an impact on surface temperature that can not be retrieved from correlation with deep oceanic δ^{18}O. This effect is a bit damped by isostatic rebound, which could absorb around a third of the thickness change, but not in phase with temperature variation [Pa1].

To apply boundary conditions as realistic as possible for the most recent period, EDC2007 temperature is used for the last 800kr and LR04_T values for the period before (by chance the two sets match quite well at −800kr). This time series will be called LR04EDC.

1.2.1.3   Accumulation rate

Two datasets exist for accumulation rate at Dome C, one from EDC2007 [Pa, Pa3] and one from AICC2012 [Baz, Ve]. When EDC2007 is time corrected as described above, the two time series match quite well. The AICC2012 is used in this work.

In the literature [P.DC, Hu, H.O] some models exist for the link between temperature and accumulation rate. These models take the form:

$$A = c \cdot 2^{\text{T}_\text{S}/10} \tag{1.24}$$

Where A is the accumulation rate in m ice-eq yr^{-1}, T_S is the surface temperature (in °C) and c = 1.5 [P.DC, Hu] or c = 2.5 [H.O]. The [H.O] model gives values too high and the [P.DC, Hu]
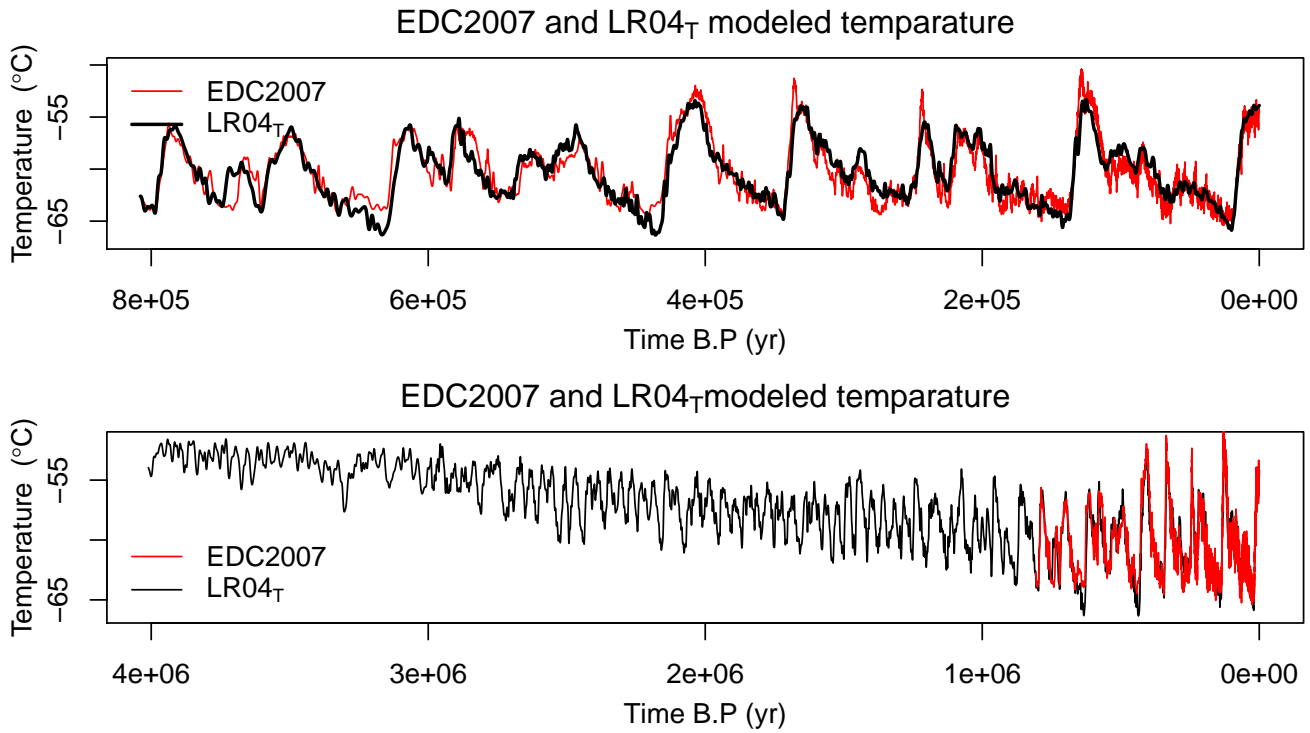
Figure 1.8: Top: $LR04_T$ modelled temperature (black) and EDC2007 (red) temperature. Bottom: Same as top with $LR04_T$ shown for the last 4Myr.

model needs a correction of -5mm yr^{-1} to match the AICC2012 values (see Figure 1.9). The model then becomes:

$$A = 1.5 \cdot 2^{(T_S - 273.15)/10} - 0.005 \tag{1.25}$$

with the temperature expressed now in K.

As expected since the $LR04_T$ fails to retrieve the interglacial temperature peak, an accumulation estimate using the $LR04_T$ temperature used in (1.25) does not fit with accumulation peaks observed during interglacial period (see Figure 1.9). The influence of temperature on accumulation rate being exponential, the underestimation of interstadial peaks is more pronounced for the accumulation rate estimate than for temperature. As for the temperature, the AICC2012 values will be used for the most recent part and then the accumulation modeled using $LR04_T$ and (1.25) is pasted to create the LR04EDC accumulation rate time series.

1.2.1.4   Ice thickness

The thickness is usually obtained from 2D models that use past accumulation rates and a thinning function [Pa], [Pa3], or directly from 3D models [P.DC.]. However the literature is poor in model linking past surface temperature and ice thickness. An EDC2007 time series for past changes in thickness relative to today is available [Pa3]. Today's ice thickness is also not precisely known. It is estimated to be H=3309m±22 in [EPICA]. However, to be comparable with borehole temperature record (see Section 1.2.1.6), the thickness is set to 3275m. This value is in agreement with the field value obtained from the last Dome C drill [S.D-J].

An empirical model is built to link thickness and temperature. First the EDC2007 thickness time

Figure 1.9: Top: AICC2012 accumulation rate (red), modelled accumulation rate using EDC2007 temperature and (1.24) with c =1.5 (green) and modelled accumulation rate using EDC2007 temperature and (1.25) (black). Bottom: AICC2012 accumulation rate (red) and modelled accumulation rate using LR04$_T$ temperature and (1.25) (black).

scale is corrected to the AICC temperature time and then a cross-correlation function between standardized EDC2007 thickness an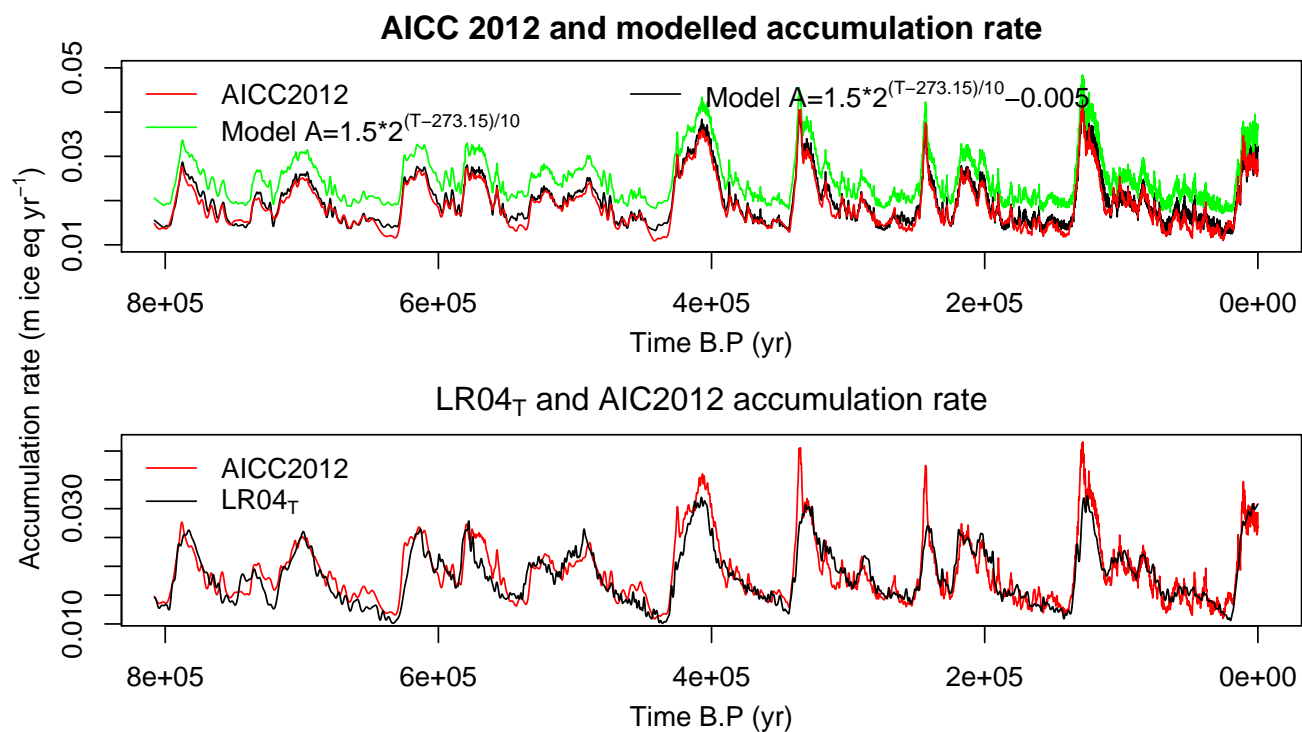d temperature is derived to find the time lag leading to the best correlation. This results in a lag of –3500yr for a correlation of 0.94 (see Figure 1.10 top panel). A lag of 3.5 kyr between climatic abrupt change and ice thickness change appears to be reasonable; due to the long adjustment time of a large ice sheet.

To retrieve ice thickness from the LR04 δ^{18}O time series, the same approach as for temperature is used, i.e.:

$$\mathrm{LR04_{thickness}} = -(\mathrm{LR04}^{-3500} - \overline{\mathrm{LR04}_{810}^{-3500}})\frac{\sigma(\mathrm{EDC2007})}{\sigma(\mathrm{LR04}_{810}^{-3500})} + \overline{\mathrm{EDC2007}} + 3309$$

Where $\mathrm{LR04}_{810}^{-3500}$ denotes the most recent 810kyr of the LR04 record shifted by -3500yr.

Figure 1.10 bottom panel shows the result of this linear model, which suffers of the same problem as the temperature reconstruction, leading to an underestimation of thickness for interglacial period of up to 50 m. To avoid abrupt discontinuities in the transient heat transport model, the thickness reconstruction is smoothed with a 10kyr moving mean filter (see Figure 1.10). The obtained thickness is coherent with the modelled thickness in [Pa].

This smoothed model is pasted to the EDC2007 data set and included into the LR04EDC time series[5].

1.2.1.5   LR04EDC time series summary

Figure 1.11 shows the 4Myr times series for temperature, accumulation rate and ice thickness established for this work.

The transition between 100 kyr and 40 kyr glacial cycles can be seen at $\sim$ 1 Myr before present. This time series also shows a decreasing mean value for the three parameters between 4 Myr and 1 Myr whereas the variability slowly increases, especially for the last 4 glacial cycles.

Figure 1.12 presents three snapshots for temperature and ice thickness for the last glacial, the end of Dome C record and a Pliocene interval. These three snapshots show the loss of temporal resolution for temperature back in time. For thickness this is not visible since the thickness time series is smoothed. From a numerical model stability point of view, smooth time series as during Pleistocene are preferable than highly variable ones.

1.2.1.6   Borehole temperature

Several temperature records exist for the Dome C borehole. In general, they all agree except for ground temperature. As shown in Figure 1.13, some records have the ground temperature at $\sim$ –2.1°C and some at $\sim$ –2.8°C. This is surprising since they are based on measurements. However, these measurements do not reach bedrock (the hole ends at $\sim$ 15 m of the bedrock). Moreover, there is a substantial uncertainty on the probe cable length and thus depth for the last hundreds of meters of the borehole measurements [S.D-J]. For these two reasons extrapolations

---

[5]Due to the smoothing, the $\mathrm{LR04_{thickness}}$ does not exactly match the EDC2007 data at the point where the 2 times series are matched. An additional smoothing is then applied for few kyr around this point.
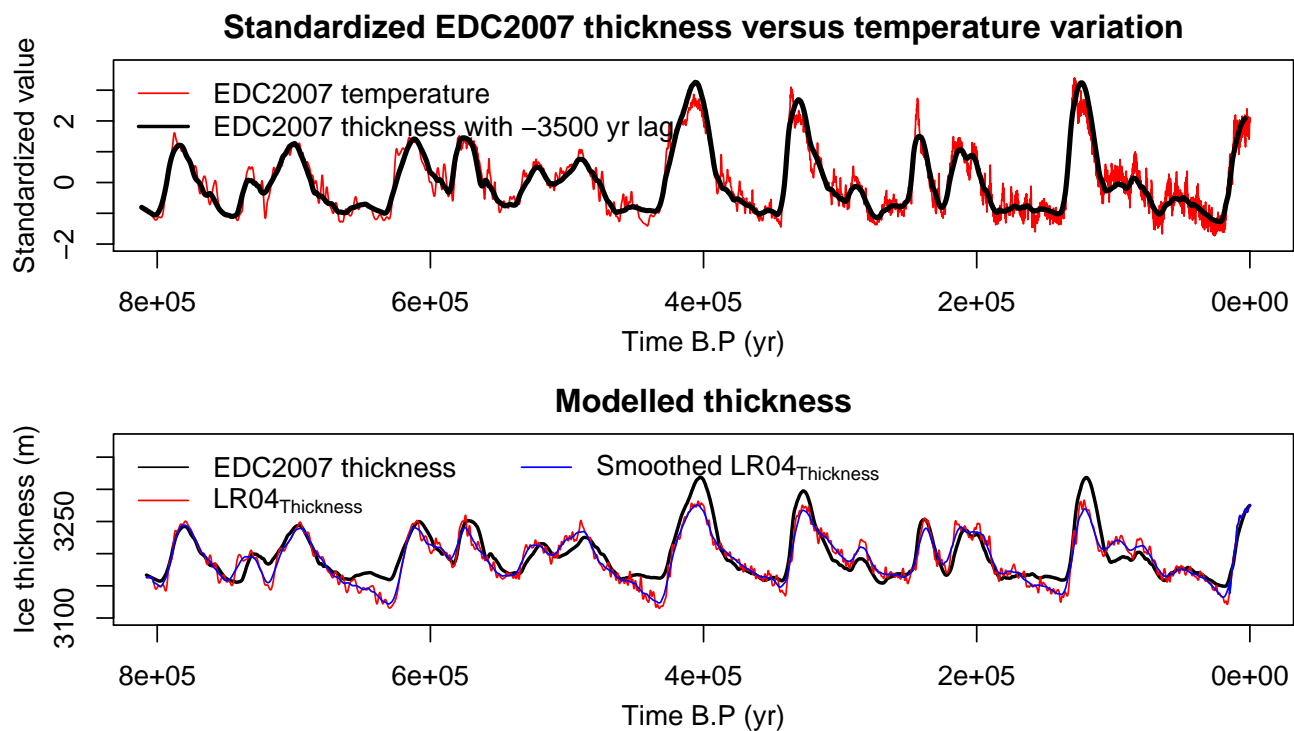
Figure 1.10: Top: EDC2007 standardized temperature (red) and EDC2007 standardized thickness with −3500yr lag (black). Bottom: EDC2007 thickness (black), modelled LR044$_{thickness}$ thickness (red), and modelled LR04$_{thickness}$ thickness smoothed (using a 10kyr moving mean filter) (black). 3275m is used as today's ice thickness
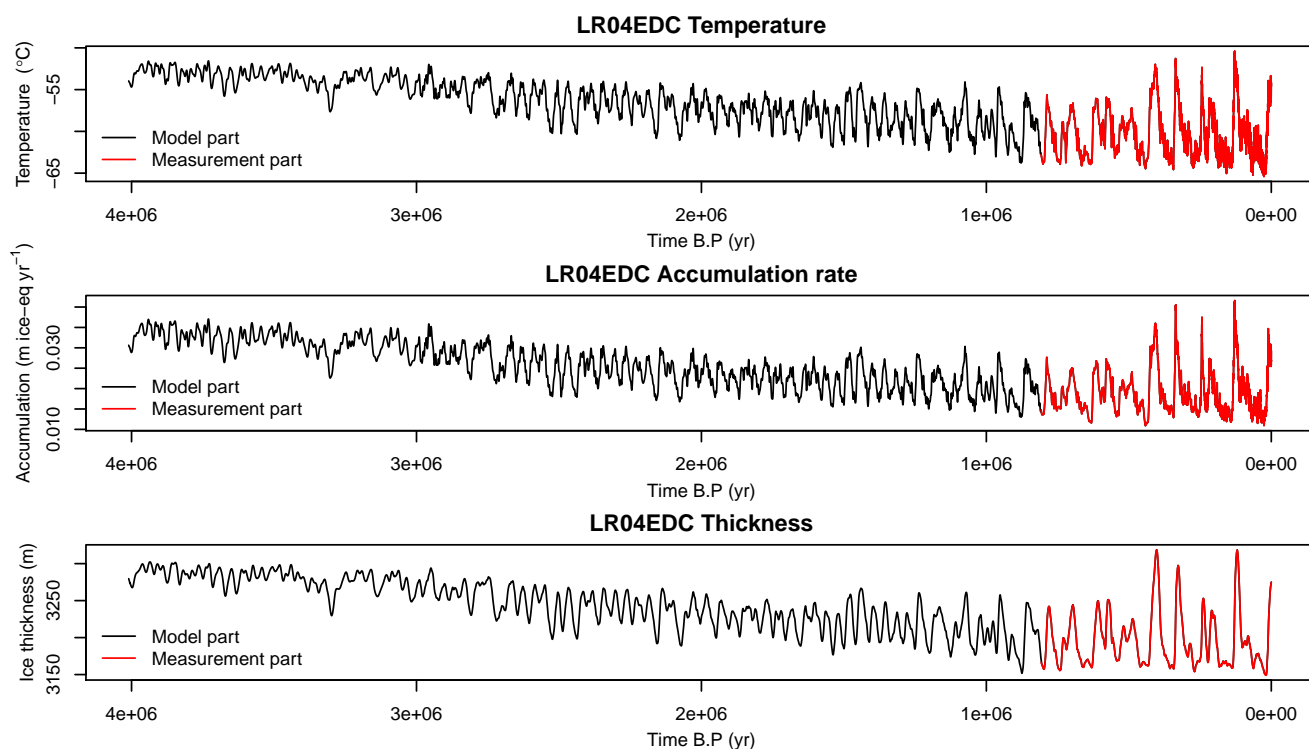
Figure 1.11: LR04EDC temperature (top), accumulation rate (middle) and ice thickness (bottom). The modeled part is in black and the part taken from the ice core record is in red.
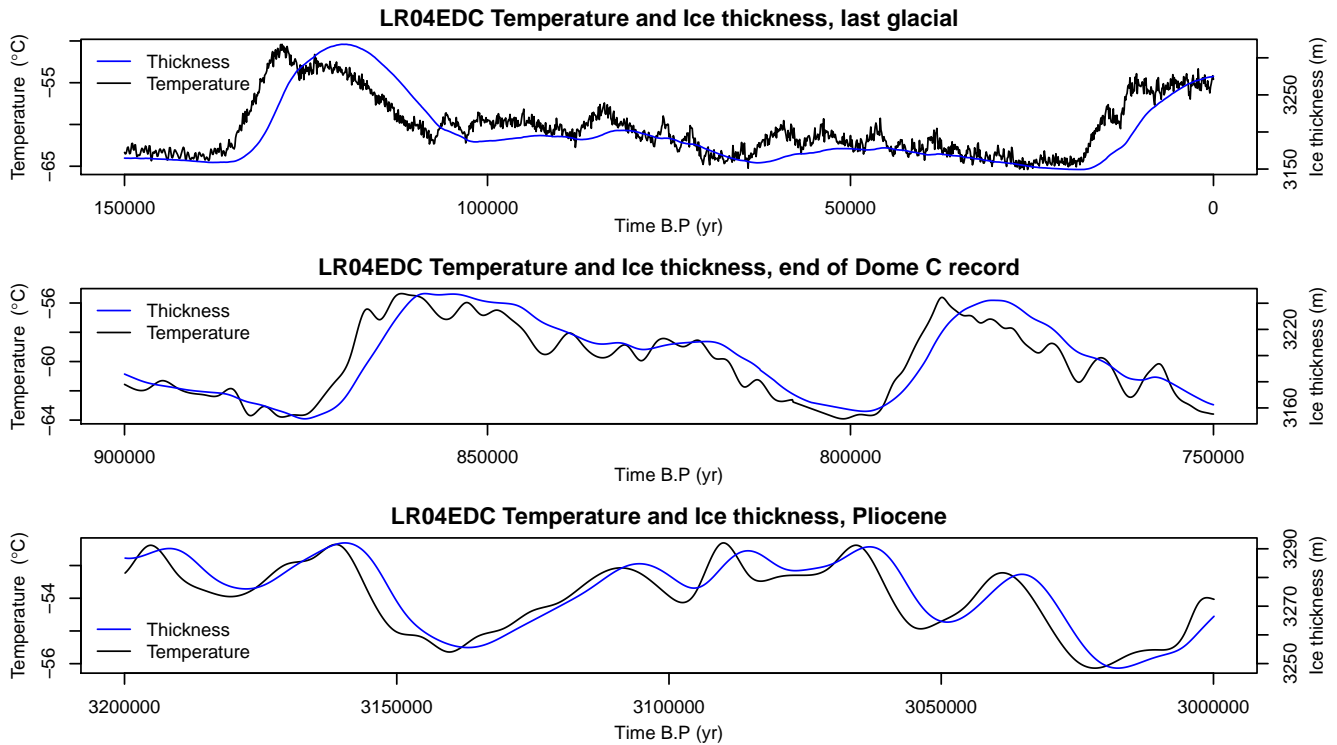
Figure 1.12: LR04EDC temperature (black) and thickness (blue) for last glacial period (top), the transition interval between ice core record and model (middle) and during the Pliocene (bottom).

have to be used to find bedrock temperature. Depending on the usage of (1.12) or (1.13) to compute the melting point (considering the ice a air saturated or not), a difference as shown in Figure 1.13 left panel occurs.

The record used in this work is from [C. Ritz, personal communication]. This record corresponds to an ice thickness of 3275m (found by extrapolation of the record until reaching the melting point), the same thickness value is then used (see Section 1.2.1.4).

Figure 1.13 also show the AICC2012 age scale used for comparison with the model.
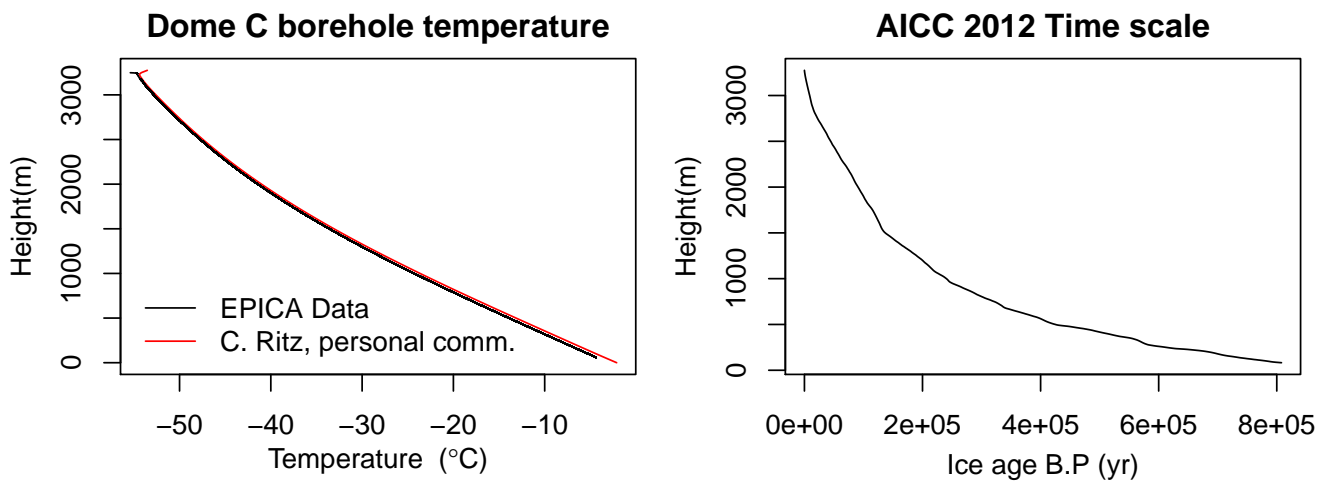
Figure 1.13: Left: Borehole temperature measurements. Right: AICC 2012 age scale.

1.2.2 Pollard-De Conto model

Alternatively, boundary conditions can also be retrieved from the 3D Ice sheet model established by Pollard and De Conto [P.DC]. This model uses a 40×40km grid and a time resolution of 5kyr to model the evolution of the Antarctic ice sheet over the last five millions years.

Data corresponding to the cell containing Dome C have been extracted (surface temperature and ice thickness). The accumulation rate is computed with (1.24) in this model. Due to its poor spatial resolution, this model fails to reproduce the dome at Dome C position. Indeed, the temperature has to be lowered by 10K and the altitude must be increased by 380m to match measurements. Moreover, a time lag of 3200yr is necessary to be in phase with the AICC2012 time series.The temperature used in the Pollard-De Conto model is shown in Figure 1.14, along with EDC2007 and LR04 temperatures.

For the last 800kyr, temperature is coherent with measurement after the −10 K correction. Nevertheless, this model predicts a variability too small for the last four glacial and interglacial cycles. Going back in time, the temperature dynamics is in phase with the Lisiecki and Raymo δ^{18}O measurement, as expected, since the boundary condition of this model are based on δ^{18}O [P.DC].

However, the temperature slowly diverges to lower values when going back in time, especially in the first 1.3 Myr of the LR04EDC time series. This could be due to the fact that surface temperature in this model depends also on altitude [P.DC] and that the modelled ice thickness, even with the 380m correction, is lower in the past (see Figure 1.15, bottom panel).

As shown in Figure 1.15 top panel, the Pollard and De Conto modelled ice thickness does also not adequately match with the EDC2007 values. In particular, the Pollard and De Conto model exhibits a too broad temporal variability in ice sheet thickness.

Due to these discrepancies between the modelled and the measured thickness for last glacial cycles, it can be concluded that the modelled values for the last 4Myr obtained by Pollard and De Conto are not more reliable than the simple model established using correlation between thickness and δ^{18}O. In the following, the simple parametrized boundary conditions will be used.

1.2.3 GRIP boundary condition

The boundary conditions at GRIP used in this work have been established using the inverse model described in [D-J3] and [Joh]. The temperature and its uncertainty are shown in Figure 1.16 left panel. Note that this temperature reconstruction fails to reproduce short-timed events in the past (such as the Younger Dryas and the Bølling-Allerød events) as they are smoothed out by thermal diffusion.

Information about ice sheet thickness is quite scarce in [D-J3] and [Joh]. A time series shown in 1.16 middle panel is established based on the few data available. The thickness maximum reached in the middle of the Holocene followed by a decreases in more recent periods is consistent with the reseluts presented in [Vi].

For accumulation rate, [D-J3] uses the following formulation:

$$A = A_0 \cdot \exp[0.0467(T - T_0) - 0.000227(T - T_0)^2] \tag{1.26}$$
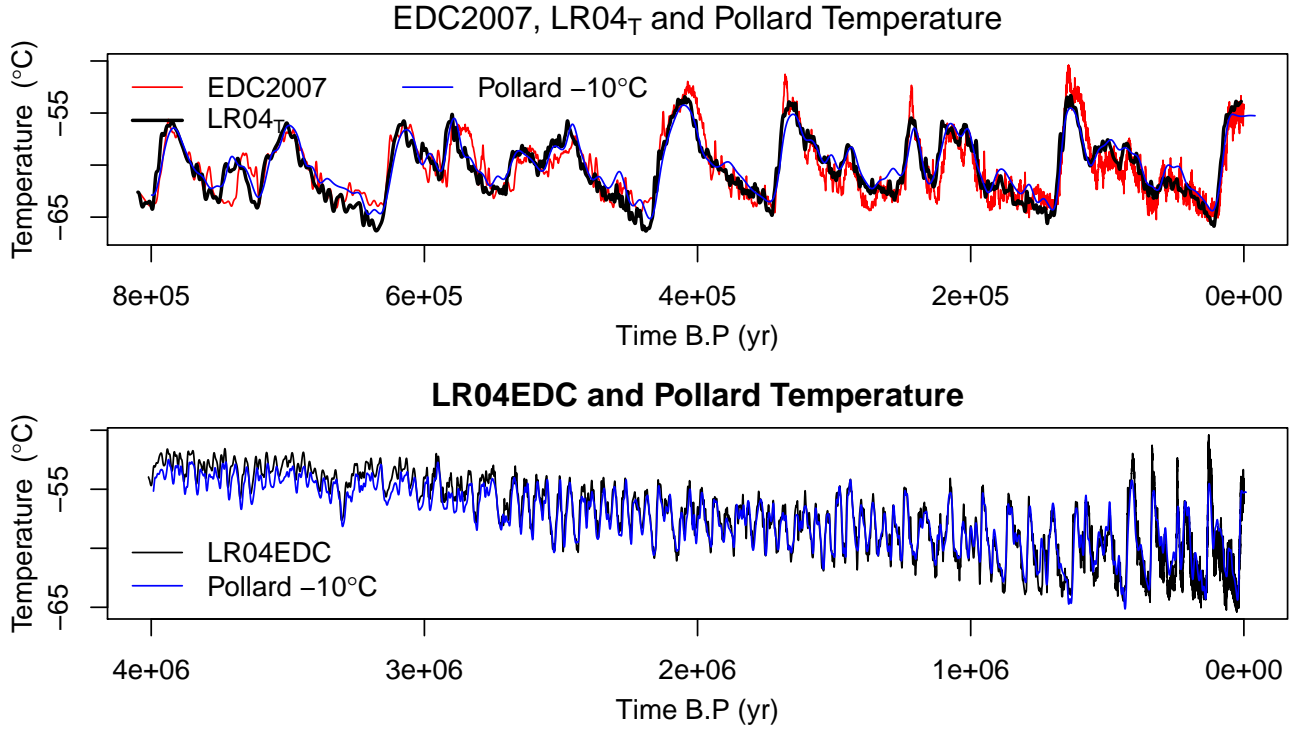
Figure 1.14: Top: EDC2007 measured temperature (red), LR04EDC modelled temperature (black) and Pollard De Conto modelled temperature with a correction of −10°C and a time lag of −3200yr (blue). Bottom: Same as top (without EDC2007 measurements) for the last 4Myr.

With $T_0 = -31.5°C$ and $A_0 = 0.35\,\mathrm{m\,ice\text{-}eq\,yr^{-1}}$ being today's values.

The age profile used is the GICC05modelext time scale described in [Ra] and [Se]. It is based upon a mix of layer counting , the NGRIP age scale model, and the correlation between events in the GRIP and NGRIP ice cores.

Since there is no melting at GRIP, the inversion of the age profile allows us to reconstruct the past accumulation rate. Indeed, taking the derivative of (1.23) gives the following:

$$\frac{\partial \mathrm{Age(z)}}{\partial \mathrm{z}} = \mathrm{w}^{-1}(\mathrm{z}, \mathrm{Age(z)})$$

Since $M(t) = 0$, (1.2) can be written as:

$$A(t) = \frac{\partial H(t)}{\partial t} - w(z, t)\omega^{-1}(\zeta(z, t))$$

Finally, combining the two previous equations gives:

$$A(\mathrm{Age(z)}) = \frac{\partial \mathrm{H}}{\partial \mathrm{t}}\Big|_{\mathrm{t=Age(z)}} - \left[\frac{\partial \mathrm{Age(z)}}{\partial \mathrm{z}}\omega\left(\frac{\mathrm{z}}{\mathrm{H(Age(z))}}\right)\right]^{-1}$$

The thickness time series being known, the accumulation rate for a given flux shape function and form factor can thus be reconstructed from the age profile.
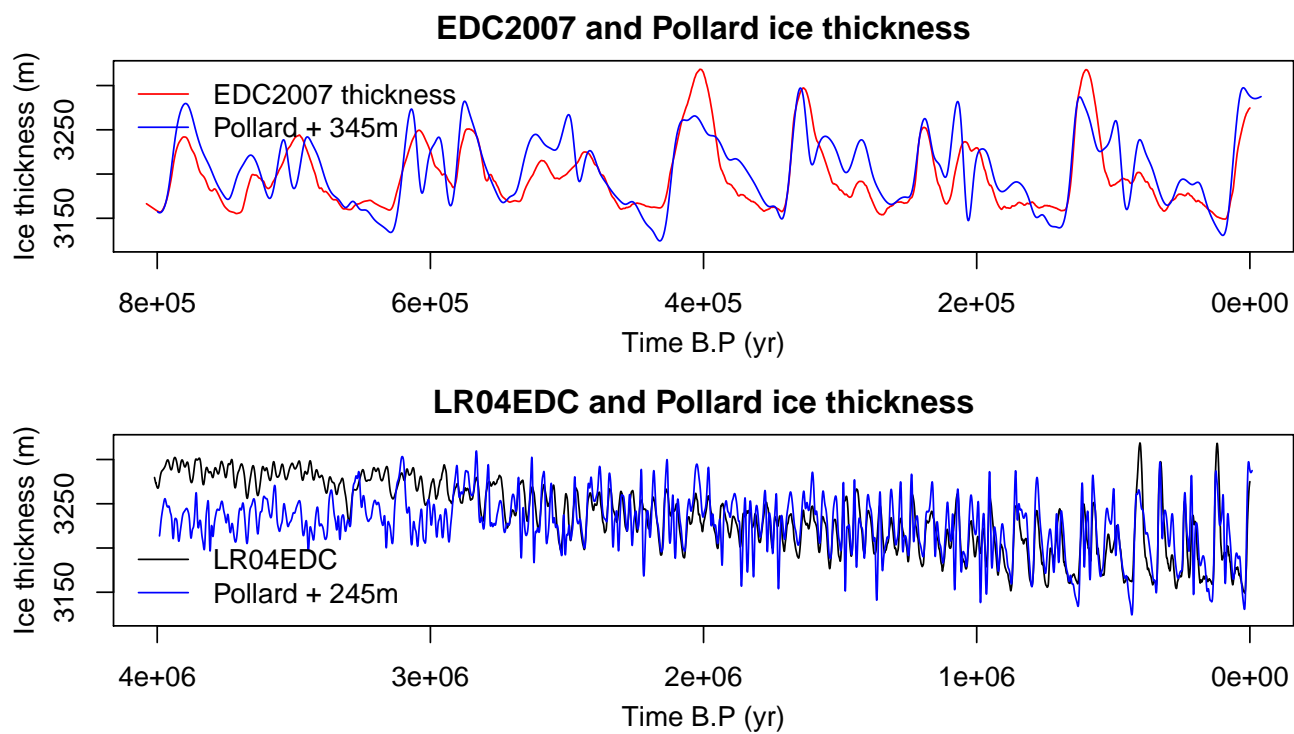
Figure 1.15: Top: EDC2007 measured thickness (red) and Pollard De Conto modelled thickness with a correction of 380m and a time lag of −3200yr (blue). Bottom: LR04EDC modelled smoothed thickness (black) and Pollard De Conto modelled thickness with a correction of 380m and a time lag of −3200yr (blue)

This reconstruction is shown in 1.16 right panel along with the accumulation rate obtained from (1.26). These reconstructions are outside the uncertainty range of (1.26), however this uncertainty is only the temperature induced uncertainty on (1.26). The accumulation rate being one of the poorest known past variables, the lower reconstructed scenarios shown on 1.16 are fully acceptable.

The borehole temperature profile used has been measured in 1994 and is described in [D-J2, Gu, Gu2, Joh].
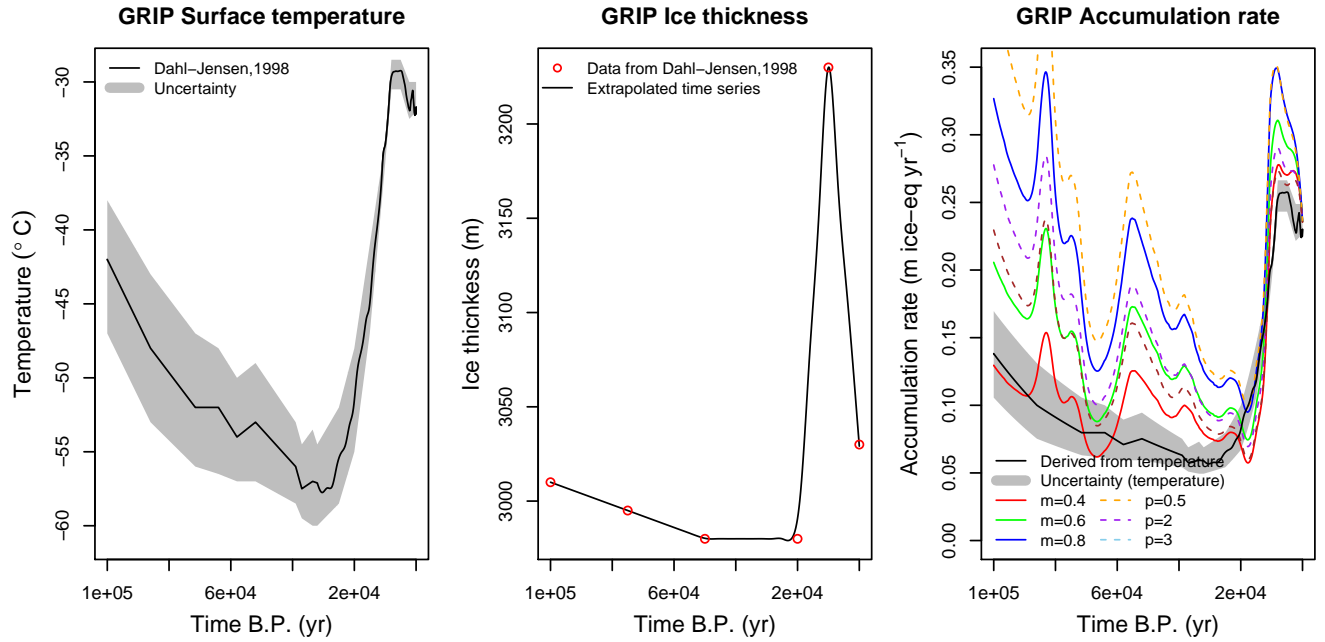
Figure 1.16: Left: Temperature reconstruction from [D-J3] and related uncertainty (grey shading). Middle: Thickness indicated in [Joh] (red dots) and extrapolated time series. Right: Accumulation rate using (1.26) and related uncertainty coming from temperature (black line and grey shading) and accumulation reconstructed by inverting age profiles using (1.3) flux shape functions (plain lines) or (1.4) (dashed lines), for various values of form factors. Note that the accumulation profiles from the age scale inversion are smoothed in the figure for readability.

1.2.4   Geothermal heat flux

The ground heat flux at Dome C is poorly known, the order of $\sim 43 \pm 20$ mWm^{-2} is given in [S.R].

In other transient models, Q_G is set as free parameter and fine tuned to produce the best age-depth relationship [Fi],[Pa]. In [Fi] a value of $Q_G = 53.5$ mWm^{-2} is obtained.

For GRIP, the value of $\sim 51 \pm 2.5$ mWm^{-2} is given in [Joh].

In this study, the geothermal heat flux will be set as free parameter (see Section 2.2.1 and Chapter 3).

1.3 From a differential equation to a numerical model

1.3.1 Explicit formulation

As equation (1.1) is discretized, any time and depth dependent quantity will be written as X_z^i, where i indicates the time step and z the depth (z = 0 being the ground and z = N the surface).

Using an Euler forward formulation for the left part of (1.1) gives [Sh]:

$$\frac{\partial T(z,t)}{\partial t} \simeq \frac{T_z^{i+1} - T_z^i}{\Delta t} \tag{1.27}$$

And using the usual formulation for second derivative and a centred difference for the first derivative *w.r.t* depth:

$$\frac{K(z,t)}{\rho(z,t)c(z,t)}\frac{\partial^2 T(z,t)}{\partial z^2} \simeq \frac{K_z^i}{\rho_z^i c_z^i}\frac{T_{z+1}^i - 2T_z^i + T_{z-1}^i}{\Delta z^2} \tag{1.28}$$

$$\frac{1}{\rho(z,t)c(z,t)}\frac{\partial K(z,t)}{\partial z}\frac{\partial T(z,t)}{\partial z} \simeq \frac{1}{\rho_z^i c_z^i}\frac{K_{z+1}^i - K_{z-1}^i}{2\Delta z}\frac{T_{z+1}^i - T_{z-1}^i}{2\Delta z} \tag{1.29}$$

$$w(z,t)\frac{\partial T(z,t)}{\partial z} \simeq w_z^i\frac{T_{z+1}^i - T_{z-1}^i}{2\Delta z} \tag{1.30}$$

Equalling (1.27) with (1.28)+(1.29)+(1.30), grouping together the T_z^i and $T_{z\pm1}^i$ terms, and writing it in a matrix form gives:

$$T_z^{i+1} = \begin{bmatrix} \frac{K_z^i\Delta t}{\rho_z^i c_z^i\Delta z^2} + w_z^i\frac{\Delta t}{2\Delta z} - \frac{K_{z+1}^i-K_{z-1}^i}{\rho c_z^i}\frac{\Delta t}{4\Delta z^2} \\ -2\frac{K_z^i\Delta t}{\rho_z^i c_z^i\Delta z^2} + 1 \\ \frac{K_z^i\Delta t}{\rho_z^i c_z^i\Delta z^2} - w_z^i\frac{\Delta t}{2\Delta z} + \frac{K_{z+1}^i+K_{z-1}^i}{\rho c_z^i}\frac{\Delta t}{4\Delta z^2} \end{bmatrix} \begin{bmatrix} T_{z-1}^i & T_z^i & T_{z+1}^i \end{bmatrix} + \dot{E}_{Iz}^i\frac{\Delta t}{\rho_z^i c_z^i} \tag{1.31}$$

Fixing as boundary condition the top temperature at the surface temperature $T_S(t)$ obtained from the LR04EDC time series (see Section 1.2.1.2 and 1.4.2) and the bottom temperature at a temperature $T_0(t)$ (see Sections 1.1.5 and 1.4.2 for more details), and defining $a = \frac{K_{z+1}^i-K_{z-1}^i}{\rho c_z^i}\frac{\Delta t}{4\Delta z^2} - w_z^i\frac{\Delta t}{2\Delta z}$, $b = \frac{K_z^i\Delta t}{\rho_z^i c_z^i\Delta z^2}$, and $S_z^i = \dot{E}_{Iz}^i\frac{\Delta t}{\rho_z^i c_z^i}$ leads to:

$$\begin{bmatrix} T_0^{i+1} \\ T_1^{i+1} \\ \vdots \\ T_{N-1}^{i+1} \\ T_N^{i+1} \end{bmatrix} = \begin{bmatrix} 1 & 0 & 0 & \dots & 0 \\ b_1^i - a_1^i & 1-2b_1^i & b_1^i + a_1^i & \dots & 0 \\ \vdots & \ddots & \ddots & \ddots & \vdots \\ 0 & \dots & b_{N-1}^i - a_{N-1}^i & 1-2b_{N-1}^i & b_{N-1}^i + a_{N-1}^i \\ 0 & \dots & 0 & 0 & 1 \end{bmatrix} \cdot \begin{bmatrix} T_0^i \\ T_1^i \\ \vdots \\ T_{N-1}^i \\ T_S^i \end{bmatrix} + \begin{bmatrix} 0 \\ S_1^i \\ \vdots \\ S_{N-1}^i \\ 0 \end{bmatrix} \tag{1.32}$$

Defining the matrix as $\mathbf{A}^i$, this reads:

$$\mathbf{T}^{i+1} = \mathbf{A}^i \cdot \mathbf{T}^i + \mathbf{S}^i \tag{1.33}$$

Numerically, this is solved using the formulation of (1.31). This explicit formulation has a major limitation: its stability condition. Indeed, as shown by a Von Neumann stability analysis [Ch, C.N.], the maximum time step is about 1 day, leading to a too long numerical computation time (about 7 hours for a 2 Myr run). This is obtained by computing the temperature profile on a daily basis with (1.33), but updating all the other parameters only once every 100 yr. Otherwise the run time is even longer.

In spite of its limitations, this method is used in this work as a test for the precision of the faster methods described below.

1.3.2   Implicit formulation

To avoid the stability limitation, an implicit scheme can be used. It consists of evaluating the right hand side of (1.27) to (1.30) at time $i + 1$ instead of i. Redoing the same development as in the previous section gives:

$$\mathbf{T}^{i+1} = - \left(\mathbf{A}^{i+1} \right)^{-1} \cdot \left(\mathbf{T}^i + \mathbf{S}^i \right)$$

The advantage of this formulation is its stability whereas the main issue is that it requires to know all the physical parameters involved in $\mathbf{A}$ at time $i + 1$. But since they are temperature dependent, they can only be approximated by their value at time i, which requires to keep the time step not to large.

1.3.3   Crank-Nicholson formulation

An improvement to the implicit scheme is the Crank-Nicholson scheme [C.N]. This scheme consists of rewriting (1.1) as:

$$\frac{\partial T}{\partial t} = \theta F_z^{i+1}(z, t, T, \frac{\partial T}{\partial z}, \frac{\partial^2 T}{\partial z^2}) + (1 - \theta) F_z^i(z, t, T, \frac{\partial T}{\partial z}, \frac{\partial^2 T}{\partial z^2}) + \frac{\dot{E}_I(z, t)}{\rho(z, t) c(z, t)} \qquad (1.34)$$

Or in other word, to use a weighted mean by a factor θ between an implicit and explicit formulation (with the internal energy term kept out). Redoing the same development as in the explicit case yields to:

$$(1-\theta)(\beta_z^i - \alpha_z^i)T_{z-1}^i + (1-(1-\theta)2\beta_z^i)T_z^i + (1-\theta)(\beta_z^i + \alpha_z^i)T_{z+1}^i + S_z^i = \begin{bmatrix} \theta(-\beta_z^{i+1} + \alpha_z^{i+1}) \\ 1 + 2\theta\beta_z^{i+1} \\ \theta(-\beta_z^{i+1} - \alpha_z^{i+1}) \end{bmatrix} \begin{bmatrix} T_{z-1}^{i+1} & T_z^{i+1} & T_{z+1}^{i+1} \end{bmatrix}$$

$$(1.35)$$

With $\alpha = \frac{K_{z+1}^i - K_{z-1}^i}{\rho c_z^i} \frac{\Delta t}{4 \Delta z^2} - w_z^i \frac{\Delta t}{2 \Delta z}$, $\beta = \frac{K_z^i \Delta t}{\rho_z^i c_z^i \Delta z^2}$ and $S_z^i = \dot{E}_{I z}^i \frac{2 \Delta t}{\rho_z^i c_z^i + \rho_z^{i+1} c_z^{i+1}}$.

Note that α and β can not be known at $t = i+1$, so they have to be approximated by their value at time i (the same holds for the ρ and c terms in S_z^i).

Defining:

$$L_z^i = \theta(-\beta_z^i + \alpha_z^i)$$

$$D_z^i = 1 + 2\theta\beta_z^i$$

$$R_z^i = \theta(-\beta_z^i - \alpha_z^i)$$

$$B_z^i = (1-\theta)(\beta_z^i - \alpha_z^i)T_{z-1}^i + (1 - (1-\theta)2\beta_z^i)T_z^i + (1-\theta)(\beta_z^i + \alpha_z^i)T_{z+1}^i + S_z^i$$

this system can be written in tridiagonal form[6]:

$$
\begin{bmatrix}
D_1^i & R_1^i & 0 & \ldots & 0 \\
L_2^i & D_2^i & R_2^i & \ldots & 0 \\
\vdots & \ddots & \ddots & \ddots & \vdots \\
0 & \ldots & L_{N-2}^i & D_{N-2}^i & R_{N-2}^i \\
0 & \ldots & 0 & L_{N-1}^i & D_{N-1}^i
\end{bmatrix}
\begin{bmatrix}
T_1^{i+1} - T_0^{i+1} \cdot L_1^i \\
T_2^{i+1} \\
\vdots \\
T_{N-2}^{i+1} \\
T_{N-1}^{i+1} - T_S^{i+1} \cdot R_{N-1}^i
\end{bmatrix}
=
\begin{bmatrix}
B_1^i \\
B_2^i \\
\vdots \\
B_{N-2}^i \\
B_{N-1}^i
\end{bmatrix}
\tag{1.36}
$$

This could be solved by inverting the full matrix [H.McC], but this is not the most efficient method. Several methods exist to solve tridiagonal systems, the algorithm described in [C.B.] is used. It is stable since $D >> L$ and $D >> L$ [Hi].

For the system:

$$
\begin{bmatrix}
D_1^i & R_1^i & 0 & \ldots & 0 \\
L_2^i & D_2^i & R_2^i & \ldots & 0 \\
\vdots & \ddots & \ddots & \ddots & \vdots \\
0 & \ldots & L_{N-2}^i & D_{N-2}^i & R_{N-2}^i \\
0 & \ldots & 0 & L_{N-1}^i & D_{N-1}^i
\end{bmatrix}
\cdot
\begin{bmatrix}
x_1 \\
x_2 \\
\vdots \\
x_{N-2} \\
x_{N-1}
\end{bmatrix}
=
\begin{bmatrix}
B_1 \\
B_2 \\
\vdots \\
B_{N-1} \\
B_{N-2}
\end{bmatrix}
$$

The following values are defined:

$$
D_i' =
\begin{cases}
D_1 & ; i = 1 \\
D_i - \dfrac{L_i}{D_{i-1}'}R_{i-1} & ; i = 2, 3 \ldots N-1
\end{cases}
$$

$$
B_i' =
\begin{cases}
B_1 & ; i = 1 \\
B_i - \dfrac{L_i}{D_{i-1}'}B_{i-1}' & ; i = 2, 3 \ldots N-1
\end{cases}
$$

---

[6]A tridiagonal form is necessary to use the algorithm described below

And then the system is solved backward:

$$
x_i =
\begin{cases}
\dfrac{B'_{N-1}}{D'_{N-1}} & ; i = N - 1 \\[2ex]
\dfrac{B'_i - R_i x_{i+1}}{D'_{N-1}} & ; i = N - 2, N - 3 \ldots 2
\end{cases}
$$

As stated before, in (1.35) the value of α and β have to be evaluated at $i + 1$ instead of i on the right hand side. To approximate these values at $i + 1$, an iterative method is used. This means that the system is solved a first time using i on both side, and then the new temperature profile is used to re-compute all the parameters and get an approximation of α_z^{i+1}, β_z^{i+1} and S_z^{i+1}. Finally, the model is solved again with these new values, .i.e:

$$
\begin{bmatrix}
D_1^{i+1} & R_1^{i+1} & 0 & \cdots & 0 \\
L_2^{i+1} & D_2^{i+1} & R_2^{i+1} & \cdots & 0 \\
\vdots & \ddots & \ddots & \ddots & \vdots \\
0 & \cdots & L_{N-2}^{i+1} & D_{N-2}^{i+1} & R_{N-2}^{i+1} \\
0 & \cdots & 0 & L_{N-1}^{i+1} & D_{N-1}^{i+1}
\end{bmatrix}
\begin{bmatrix}
T_1^{i+1} - T_0^{i+1} \cdot L_1^{i+1} \\
T_2^{i+1} \\
\vdots \\
T_{N-2}^{i+1} \\
T_{N-1}^{i+1} - T_S^{i+1} \cdot R_{N-1}^{i+1}
\end{bmatrix}
=
\begin{bmatrix}
B_1^i \\
B_2^i \\
\vdots \\
B_{N-2}^i \\
B_{N-1}^i
\end{bmatrix}
\tag{1.37}
$$

As for the density calculation (Section 1.1.3), this could be iterated until reaching a stable value, see Section 2.3.

1.4 Technical details

1.4.1 Boundary condition in their discrete form

The surface temperature time series is linearly extrapolated with a point every 100 yr. The same holds for ice thickness and accumulation rate.

In the model run, the effective ice sheet thickness (i.e the number of cells) is the integer part of the thickness, i.e each vertical layer has a thickness of 1 m. However, the thickness value used to compute the velocity and the melting temperature is the real thickness (to avoid discontinuity when the thickness jumps to the next integer).

At the end of every time step, the thickness for the next time step is taken and rounded. If the future ice thickness (from LR04EDC) is not equal to the previous one, some layers are added on the top with a temperature corresponding to the surface temperature (if the future thickness is larger) or a spline is used to reduce the whole temperature profile to the needed number of layer (the spline follows the form of the velocity profile, i.e. the flux shape function (see Section 1.1.2)).

1.4.2 Density, melting, thermal conductivity, heat capacity and velocity in discrete form

At the beginning of every time step, the density profile is computed using the temperature profile from the previous step (T_z^i) and the accumulation rate from LR04EDC. The density profile ρ_i^z is obtained with (1.6) and (1.7).

Then the thermal conductivity K_z^i and heat capacity c_z^i are computed with (1.8), (1.9) or (1.10) and (1.11).

The density profile allows us to compute the pressure at the bottom $P^i = \sum_{z=0}^{z=H} \rho_z^i \Delta x$ and from this the melting temperature T_M with (1.12).

To compute the melt rate, it is first checked if there is enough energy available to reach or stay at the melting point during this time step by computing:

$$Q_G + K_0^i \frac{T_1^i - T_M}{\Delta z}$$

With two possibilities:

1. The result is larger than zero: it will be possible to melt some ice. The new bottom temperature T_0^{i+1} is then T_M. The energy needed (or released) to reach this temperature is computed by assuming a locally linear temperature profile and then transformed into a flux over one time step:

$$Q_{eq} = -\rho_0^i c_0^i \left[M^{i+1} \frac{T_M - T_1^i}{2} + \frac{T_M - T_0^i}{2} \frac{\Delta z}{\Delta t} \right]$$

The melt rate is then obtained by solving (1.15):

$$M^i = \frac{Q_G - \rho_0^i c_0^i (T_M - T_0^i)\Delta z/(2\Delta t) + K_0^i \frac{T_1^i - T_M}{\Delta z}}{\rho_0^i (L + c_0^i(T_0^i - T_M) + c_0^i(T_M - T_1)/2)} \tag{1.38}$$

2. The result is smaller than zero: no melting occurs, M^i is set to 0.

   As explained in Section 1.1.5, it this case the model only considers a cooling of the basal ice (no possible water refreezing or cooling of the bedrock).

   The new bottom temperature is obtained by solving (1.38) with $M^i = 0$ and a corrected Q_{eq} set to 0[7]:

$$Q_G = K_0^i \frac{T_1^i - T_0^{i+1}}{\Delta z}$$

$$T_0^{i+1} = T_1^i - Q_G \frac{\Delta z}{K_0^i} \tag{1.39}$$

---

[7]In this case it is assumed that the temperature will reach the equilibrium within a time step Δt and the exact energy budget is not important.

The new T_0^{i+1} is then used as boundary condition.

Finally, the velocity is calculated with the chosen flux shape function (see Section 1.1.2).

When performing the second pass for the Cranck-Nicholson scheme, all of the following values are replaced in (1.38) by their mean value over the time period:

$$\rho_z^i \to \frac{1}{2}(\rho_z^{i+1} + \rho_z^i)$$

$$c_0^i \to \frac{1}{2}(c_0^{i+1} + c_0^i)$$

$$K_0^i \to \frac{1}{2}(K_0^{i+1} + K_0^i)$$

$$T_z^i \to \frac{1}{2}(T_z^{i+1} + T_z^i)$$

1.4.3   Programming details and profile

The model is developed in C. The chosen time step Δt is 100 yr and the height step Δz is 1 m. When the explicit formulation is used, $\Delta t = 100$ yr is kept for the update of all the physical parameters, changes in boundary conditions and computation of the melt rate, but an additional inner loop updates the temperature profile with $\Delta t = 1$ day.

The Crank-Nicholson parameter θ is set to 0.7. Despite the fact that Crank-Nicholson scheme is supposed to be stable for a simple heat equation, the formulation used here with advection, changing thickness and temperature dependent parameters ρ, c and K produced some instabilities for $\theta < 0.6$ and $\Delta t = 100$ yr. The chosen value for theta corresponds to the best fit with the explicit scheme output (see Section 2.3).

The model can receive as free parameter the form factor, the ground heat flux, some temperature correction for the glacial periods and/or the Holocene, some accumulation rate correction, and the valley depth, width, and flat bottom width. The model accepts several values for free parameters (provided in tables) and automatically loops through the whole set of given parameters. The output can be temperature and age profile for today, melt rate record over the time span of the run, and full temperature profile history (one profile every 100 yr provided in a matrix) with each file named with the used free parameters values. See more details on the source code on Appendix D.

The execution time for a 4Myr rune is divided as follows: $\sim 32\%$ for the computation of physical parameters (w,ρ,k,cp,α and β), $\sim 32\%$ for the computation of the internal energy production and lateral conduction, $\sim 24\%$ for the tridiagonal solver algorithm, and $\sim 9\%$ to compute melt, scale thickness and split the work between functions. The remaining $\sim 3\%$ are spent for initialization, reading data from files and writing output into files. These numbers correspond to runs with full complexity (i.e. all physical processes described in Chapter 1 turned on) and are obtained using the gprof UNIX utility [Gr].

All the code is written using usual C libraries (stdio.h, stdlib.h, math.h and time.h), meaning that all the solving algorithms have been implemented by hand. The only unusual library used is the open source Open MP library (www.openmp.org) allowing multiprocessor computation to speed up the code. Note that the tridiagonal system that has to be solved ($\sim$3000$\times$3000 matrix) is not big enough to implement algorithms that really take profit from processor splitting ([Ma]). Multi processing is used when several runs are performed with different values for the frees parameters. By default, the values chosen for the form parameter are distributed over all the core of the computer, meaning that a maximum efficiency is obtained if the number of form parameter value is a multiple of the number of core.

With a five-year-old common computer, one run with full complexity for 4Myr takes about 150 seconds. When using multiprocessing for runs with varying free parameters values, the run time is divided by the core number. When turning off the valley effect, the run time is almost divided by 2. This means that with a 4 core computer and without valley effect, a run with 1000 different combination of free parameters takes around 5 hours (10 hours with valley effect).

Some adjustments are needed in the description given in Section 1.3 due to some computational limitation. When computing density, the $\mathcal{Z}$ terms rapidly diverge (Section 1.1.3). Since the density is proportional $\mathcal{Z}/(\mathcal{Z}+1)$, this divergence is perfectly natural but a too big $\mathcal{Z}$ value can not be handled by the computer. To avoid this issue the density is directly set to $\rho_{\text{ice}}(\text{T}_{\text{z}})$ for depth larger than 1000 m (that has no effect on the final density up to 8 digits).

Plots are produced with R and GnuPlot and the IDE used in C is Code::Blocks meaning that this whole thesis is made using free and open source software.

Chapter 2

Spin up, sensitivity test and model comparison

In this chapter, different aspects of the model are tested. First, the necessary time for spin up is established. Then, the sensitivity of the model to all internal parameters is tested to infer if the model reacts correctly and to quantify the impact of these parameters on the output of the model (i.e. recent temperature profile, melt rate history and age profile). Finally, the different schemes of the model are tested (see Section 1.3) and the model is tested against other models.

2.1   Spin up

The model is spun up before each run with boundary conditions corresponding to the first value of the boundary condition times series. The initial temperature profile is set to a linear profile with the bottom temperature set at melt temperature for the runs at EDC and to a quadratic profile with bottom temperature at –9°C for runs at GRIP (i.e almost today's ground temperature, see section 1.2.3) .

Figure 2.1 shows the evolution of the spin up temperature values for GRIP and EDC conditions (respectively boundary condition at 100 and 150 kyr B.P., with m = 0.4 and 0.5, and with $Q_G = 54$ and 55 mWm^{-2}, both using [Fi] flux shape function and [C.P] firn thermal correction, see Sections 1.1.2 and 1.1.4).

Regarding melt rate, it converges in about 75 kyr to its equilibrium value (changes between 100 kyr and 150 kyr are of order 5%).

Note that when changing boundary conditions to other physically acceptable values, a similar time needed to reach equilibrium. A duration of 150 kyr for the spin up is then sufficient.
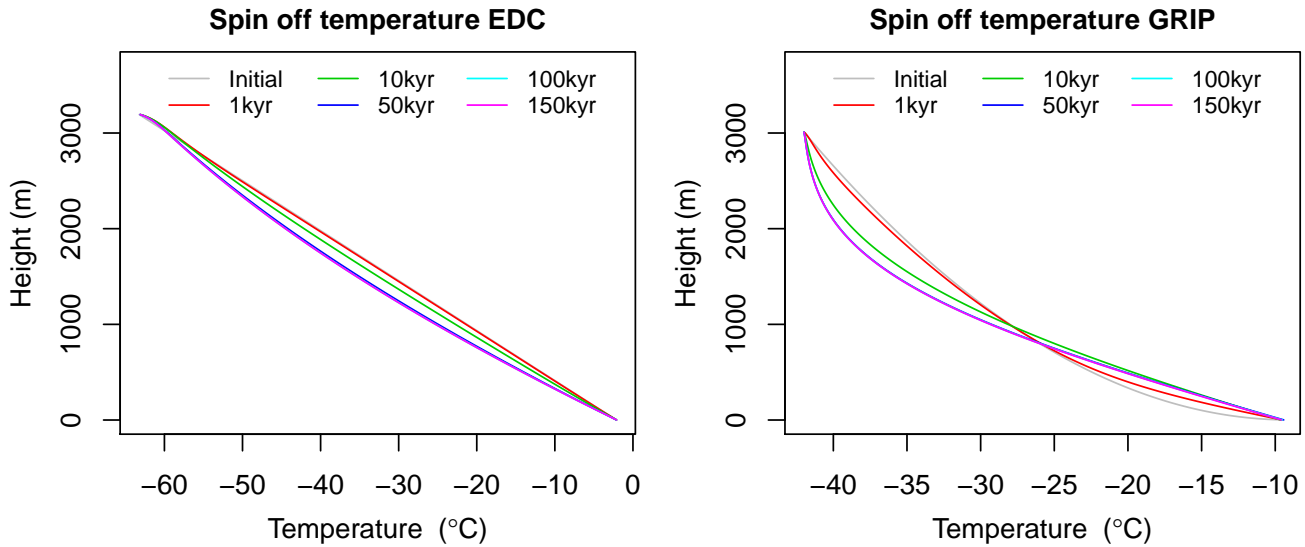
Figure 2.1: Temperature profile for different time after the beginning of spin up. Left: EDC. Right: GRIP.

2.2 Sensitivity test

2.2.1 Physical parameters

2.2.1.1 Thermal conductivity and density

Two formulations for the impact of the firn layer on thermal conductivity are tested ((1.9) from [C.P] and (1.10) from [Sc], see Section 1.1.4). The output of the model without firn correction is also tested. The result is shown in Figure 2.2 (run for 1 Myr at EDC using [Fi] flux shape function with m = 0.4 and $Q_G = 54$ mWm^{-2}).

The figure shows that [Sc] formulation gives a slightly warmer upper profile than the [C.P] one, whereas the bottom part of the temperature profile and the melt rate are quite similar. When no firn thermal conductivity correction is included, the profile is colder, meaning that firn insulation, even in warm period, helps to retain ground heat in the ice sheet. The difference between the [Sc] and [C.P] formulation is not too large but also not negligible, showing the importance of having a better knowledge of firn properties. Since the [C.P] formulation is faster in the model (no exponential to compute, which is quite slow in C), this formulation will be used unless something else is specified.

Figure 2.2 also shows that having a realistic density profile mainly affects the output through thermal conductivity change (i.e. the profiles with no firn correction on density and constant density are really close). Nevertheless, the difference between profiles with and without firn correction thermal conductivity ($\sim$ –0.5°C) show the importance of having a real density profile in the model.

As can be expected, changing the thermal conductivity to smaller values for the whole profile gives a cooler profile in warm periods whereas higher conductivity gives a warmer profile. However, at ground level, higher conductivity leads to higher downward cold flux that can exceed the ground heat flux and then lead to no melting and thus colder ground temperature (see the profile for

K+10%).

Finally, the model handles transitions between phases with and without ground melting properly. Indeed, the K[C.P]+5% run (orange line on the right panel of Figure 2.2) goes through some phases where there is no melting and resumes to melting in a coherent manner in comparison to the melt rate history of the other runs. Moreover, the temperature profile for the same run (orange line on the left) show the expected small decrease in basal temperature since today's melting is zero.
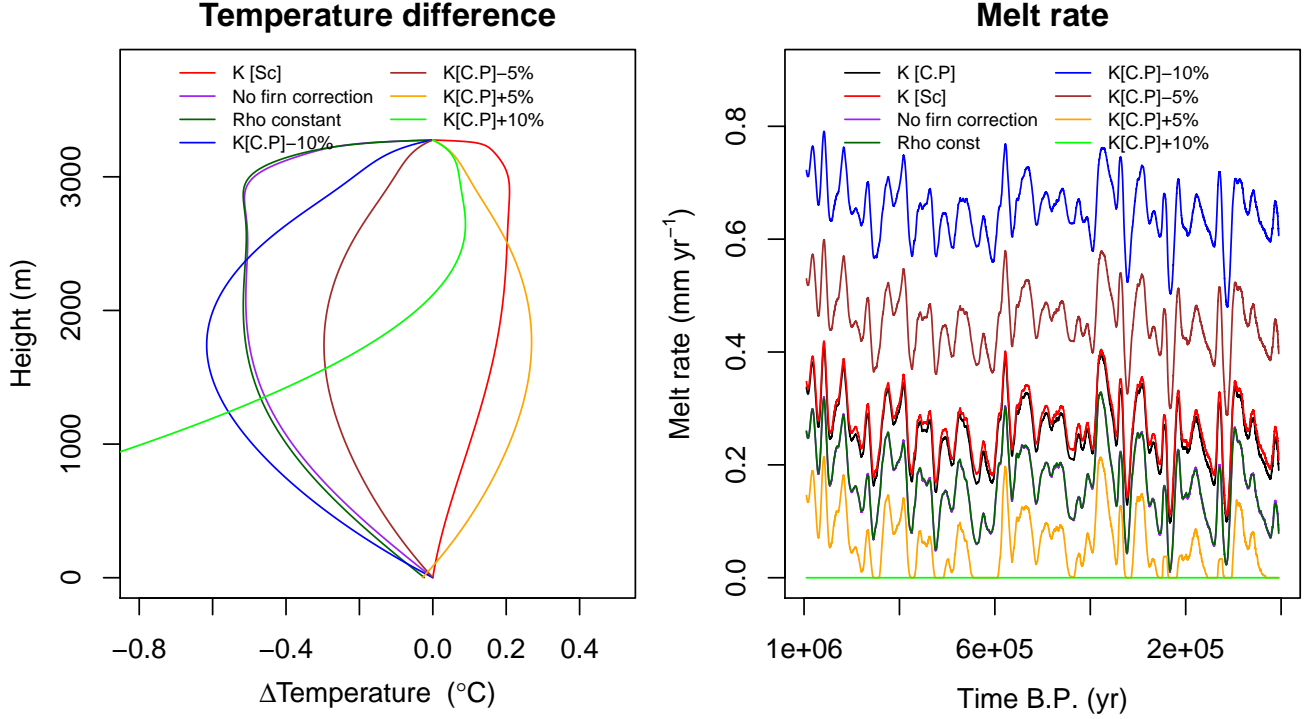
Figure 2.2: Left : Different between temperature profiles (for different values of thermal conductivity) and the temperature profile obtained using K[C.P]. The dark green profile uses a constant density profile (920 kg m^{-2}) whereas the other profiles use density as described in 1.1.3. When a percentage change is indicated, that means that this change is locally applied to the whole thermal conductivity profile. Left: Melt rate for the same set of runs. Runs for 1 Myr at Dome C using [Fi] flux shape function with m = 0.4 and Q_G = 54 mWm^{-2} and the LR04EDC time series.

2.2.1.2   Velocity and ground heat flux

The model is run with [Fi] (see (1.3)) and [Pa] (see (1.4)) flux shape functions with various values for the form factors. Output is shown in Figure 2.3 (the ground heat flux for this 1 Myr EDC run is set to 54 mWm^{-2}). Both flux shape functions give similar output for temperature whereas they disagree in age (i.e. melt rate). This difference is due to the different temperature gradient they have close to the ground (see Figure 1.1).

When reducing the ground heat flux there is as expected no melting and thus a colder ground temperature (see Figure 2.4). Above the melting threshold, the ground temperature is at melting point and the temperature value along the whole profile slightly decreases as the ground heat flux increases. This effect is due to the higher melt rate that induces a higher vertical downward velocity and thus more cold advection from the top of the ice sheet.
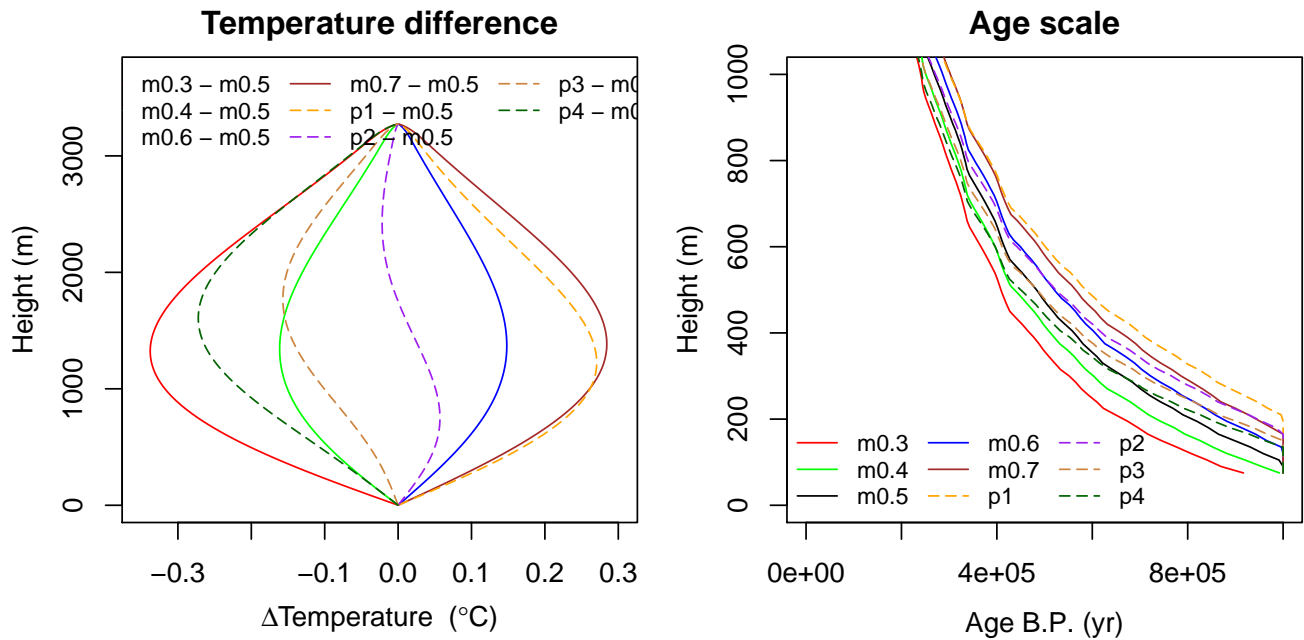
Figure 2.3: Left : Temperature profile for [Fi] (plain lines) and [Pa] (dashed lines) flux shape function for various values of the form factor, minus temperature profile with [Fi] flux shape function and m=0.5. Right: Age profile for the same set of run. Runs for 1 Myr at Dome C using $Q_G = 54$ mWm^{-2} and the LR04EDC time series.
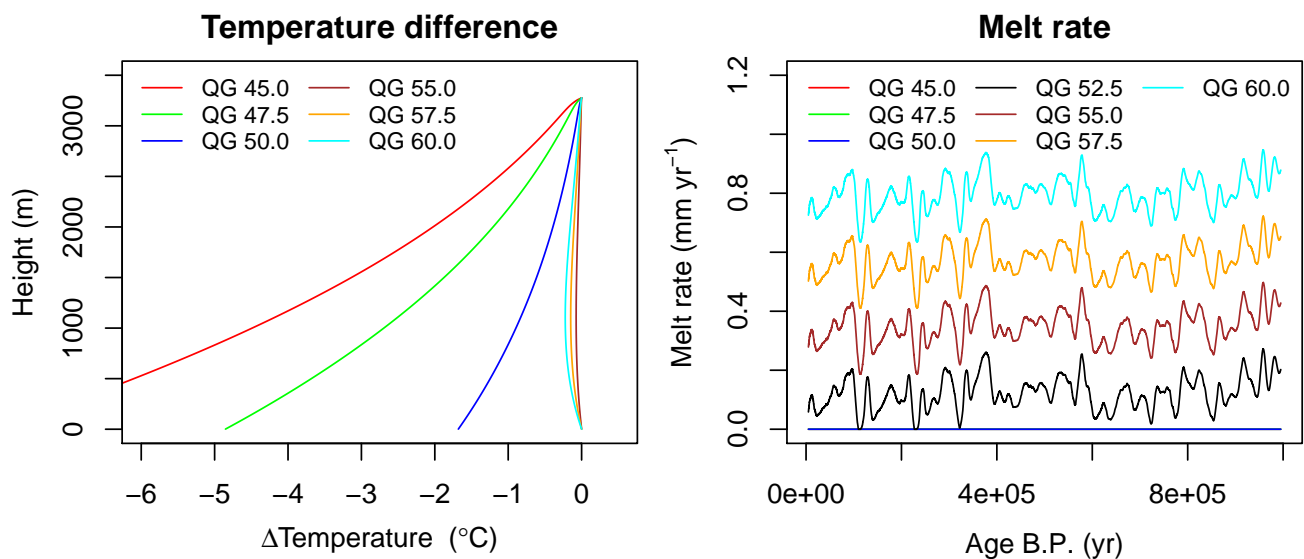
Figure 2.4: Left : Temperature profile for different ground heat flux values (in mWm^{-2}) minus profile with $Q_G = 52.5$ mWm^{-2}. Right: melt rate for the same ground heat flux values. Run for 1 Myr at Dome C with [Fi] velocity profile and m = 0.4.

2.2.1.3   Valley effect and internal energy production

The effect of having the drill site above a valley is tested for different values of ΔH, L and f (i.e. valley depth, width, and flat valley bottom width, see 1.1.7). The results are shown in Figure 2.5 and Figure 2.6. A deeper and thinner valley increases the temperature, but small ground flat areas surprisingly gives colder profiles than large ground areas. This is due to the fact that reducing the flat area diameter leads to higher temperature near bedrock (which can be seen for blue plain lines in the lower two panels of Figure 2.5) and thus higher melting (see Figure2.6) leading to a higher downward velocity and thus a colder profile in general. The elevation of the temperature when the flat area radius is reduced is due to the proximity of the valley cliffs which are at melting temperature and thus warmer than the ice column.

The topography has an important influence on the melt rate (and thus age profile) and small changes in valley parametrization have a non negligible impact on melt rate, as shown in Figure 2.6. This impact on the melt rate is larger than the usual uncertainty given in the literature for melt rate values (see [Pa, D-J3]). Thus, a good parametrization of topography is essential for a reliable determination of the ground heat flux.
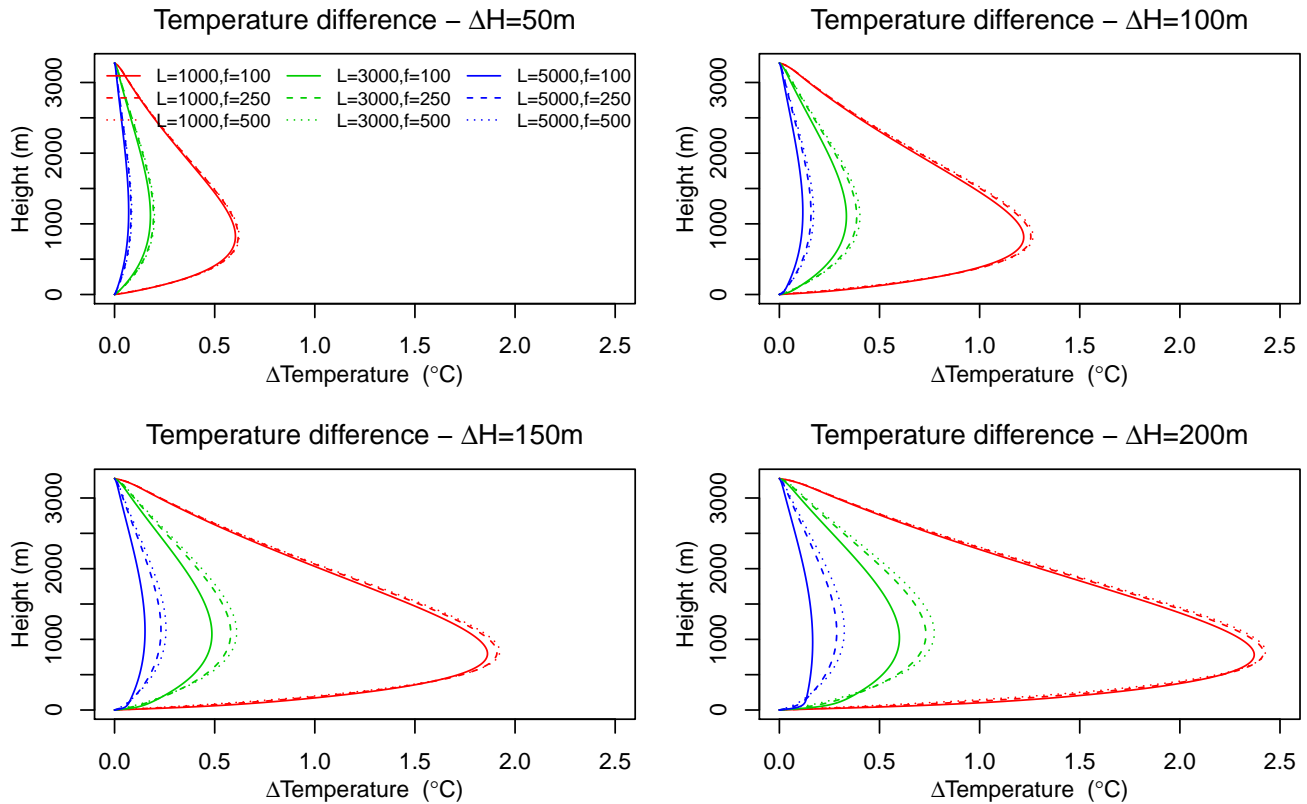
Figure 2.5: Effect of valley topography on temperature profiles (compared to a run without valley) for different values of ΔH, L and f.

Results for the internal energy production (see 1.1.6) test are presented in Figure 2.7. With parameters from [D-J] (see Appendix B) the effect on temperature and melting is negligible. Since the used parameters hold for an ice sheet at equilibrium, one can imagine that during periods of high thickness changes there is more internal ice displacements and thus more internal energy. When testing by increasing internal energy by factors 10 and 100 for periods of fast thickness
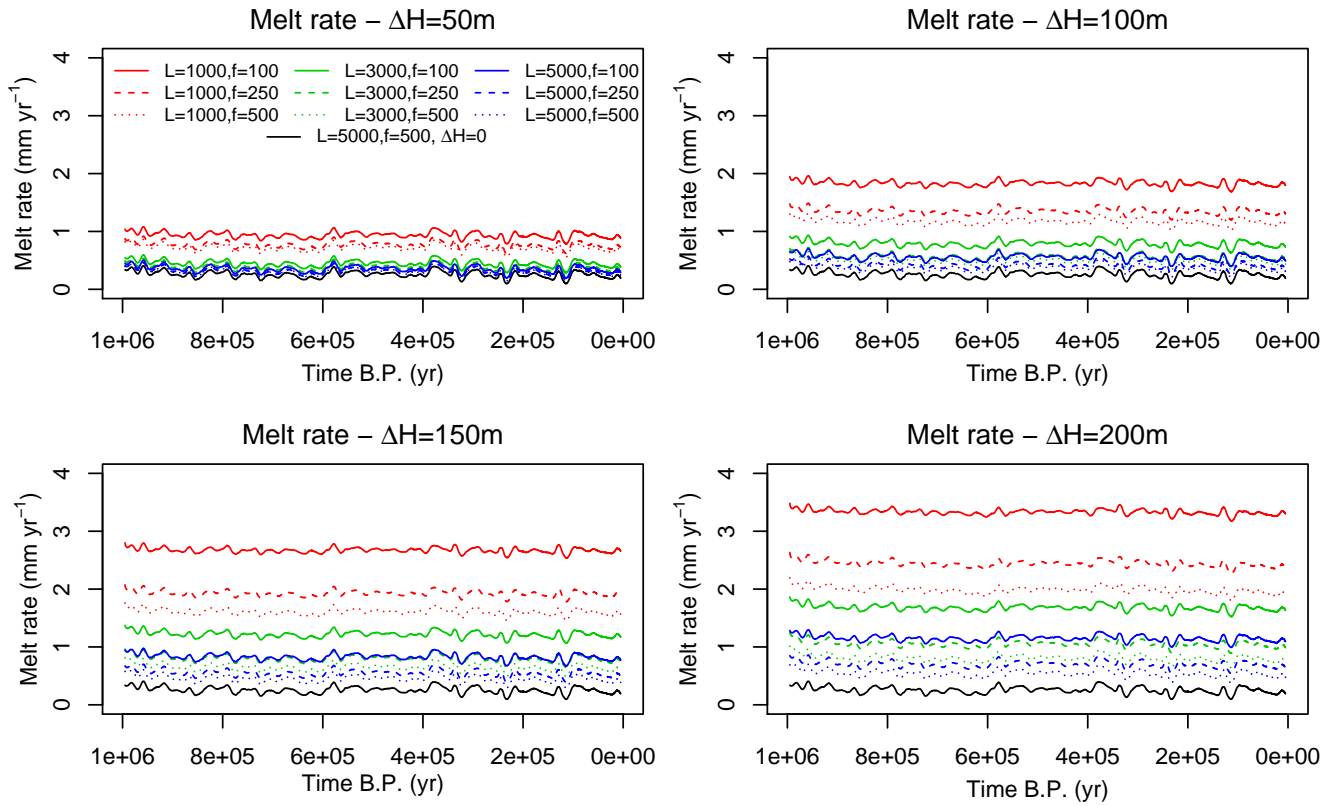
Figure 2.6: Effect of valley topography on melt rate history for different values of ΔH, L and f.

changes, the effect is of order $\sim 0.02°C$ and $\sim 0.15°C$. Thus only a 100 times increase factor gives observable impact on the temperature profile, but this amount of internal energy production seems quite unlikely.

Two runs are performed to separate the effect of compaction heat and deformation heat. The bottom part of the profile with compaction heat only is slightly colder. This is explained by the thermal expansion of the ice, i.e. the density decrease toward the ground and thus directly applying (1.17) leads to a negative compaction energy.

2.2.1.4 Sensitivity test summary

The three sets of sensitivity tests performed show some physically expectable outputs and provide evidence for some interesting behavior of the model. The firn density parametrization and thermal conductivity correction are major concerns for modeling the temperature and age profiles. In addition, bedrock topography can have a non-negligible influence on temperature and an important impact on the melt rate and thus determination of the ground heat flux. The form factor has a moderate impact on temperature and age profiles. The ground heat flux has really little impact on the temperature profile if there is some melting but, as expected, a large impact on melt rate. Finally, internal heat production, based on a equilibrium state ice divide model, has a really small influence.
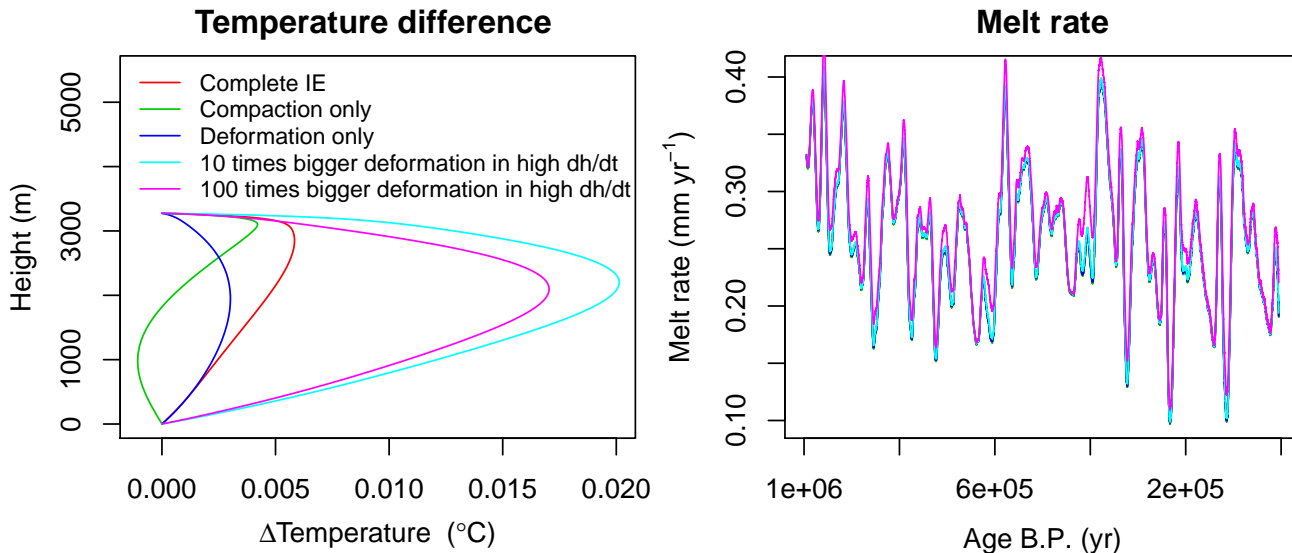
Figure 2.7:   Effect of internal energy production on temperature profiles (compared to a run without internal energy). The profile for the run with an increase by a factor 100 on deformation heat for period of high thickness change (purple line) is divided by 10 to fit to the temperature scale.

2.3   Different scheme comparison

The model is tested against the explicit and implicit scheme. First, the impact of the number of iterations in the Crank-Nicholson scheme is tested (as explained in detail in 1.3.3, parameters at $t + 1$ are not known, so multiple iterations can be performed using previous output to compute parameters at $t + 1$). For the whole section, the model is run with form factor m = 0.5 and $Q_G = 54$ mWm^{-2}.

Figure 2.8 shows the transient difference between 1 and 2 pass and between 2 and 3 pass for a C-N scheme. These runs are performed with internal energy production and valley effect. When the valley effect is not included, the difference between 1 and 2 pass is between −10 and +15 mK and the difference between 2 and 3 pass is of order ±1 mK.

The biggest difference observed when the valley effect is included is due to the fact that the lateral heat transport is computed using the mean of the temperature at the beginning of the time step and at the end of the time step (obtained from the previous pass). When only one pass is performed, only the temperature at the beginning of the time step is used, leading to a bigger gradient and thus a bigger heat flux.

Figure 2.8 right panel shows that two passes are sufficient. Indeed, additional passes increase the accuracy of order few mK only, far below the uncertainty due to boundary condition or physical parametrization of the ice sheet (see Section 2.2). Moreover, this figure shows that the difference due to pass number remains stable (with some oscillations) and is not producing a growing error.

Due to the valley error described above, to compare C-N with implicit and explicit scheme the valley effect must be turned off. Indeed, for the explicit formulation the extremely slow computation is prohibitive to make multiple passes while keeping a reasonable run time. It can be seen in Figure 2.9 that the three schemes agree quite well with the closest to the explicit output being the C-N scheme with $\theta = 0.6$. However, with $\theta = 0.6$ and smaller, some numerical oscillations appear
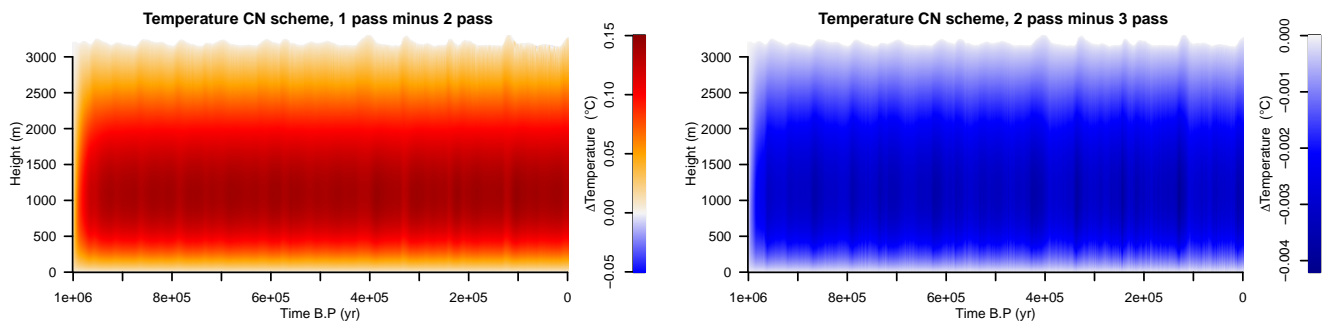
Figure 2.8: Left: Transient temperature difference between C-N scheme with one pass and two pass. Right: Transient temperature difference between C-N scheme with two pass and three pass. For both the valley effect is turned on with L = 5000 m, f = 500 m and ΔH = 100 m

.

at the surface, especially for recent periods. This is because the boundary condition time series are more highly resolved the closer we get to today and then exhibit a higher high frequency variability whereas back in time the time series are more smoothed (see Section 1.2). Coupled with the big time step used (100 yr), small θ values, i.e. bigger share of the explicit part in the C-N scheme, produces the oscillations shown in Figure 2.9 first panel. When increasing the θ value, the numerical oscillations decrease but the error grows, as shown in the second and third panel of Figure 2.9, where the third panel with $\theta = 1$ corresponds to an implicit scheme. The best value of θ to have both small numerical oscillation and error is $\theta = 0.7$, this value will then be used in the model.

Note that only 1 Myr output is shown here, but when run for 4 Myr, the model output for the last 1Myr is exactly the same, showing that there is no growing error propagating in the C-N model compared to the explicit scheme.

When a second pass is included (Figure 2.9 last panel), the temperature output seems to be less good than with one pass only. Indeed in this case there is a bigger difference with respect to the explicit scheme.[1] Nevertheless, this is probably because the C-N 2 passes run is more accurate than the explicit scheme and the difference shown in the figure is actually more the error of the explicit scheme. Indeed, the C-N scheme is considered as more accurate because it uses surface temperature both at the beginning and end of the time step and has a more accurate melt rate computation. Moreover, in the explicit scheme all the physical variables are updated only every 100 kyr for computational time purpose (except temperature profile which has a time step of one day) there thus not a better temporal resolution in the explicit scheme.

2.4 Comparison with a simple steady state model

The model used in [Fi] offers a good comparison point. However, this model has several differences with the model developed in this thesis: it uses constant ice density (at 921 $\mathrm{kg\,m^{-3}}$), a simple formulation (1.8) for thermal conductivity, constant boundary conditions (set as the mean values for the last glacial) and no internal energy production. The ground heat flux is given and the melt rate is deduced from the basal heat flux balance required to have basal ice at the melting

---

[1] The difference between the 1 pass and 2 passes C-N scheme in these runs without valley effect is between –5 and +10 mK.
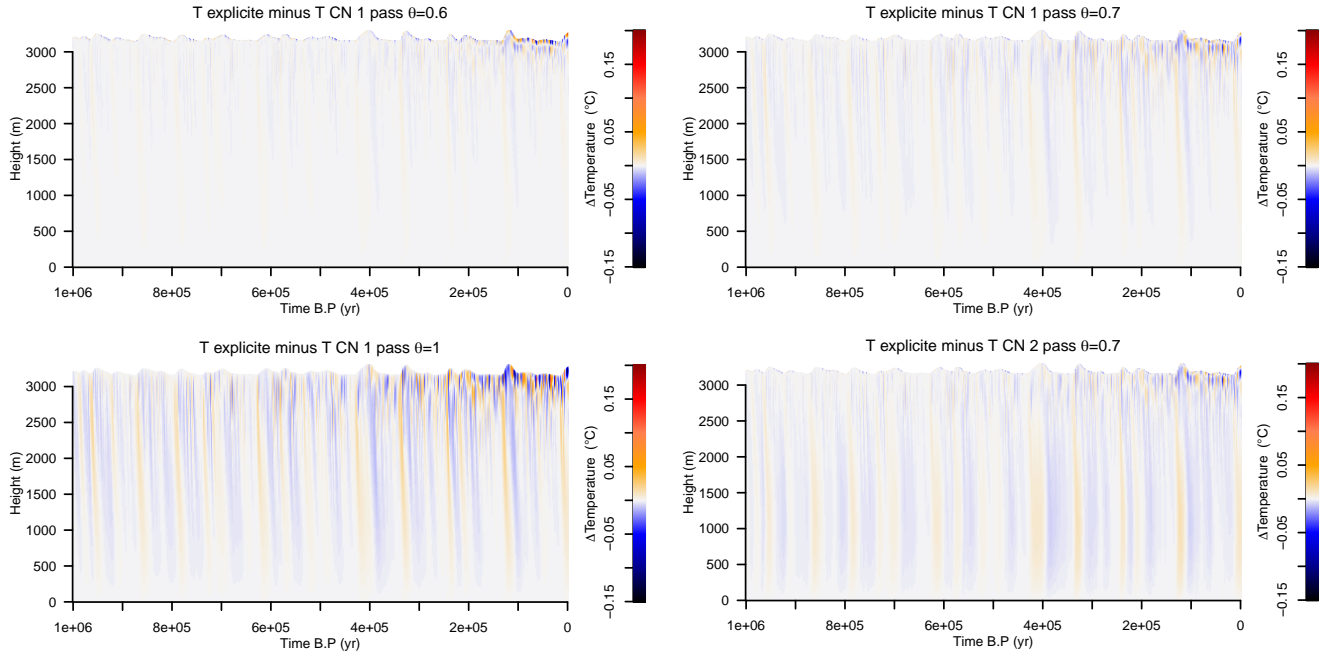
Figure 2.9:   Top left: Transient temperature difference between explicit and CN scheme with one pass and $\theta = 0.6$. Top right and bottom left: Same as top left but with $\theta = 0.7$ and $\theta = 1$ respectively. Bottom right: Same as top right but with 2 pass. For all the runs, no valley effect is taken into account
.

temperature. The model is run for 500kyr and if at the end the bottom temperature is bigger than the melting point, the melt rate is incremented and the model is run again until a bottom temperature smaller than the melting temperature is reached. Note that the flux shape function is (1.3) with m=0.5, and the age is obtained by numerical integration of $1/w$.

The model developed in this thesis easily can be tuned to reproduce the same physics, with the only difference being the melt rate calculation. This difference for the melt rate is not a problem, it is rather a strong coherence arguments for the two models if the final results are concordant.

Two runs have been accomplished with two different sets of boundary conditions:

1. Run 1: $H = 3151$ m, $Acc = 0.0191$ m ice eq yr^{-1}, $T_s = 213$ K and $Q_G = 59.4$ mWm^{-2}

2. Run 2: $H = 3000$ m, $Acc = 0.025$ m ice eq yr^{-1}, $T_s = 220$ K and $Q_G = 53.5$ mWm^{-2}

The temperature profile at the end of the run and the age depth relationship for the two models are compared in Figure 2.10. Note that Fischer's model is run for 500kyr whereas this thesis' model is run for 1Myr (because of the age model), but as shown in previous section, equilibrium is reached long before 500kyr, so this difference in run time has no effect on the final result.

The temperature profile produced by the two models are very similar (Figure 2.10 top panel). Note that the linear deviation between the surface and the bedrock, reaching 0.05K for run 1 and 0.04K for run 2, is due to the fact that Fischer's model use bottom temperature only for inversion that is not exactly set at T_M. The positive result is coherent with the fact that Fischer's model runs until getting a bottom temperature smaller than T_M. The relevant value for the comparison is then the spread of the points, which is of order 0.01K. It can then be concluded that the two model agree almost perfectly in temperature.

Regarding melt rate, the transient model obtains M=6.77 and M=3.98 mm yr^{-1} and [Fi] model M=6.7 and M=4.0 mmyr^{-1}. The higher value for the latter are perfectly coherent since they correspond to the first step above the value found by the transient model ([Fi] model increments the melt rate by 0.1 mm yr^{-1} per loop). This result shows that the more complicated melting formulation developed for the transient model is consistent with the simpler [Fi] melting formulation when applied in a steady state run.
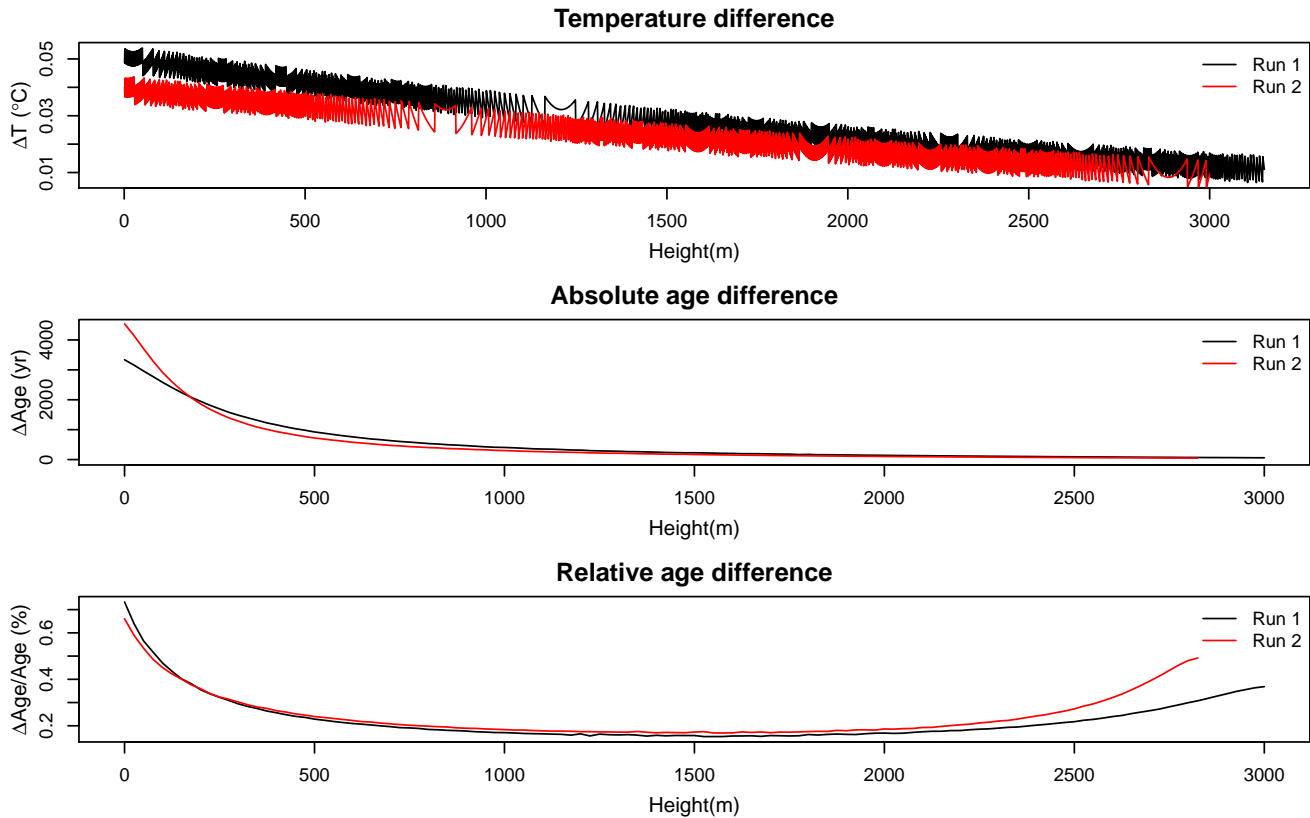
Figure 2.10: Top: Temperature output of the model developed for this thesis minus output of [Fi] model for the parameters given in the text. Middle and bottom: Comparison of age scale output of the model developed for this thesis with [Fi] model, for the parameters given in the text.

The two age models (Figure 2.10 middle panel and bottom) are also in a good agreement. The divergence on the right side of the bottom panel is artificial (due to the fact that relative value is plotted and age tends to zero at the surface. The closer we get to the ground, the more the melt rate becomes dominant in the age depth profile and the two profile starts to diverge (because of different M), but with a really reasonable difference (0.5% at the bottom).

In conclusion, the model developed for this thesis is fully coherent with [Fi] model when reduced to the same physics and boundary conditions.

2.5 Summary of chapter 2

In this chapter, the necessary spin up time has been established to 150 kyr. Several sensitivity tests have been performed and have shown the correct physical behavior of the model. It has been shown that the firn density parametrization and the related thermal conductivity correction are key information for modeling the temperature and age profile and, in addition, that bedrock

topography can have a non-negligible influence on temperature and an important impact on the melt rate, directly influencing the determination of the ground heat flux. The ground heat flux and the form factor values have the expected impact, whereas the internal heat production is shown to have a negligible influence on the model.

The different schemes of the model have been compared and is has been shown that the C-N scheme with $\theta = 0.7$ is reliable and is the best compromise between speed and accuracy. The importance of the second pass when the valley effect is present has been demonstrated. Finally, the model has been tested in simpler steady state conditions and has shown a really good agreement with the model used in [Fi].

Chapter 3

Application of the model and discussion

In this final chapter, the model is run for two sites, GRIP and Dome C, where the borehole temperatures have been measured and where other models exist for the age scale. The aim of the GRIP run is to solely validate the model, whereas the run at Dome C serves as a second validation and also is used to determine the value of the ground heat flux and the form factor for Dome C and its surroundings. In addition, sensitivity to boundary condition changes and eventual corrections for both GRIP and Dome C are discussed.

In the third part, the model is used to describe the ideal conditions for an oldest ice site. To do so, the model is run with the free parameters values and eventual boundary condition corrections found for Dome C, and with various values of the ice sheet thickness. The basal temperature and melt rate along with the ice age are discussed and the ideal thickness to find 1.5 Myr old ice is defined.

3.1   Experiment 1: Test at GRIP

The aim of the test at GRIP is mainly to validate the model by looking if it is able to reproduce the measured borehole temperature and to fit with another age-depth model using a ground heat-flux comparable to what is found in the literature. For this purpose, several runs are performed with different sets of boundary conditions.

An important reason to test the model at GRIP is that the ground heat flux has a total different influence than at EDC. Indeed, at EDC the ground temperature is fixed at the melting point and thus the ground heat flux mainly influences the age profile through melting. On the contrary, at GRIP the age profile is only determined by accumulation rate and thickness change and the ground heat flux only fixes ground temperature. When performing tests for other locations in Antarctica, the model will have to jump between melting and non-melting phases, it is thus important to perform a test as at GRIP to see how the model behaves without melting.

Note for the whole GRIP experiment, no hole effect or internal energy are taken into account. The model is spun-up during 150kyr and run for 100kyr.

3.1.1   Run 1: Using calculated accumulation rate

Several runs are performed with both Fischer's (1.3) and Parrenin's (1.4) flux shape functions, and with various values for the ground heat flux Q_G and the form factors m or p. The temperature and thickness used are the time series described in Section 1.2.3 and the accumulation rate is derived from (1.26).

Top panels of Figure 3.1 shows the results for the two velocity profiles (for each value of the form factor, only the ground heat flux value giving the best temperature profile is shown). For velocity as in (1.3) the best temperature fits are obtained with $0.6 < m < 0.7$ and $0.049 < Q_G < 0.050 \, \mathrm{W \, m^{-2}}$, and for velocity as in (1.4) the model gives $1.5 < m < 2$ and $0.049 < Q_G < 0.050 \, \mathrm{W \, m^{-2}}$. The values for Q_G are close to what is obtained in [D-J3] ($0.0513 \pm 0.0002 \, \mathrm{W \, m^{-2}}$) and in perfect agreement with [Joh] ($0.0497 \pm 0.0002 \, \mathrm{W \, m^{-2}}$ for models with dynamic thickness).

A first important indication is that the modelled temperature fits with the borehole temperature, meaning that the thermodynamics model is equivalent to [Joh] and [D-J3] models. The deviation of few tenth of degrees from borehole temperature for the best fits can easily be explained by the large uncertainty in the boundary condition time series.

However, when looking at age depth model (Figure 3.1 bottom panels), the ground heat flux and form factor values giving good temperature profile produce age profile clearly disagreeing with the GICC05modelext time scale, especially for Parrenin's flux shape function which disagree for all form factor values. Nevertheless, this result is somewhat expected since the boundary time series used is established by temperature inversion only and thus the obtained time series for temperature and accumulation rate do not match, *a priori*, with the age depth model. The age depth profile computation could have been used in [D-J3] as an additional criteria on all the acceptable scenarii they found for past surface temperature and accumulation rate to refine the selection, but this was not the case.

Regarding the age scale obtained in the model, note that the model can only compute age below 100 kyr (because the time series duration is 1 Myr) and is set to compute the age from 300 m above bedrock (with one point every 10 meters), whereas the GICC05modelext reaches 103 kyr and starts at 275 m above bedrock, explaining why the GICC05modelext line is longer in all the age plots.

3.1.2   Run 2: Using reconstructed accumulation rate

To get a better age depth profile, the model is run using accumulation from the GICC05modelext inversion as shown in Figure 1.16. In this case, for any form factor value a perfect fit for age is obviously obtained (Figure 3.2 bottom panels). Since the accumulation reconstruction (from GICC05modelext inversion presented in Section 1.2.3) and the age computation at the end of the model run by numerical integration of vertical velocity are totally independent, this result indicates that the numerical integration in the model to retrieve age is implemented correctly.

The reconstructed accumulation time series by GICC05modelext inversion used along with the temperature reconstructed by [D-J3] fails to accurately reproduce the borehole temperature record (Figure 3.2 top panels), but the difference is reasonable (few tenths of degrees) and is explained by the uncertainty in past temperatures. However, the form factor value used to get good fits (m = 0.8 and p = 0.5) corresponds to elevated past accumulation rate that can be considered
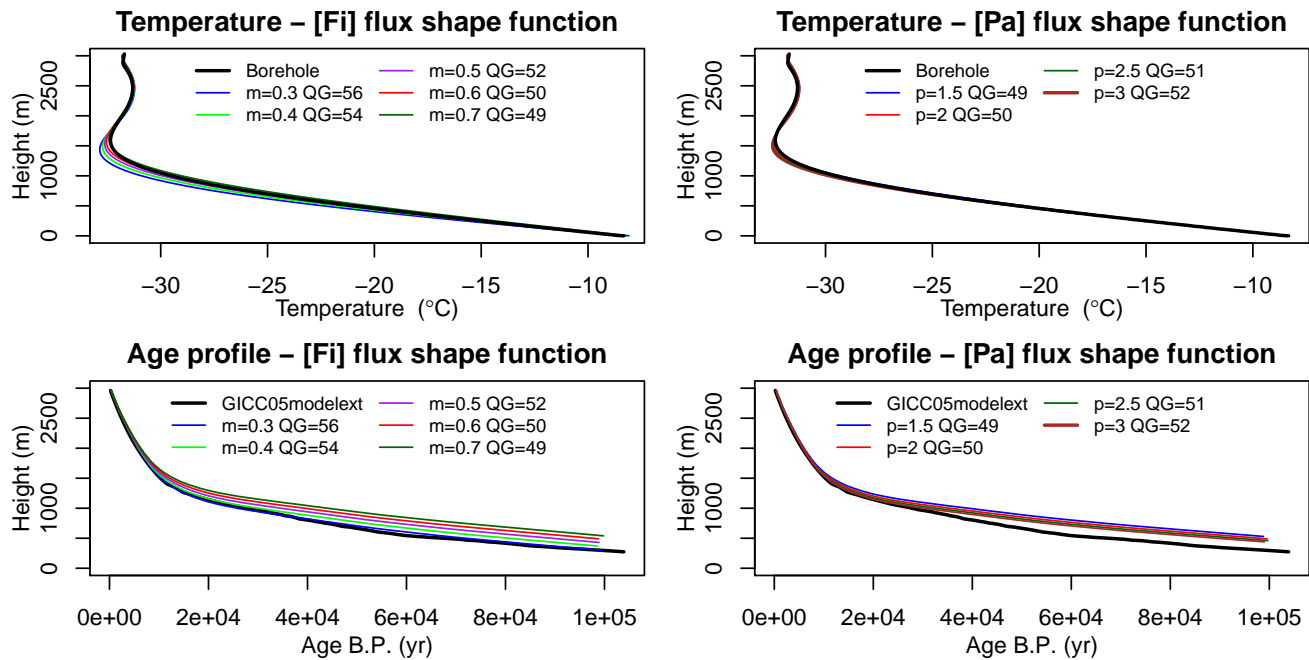
Figure 3.1:   Top: Borehole temperature measurement (black) and temperature profile obtained with Fischers's velocity (left) and Parrenin velocity (right) established accumulation rate from (1.26). Bottom: Idem for age depth model, with GICC05modelext in black. Coloured curves show output for the different form factor and ground heat flux (indicated in mWm^{-2})

as likely not realistic (see Figure 1.16). Moreover, the values obtained for Q_G are very high in comparison to the literature [Joh, D-J3].

Since all information from the age profile is lost when a reconstructed accumulation rate as used in this run, only the temperature profile remains to retrieve information. It becomes then more difficult to use the model to determine precisely the form factor. With Q_G being dependent on the chosen form factor, the same argument applies.

In summary, to establish the values of Q_G and m or p precisely, an accurate time series for accumulation rate is necessary and this time series needs to be independent of the form factor, i.e. not derived from the age model but from ice core analysis or from another proxy.

3.1.3   Run 3: Changing past temperature

To see if the model is able to reproduce both temperature and age profile with accumulation independent of the flux shape function, a third set of runs is performed using a surface temperature time series corresponding to the upper bound of the uncertainty range of [D-J3] temperature before 10 kyr B.P. (see Figure 1.16 left panel) and with accumulation computed from (1.26).

Results for temperature and age scale are shown in Figure 3.3. As with mean [D-J3] temperature, [Pa] flux shape function fails to reproduce the age depth profile. Moreover, the temperature profile does not match well with the borehole measurement. With [Fi] flux shape function, reasonable temperature profile and age scale are obtained with m = 0.4 and Q_G = 0.052 mWm^{-2} (exactly the same value as found in [D-J3]).

Temperature – [Fi] flux shape function

Temperature – [Pa] flux shape function

Age profile – [Fi] flux shape function

Age profile – [Pa] flux shape function
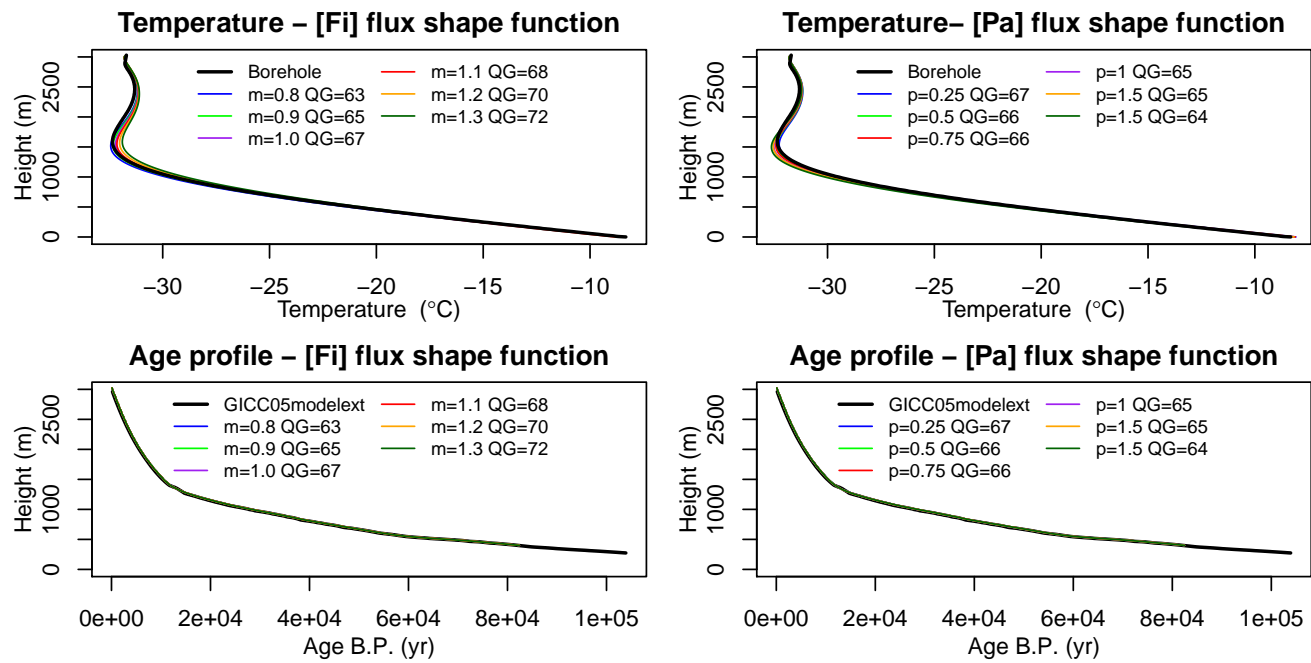
Figure 3.2: Top: Borehole temperature measurement (black) and temperature profile obtained with Fischers's velocity (left) and Parrenin velocity (right) established with reconstructed accumulation rate (using GICC05modelext age model). Bottom: Idem for age depth model, with GICC05modelext in black. Coloured curves show output for the different form factor and ground heat flux (indicated in mWm^{-2})

Temperature
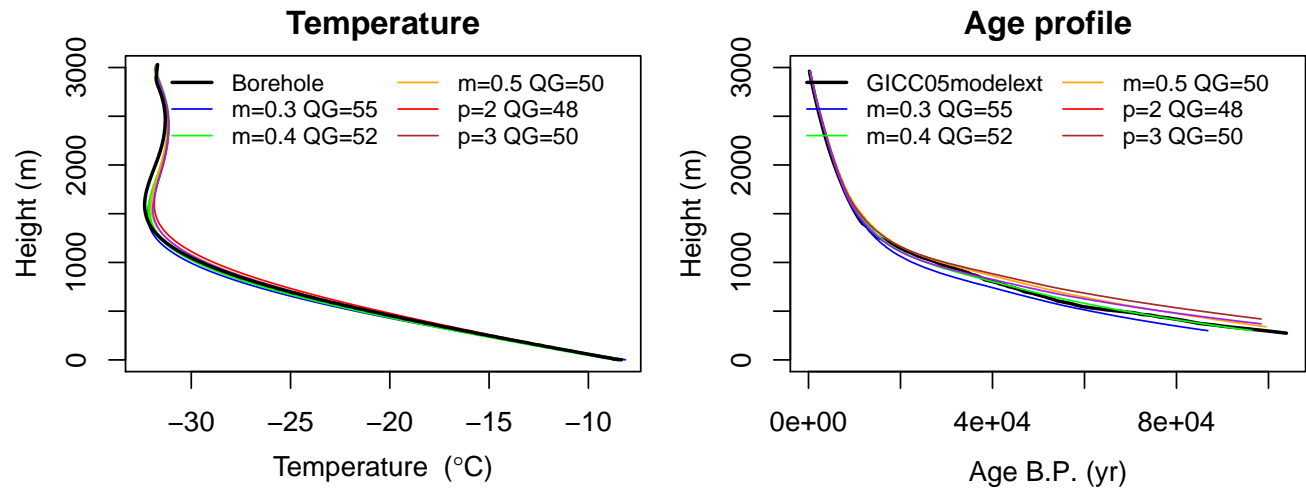
Age profile

Figure 3.3: Left: Borehole temperature measurement (black) and temperature profile obtained with [Fi] and [Pa] flux shape functions (indicated respectively by m and p in the legend) established accumulation rate from (1.26). Right: Idem for age depth model, with GICC05modelext in black. Coloured curves show output for the different form factor and ground heat flux (indicated in mWm^{-2})

3.1.4   Results of experiment 1

The three sets of runs performed for this experiment give important information on the model and its usage:

1. The first run shows that the heat transfer in the model is coherent with the [D-J3, Joh] model.

2. Results found for Q_G in the first and last runs are coherent with the values found in [D-J3, Joh]. It can then be deduced that ground heat flux is treated consistently in the model.

3. The perfect age scale obtained with reconstructed temperature in the second confirms the correctness of the age computation.

4. Runs 2 and 3 show that in order to establish more accurately Q_G and the form factor value, accumulation rate must stay independent of the form factor.

5. By testing additional time series for temperature, accumulation rate and ice thickness (all lying in the uncertainty range), this model can certainly produce a better output (e.g. with a Monte-Carlo approach as in [D-J3]).

In conclusion, this test at GRIP is a robust validation of the physics of the model, whereas the large uncertainty on past boundary condition do not allow an accurate definition of the form factor and heat ground heat flux (even if the values found for the ground heat flux are perfectly in agreement with the literature). Unfortunately, the vertical velocity model used in [Joh, D-J3] is not indicated, it is thus not possible to infer the validity of the values found for the form factor.

3.2   Experiment 2: Test at EDC

The purpose of this second experiment is to perform a second validation of the model and to define if the LR04EDC time series give adequate results and to determine the value of the ground heat flux and of the form factor for Dome C and its surrounding. These values will be used in the last experiments of this thesis. In addition, some corrections on the boundary conditions will be discussed.

Finally, the model is run at Dome C in a steady state mode with the mean values of the LR04EDC time series as boundary conditions and with parameters given in [Fi]. The aim is to infer if steady-state models can give adequate results and to discuss the transient behavior of the model.

3.2.1   Run 1: LR04EDC boundary condition

As for GRIP, the model is run with both Fischer's (1.3) and Parrenin's (1.4) velocity profile and various values for the free parameters Q_G, m or p, and ΔH. The surface temperature, accumulation rate, and ice thickness are the LR04EDC time series (see Section 1.2.1).

The internal energy contribution for both firn compaction and ice deformation are included. Figure 3.4) presents the difference between the borehole temperature record and age scale found in the literature (see Section 1.2.1.6) and the output of the model. In the figure, Q_G is ranging from 56 to 60 mWm^{-2} for [Pa] flux shape function and from 55 to 59 mWm^{-2} for [Fi] flux shape function. This corresponds to the range giving acceptable age scale. ΔH is equal to 0 or 100m (with L = 5000 m

and f = 500 m). On Figure 3.4 left panels, the two groups seen for each color correspond to the two values of ΔH, $\Delta H = 100$ being the warmer output, whereas on the right panels (age) ΔH does not have a significant impact. Regarding ground heat flux values, lower heat flux induces colder and older output (respectively lines on the left of left panels and on the top of right panels) and higher heat flux induces the opposite.

Although acceptable results can be obtained for the age scale modeled, the temperature profiles are too cold for all the combination of free parameters. As seen in Section 2.2, reasonable changes in the physical parameters of the model can not explain this temperature difference. A valley effect parametrized with L = 1000 m instead of L = 5000 m could produce a warm enough profile (see Section 2.2.1.3), but [Fo] suggests a really wider hole. Note that from [Fo] it is not clear whether the drill site is above a valley or an almost circular hole. Being above a hole would more or less double the lateral heat flux contribution, but Section 2.2.1.3 shows that the ΔH, f and L values used here would warm the profile by 0.2 K only. This is not enough to explain the difference observed in 2.2.1.3.

Regarding internal energy production, the hypothesis of a higher energy production during periods with high thickness variation (glaciation/deglaciation) is discussed in Section 2.2.1.3, but Figure 2.7 shows that an increase of a factor more than 100 of the deformation energy production during high thickness variation period is needed.

All the temperature outputs on Figure 3.4 are colder than the borehole measurement in the first few meters, then show a warmer peak and finally exhibit a colder difference for the main part of the profile. The difference in the upper part is due to the seasonal effect on the borehole temperature record. Indeed the field season takes place during summer and the temperature cold difference is present on the first 20 meters of the borehole record in agreement with what can be expected for seasonal variation [C.P]. The warmer peak (between 50 and 250 m deep) can be explained by the uncertainty in the boundary condition time series. At this depth, the ice temperature is mainly determined by the surface temperature occurring between 2 and 6 kyr B.P. With the time step used (100 yr), this represents only 40 points. If few of them correspond per chance to years slightly warmer than the average and since there is not a lot of time to diffuse the heat, this output of a few tenth of degrees warmer than borehole measurement is acceptable. Moreover, this peak could also be due to an overestimation of the heat generated by the firn compaction (see Figure 1.4).

A last information from Figure 3.4 is the output using free parameters values as obtained in [Pa][1] and [Fi]. In both cases, the temperature suffers from the same problem and the age is highly overestimated close to the bedrock. Moreover, the ground heat flux value obtained by [Fi] (53.5 mWm^{-2}) lies outside the acceptable range found with the transient model. Regarding the [Pa] model, this can be explained by the different accumulation rate computation and the fact that a constant basal melting is used in [Pa]. For [Fi], this result illustrates the impact of having a transient model versus a steady state one (see Section 3.2.3 for more details). Moreover, since [Pa] does not compare the temperature output to measurements and [Fi] obtains a temperature profile that is deviating from the borehole record (because it uses as surface temperature the mean value over the last glacial cycles), it is not too surprising that their result for free parameters does not produce good results when inserted in our transient model.

---

[1][Pa] does not give a value for the ground heat flux, but directly takes the basal melting as free parameter. The ground heat flux value giving a mean melt rate comparable to what is obtained by [Pa] is used, i.e. $Q_G = 57 \text{ mWm}^{-2}$ to get $\bar{M} \simeq 6 \text{ mm yr}^{-1}$.

In conclusion, the transient model developed for this thesis used with the LR04EDC time series clearly fails to reproduce the borehole temperature measured at Dome C, even when including some additional heat sources neglected in other models (i.e. internal energy and valley effect). As seen in section 2.2, changing physical parameters such as heat conduction by a reasonable amount can also not explain the too cold output of the transient model. This is why in the next Section changes in boundary condition time series are discussed.
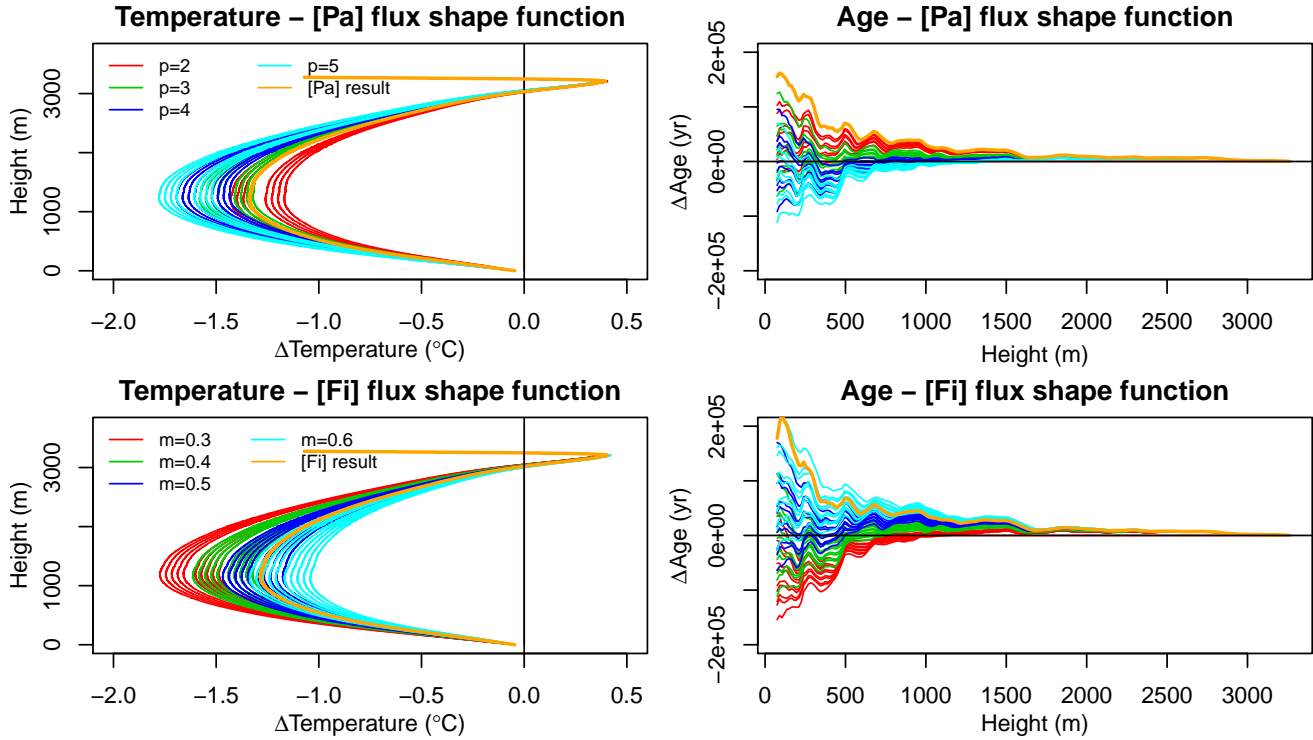
Figure 3.4: Left: Difference between the temperature profile obtained with the model and the borehole temperature record [Catherin Ritz, personal communication]. Positive values indicate that the model output is warmer than the measurements. Right: Difference between the age output of the model and the AICC2012 age scale. Positive values indicates older ice in the model. Top: Runs using the [Pa] flux shape function. Bottom: Runs using the [Fi] flux shape function. The colors indicate the different form factor values and the orange lines indicate the runs with free parameters values as in [Pa] (top) or as in [Fi] (bottom).

3.2.2   Run 2: Changing past temperature and accumulation rate

To obtain a better temperature profile, the model is run with a warmer temperature for past glacial periods. Since the [Fi] flux shape function produces slightly better temperature output (see Section 3.2.1), only this formulation is used here. More than 20'000 different combinations of free parameters and boundary condition corrections are tested.

The temperature correction can be implemented in two ways: either the temperature is shifted for the periods considered as cold periods[2], or the whole surface temperature time series can be linearly

---

[2] The periods considered as glacial are 15'000 to 110'000 yr B.P., 135'000 to 190'000 yr B.P., 220'000 to 235'000 yr B.P., 250'000 to 320'000 yr B.P., 340'000 to 390'000 yr B.P, 430'000 to 480'000 yr B.P., 530'000 to 560'000 yr B.P., 630'000 to 670'000 yr B.P., 740'000 to 760'000 yr B.P., 795'000 to 810'000 yr B.P., 870'000 to 930'000 yr B.P.

squeezed, maintaining the same temperature for today and adjusting the LGM temperature to a chosen value. Accumulation rate can either be recomputed using the corrected temperature time series and (1.25) or the LR04EDC accumulation rate time series can be used. To reduce the warm peak observed for the top hundreds meters on Figure 3.4, the surface temperature is reduced for the last 2 millenia. The time series obtained by changing only glacial temperature or squeezing the whole time series along with the accumulation rate re-computer from (1.25) are shown in Figure 3.5. Re-computing the accumulation rate leads to a substantial change compared to the LR04EDC time series.
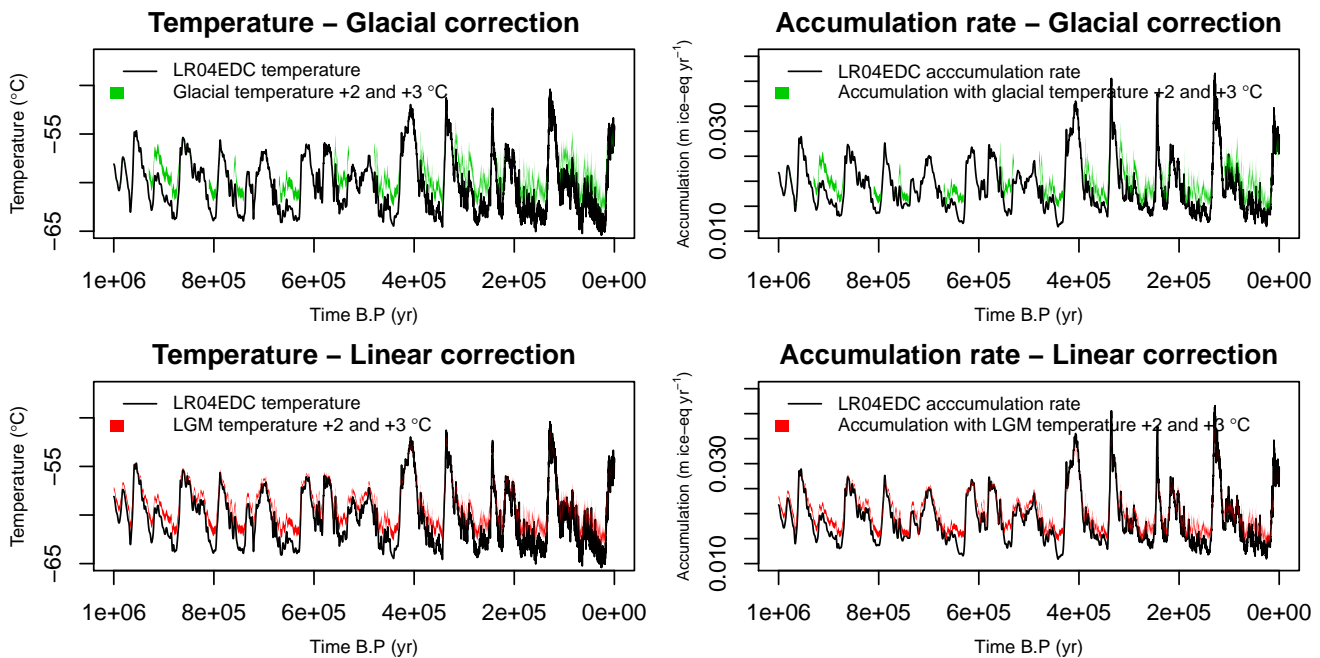
Figure 3.5: Example of boundary condition time series correction. All of them have a correction of −1°C for the last 2′000 yr. Top : Temperature and accumulation rate computed from (1.25) with a temperature correction between 2 and 3°C during glacial periods. Bottom: Temperature and accumulation rate computed from (1.25) with a temperature linear correction between 2 and 3°C for LGM and fixed today's temperature.

The four combinations of temperature and accumulation correction are tested and in every case accumulation rate needs an additional correction to give a reasonable age scale. The results for the four combinations are shown in Appendix C. The best temperature profile and age scale are obtained by using a surface temperature time series corrected only for the glacial periods and with the LR04EDC time series slightly increased for the accumulation rate, this combination of corrections is then used, but the linear temperature squeezing correction gives also good output and similar values for the free parameters.

Tables 3.1 and 3.2 and Figure 3.6 present the values of acceptable free parameters as well as the output of the model. Figure 3.7 shows the corresponding time series for boundary conditions. Note: for this section and the next one, age scale is always shown between 75 m above bedrock and the surface, i.e. the depth covered by actual Dome C ice core.

The values found for Q_G, M and m are perfectly in agreement with [Fi] (and with [Pa] for M[3])

---

[3]And in to extent for m. Indeed, the values of p found in [Pa1] (1.5<p<2.5) give flux shape function really close to 0.45<m<0.5, see Figure 1.1.
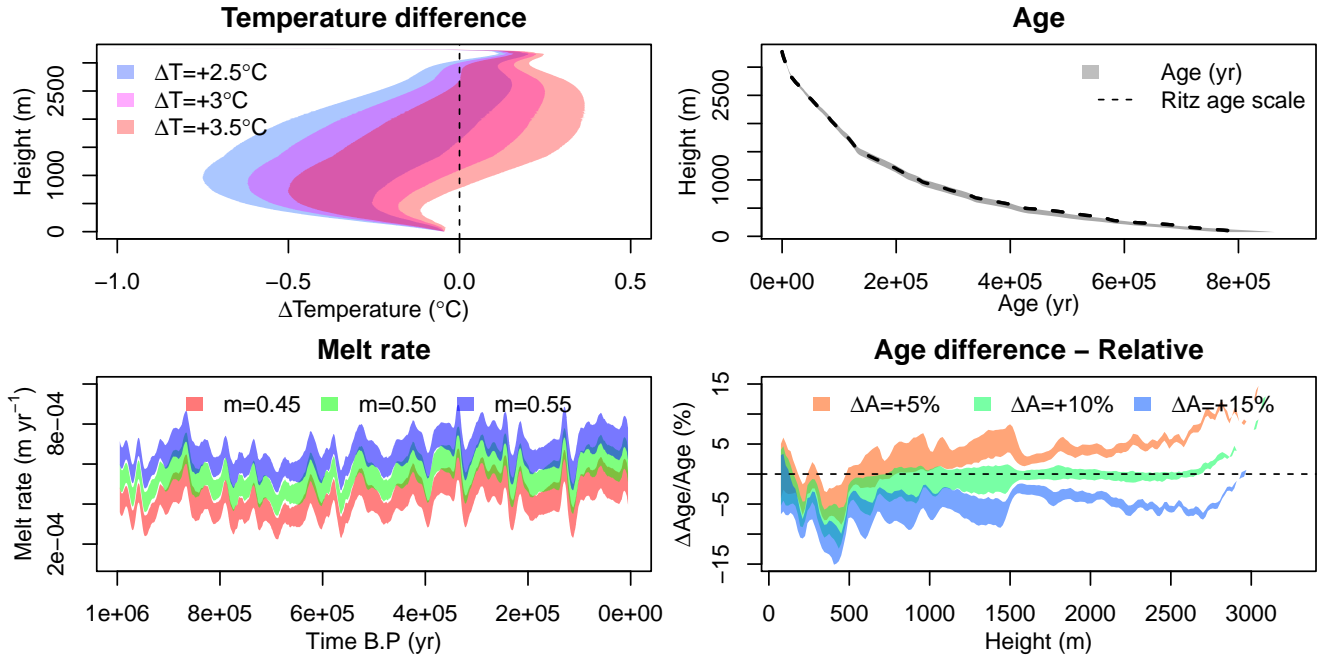
Figure 3.6: Best output obtained for Dome C. For each variable shown (except the age scale), the values of the free parameter having the most important impact on this variable are shown. Top left: Temperature difference between model output and Catherine Ritz borehole record [personal communication]. Colors indicate different glacial temperature corrections. Bottom left: Melt rate. Colors indicate different values for the form factor. Top right: Age output of the model for different values of the free parameters (gray shade) and AICC2012 age scale [Baz, Ve] (dashed line). Bottom right: Relative difference between age output of the model and Catherine Ritz age scale, colors indicate different values of the accumulation rate correction.

Table 3.1: Range of cold period temperature correction ΔT, accumulation rate correction ΔA and valley width L giving acceptable output for Dome C with value for form factor and ground heat flux as in Table 3.2.

ΔT (K)	ΔA (%)	L (m)
$\in (+2.5, +3.5)$	$\in (+5, +15)$	$\in (3000, 5000)$

Table 3.2: Value of the ground heat flux Q_G for the different accepted values of the form factor m and valley width L.

m	L	Q_G (mWm^{-2})
0.45	3000	52
0.45	5000	53
0.50	3000	53
0.50	5000	54
0.55	3000	54
0.55	5000	55

and the correction in accumulation rate is acceptable since there is an important uncertainty on past accumulation rate.

The correction made on the boundary condition time series can be considered as real changes on the past temperature and accumulation rate, or as mathematical corrections to replace some unknown processes happening at Dome C that are not described in the model. Additional discussion on these corrections take place in the Section Summary and additional consideration at the end of this work.

In spite of the need for some corrections to the boundary condition time series, the output of this run is considered as the best output for Dome C achievable with the 1D transient model developed here. Indeed, in the previous experiment (see Section 3.2.1) and in the sensitivity test performed in the second chapter, all other attempts made to reduce the difference observed for the temperature profile have failed. Consequently, the best values for the corrections of the time series and for the free parameters found in this experiment and presented in Tables 3.1 and 3.2 are considered as the relevant value for Dome C and will be used for the study of potential oldest ice sites in Section 3.3.
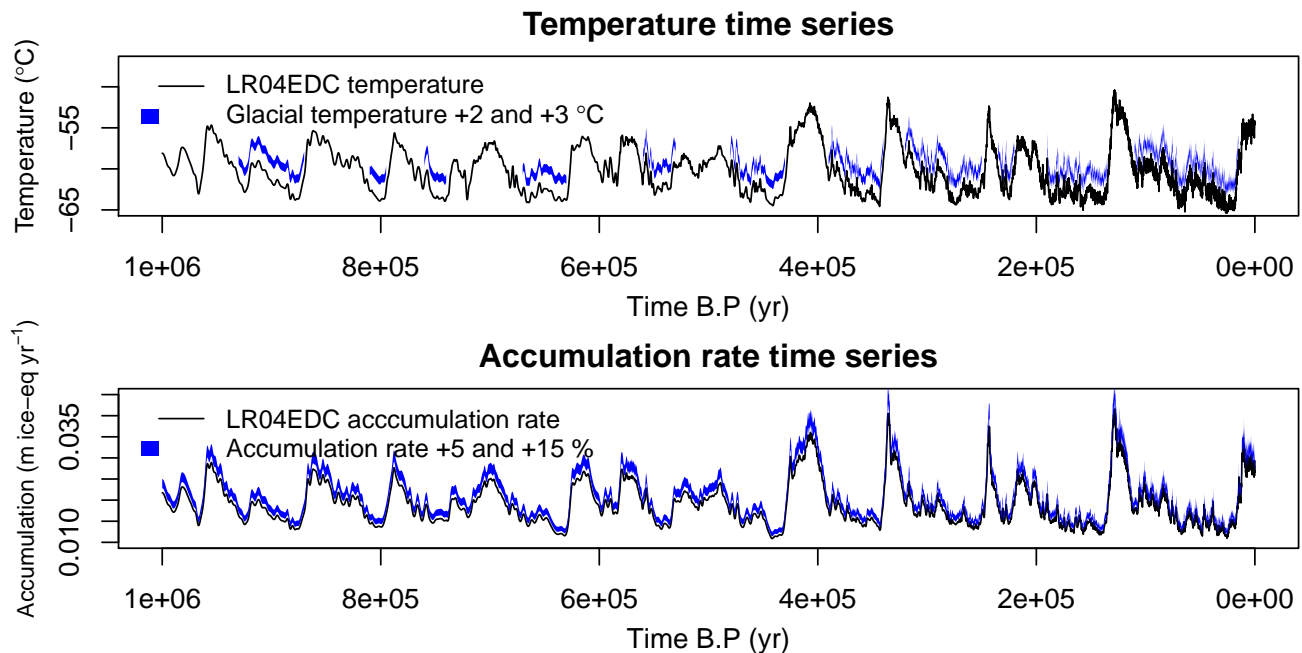
Figure 3.7: Corrected time series used for Dome C run. The blue areas represent the LR04EDC temperature time series corrected by values between +2 and +3°C for glacial periods (as defined in footnote 2) and the LR04EDC accumulation rate time series with a correction of +5 to +15 %.

3.2.3   Run 3: Transient behavior of the model

The aim of this run is first compare the transient model with the steady state model described in [Fi] and second to infer how the use of transient boundary condition influences the output of the model, especially the melt rate.

The model is ran with [Fi] boundary condition for accumulation rate (A = 0.0191 m ice-eq yr^{-1}), surface temperature (T$_S$ = 213 K) and ice thickness (H = 3151 m ice-eq) with constant density,

and using [Fi] value for free parameters ($Q_G = 53.5$ mWm^{-2}, m $= 0.5$). Four runs are performed: one with and one without valley effect ($\Delta H = 100$ m and L $= 3000$ m), the third one with valley effect and with transient thickness, and the fourth with [Fi] boundary conditions, no valley effect, but with K and c constant over the entire ice column, computed for an ice at melting temperature (this is how [Fi] obtains the best results). Boundary conditions values used in [Fi] are very close to the mean of the LR04EDC time series over the last million of years ($\bar{A} = 0.01905$ m ice-eq yr^{-1} and $\bar{T}_S = 212.96$ K for LR04EDC). The output is compared with a run using LR04EDC corrected and non-corrected boundary condition, and using $Q_G = 53$ mWm^{-2}, m $= 0.5$, $\Delta H = 100$ m, and L $= 3000$ m. For the corrected LR04EDC run, $\Delta T = 3°$C and $\Delta A = +10\%$ are used.

The comparison for borehole temperature, melt rate, and age scale is shown in Figure 3.8. In the first panel, [Fi] boundary condition runs with K and c computed with real ice temperature suffers the same problem as the non-corrected LR04EDC runs, i.e. the bottom part of the temperature record is too cold compared to the berohole record (the upper part of [Fi] is too cold due to the usage of mean value for surface temperature).

As expected, the [Fi] run with valley effect and transient thickness agrees quite well with non-corrected LR04EDC for age-scale, showing that mean accumulation rate can be used without losing too much accuracy. Nevertheless, when constant thickness is used the melt rate drops down, leading to much higher basal ice age. This is due to the zero value of $\frac{\partial H}{\partial T}$ in the vertical velocity computation, which biases the age scale computation.
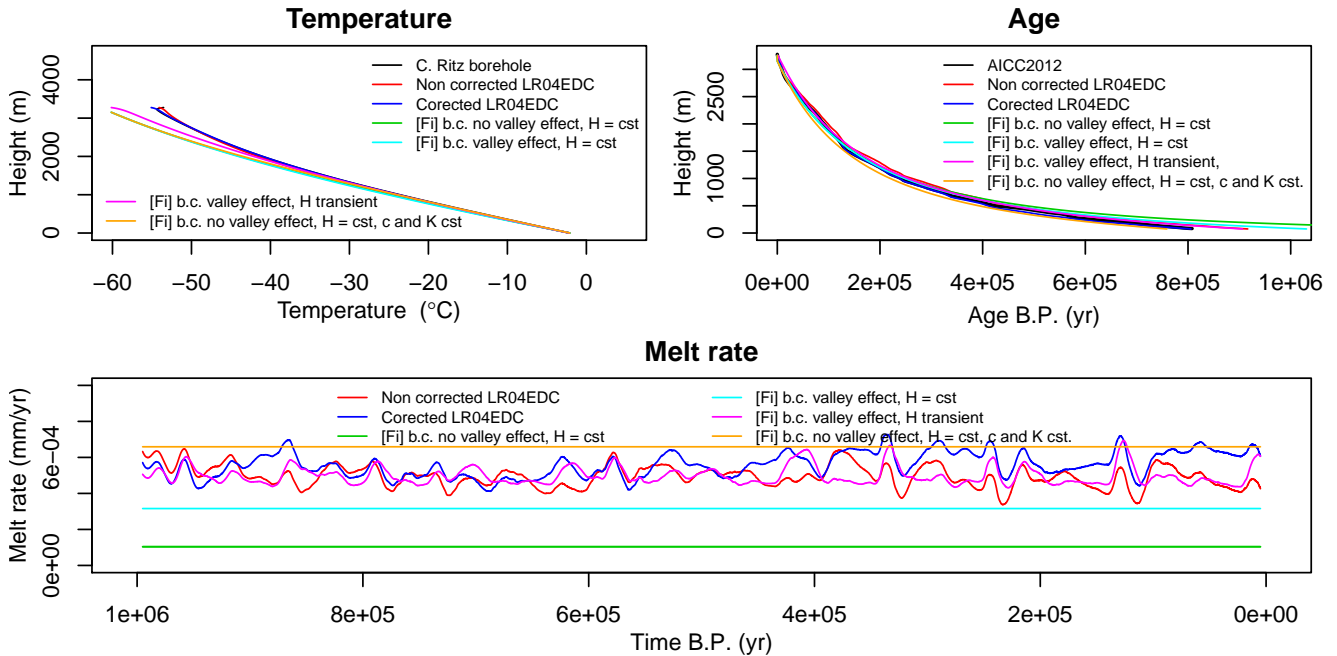
Figure 3.8: Comparison of runs for temperature (top-left), age scale (top-right) and melt rate (bottom) using LR04EDC corrected and non corrected and [Fi] boundary conditions. The orange line represent the best output shown in [Fi].

All [Fi] runs with temperature dependent K and c and the non-corrected LR04EDC run overestimate the basal ice age. This is due to a temperature gradient too high close to the bedrock (see first panel) leading to a basal melting too low (see lower panel). The temperature correction on LR04EDC leads to a correct temperature profile and thus a correct gradient close to the

bedrock[4].In [Fi], the temperature gradient issue is tackled by using a constant thermal conductivity K and heat capacity c computed using melting ice temperature (orange line in Figure 3.8). The output with corrected c and K and [Fi] boundary conditions slightly overestimate the melt rate and thus underestimate the basal ice age[5], as shown in second and third panels of Figure 3.8. In both cases the correction is quite unphysical but the two outputs agree quite well ([Fi] requires $Q_G = 53.5$ mWm^{-2} and M = 6.68 and the transient model $52 < Q_G < 55$ mWm^{-2} and $3.8 < M < 7.3$mmyr^{-1} in general and $52 < Q_G < 55$ mWm^{-2} and $3.8 < M < 7.3$mmyr^{-1} for m = 0.5). Nevertheless, [Fi] runs with transient thickness or constant thickness, show that the use of transient boundary condition has an impact on the result. Furthermore, the fact that [Fi] values for Q_G, M and m are in the accepted range of the transient model does not mean that both models are equivalent. Indeed, by adjusting Q_G and M and correcting past temperature or K it is always possible to get an age scale in agreement with AICC2012.

In Figures 3.9 and 3.10, the transient behavior of the model for Dome C is shown. Eight runs are performed with $Q_G = 53$ mWm^{-2}, m = 0.5, $\Delta H = 100$ m and L = 3000 m and all of the eight combinations of transient or constant mean values for T_S, A and H. The corrected LR04EDC with $\Delta T = 3°C$ and $\Delta A = +10\%$ is used. In the temperature profile, the largest impact comes from the use of transient or constant values for T_S (left and right branch on Figure 3.9 first panel). The two vertical sub-branches correspond to runs with transient or constant value for the ice thickness, changing today's thickness by few tens of meters. For the ice age, the main difference is found between the run with transient and the run with constant thickness, showing that the use of mean accumulation rate only cancels the few irregularities of the curve but does not impact the bottom ice age. The difference observed when thickness is constant or not is of order $25'000$yr and is in the uncertainty range of the model output. This difference occurs because the use of a constant thickness value cancels all the $\frac{\partial H}{\partial t}$ information. Since the thickness is different at the beginning and at then end of the time series, the mean of $\frac{\partial H}{\partial t}$ is not equal to zero. Moreover, the thickness derivative is weighted by the flux shape function in the vertical velocity formulation (1.2). When integrating the velocity profile to retrieve the age scale, $\frac{\partial H}{\partial t}$ is thus expected to have an influence even if its mean value over time is zero.

Figure 3.10 illustrates the effect of the different boundary condition time series on melting. First, the temperature increase during warm periods reaches the bottom and then influences the melt rate after few tens of thousands of years. Next, the ice slowly cools down and the melt rate decreases. It can be observed that the Holocene warm temperatures have not reached the bottom yet. The influence of accumulation rate and ice thickness changes are, as expected, more direct since they directly influence the vertical velocity function used in this model. For accumulation, the peak observed during warm periods leads to lower melt rate values because higher downward velocity means a bigger cold flux to the ground. For $\frac{\partial H}{\partial t}$, the situation is the opposite because it has a negative influence on the vertical velocity in (1.2). A comparison of middle and lower panels of Figure 3.10 shows that the three boundary conditions have an important impact on melt rate. Indeed, if temperature and accumulation seem to induce a greater variability on the melt rate than thickness changes (middle panel), they partially cancel when combined and $\frac{\partial H}{\partial t}$ remains an

---

[4]Changes in accumulation rate value have little impact on melting (see bottom panels of Figure 3.6) and, therefore, basal age. The main influence of accumulation rate on the age scale is above 250 meters above bedrock, as predicted by (1.2).

[5]Using his model, [Fi] finds M = 0.66 mm yr^{-1}. When [Fi] boundary condition, K and c are used in the model being developed here, the obtained melt rate is M = 0.659 mm yr^{-1}, showing once more the ability of the C model to reproduce [Fi] outputs.
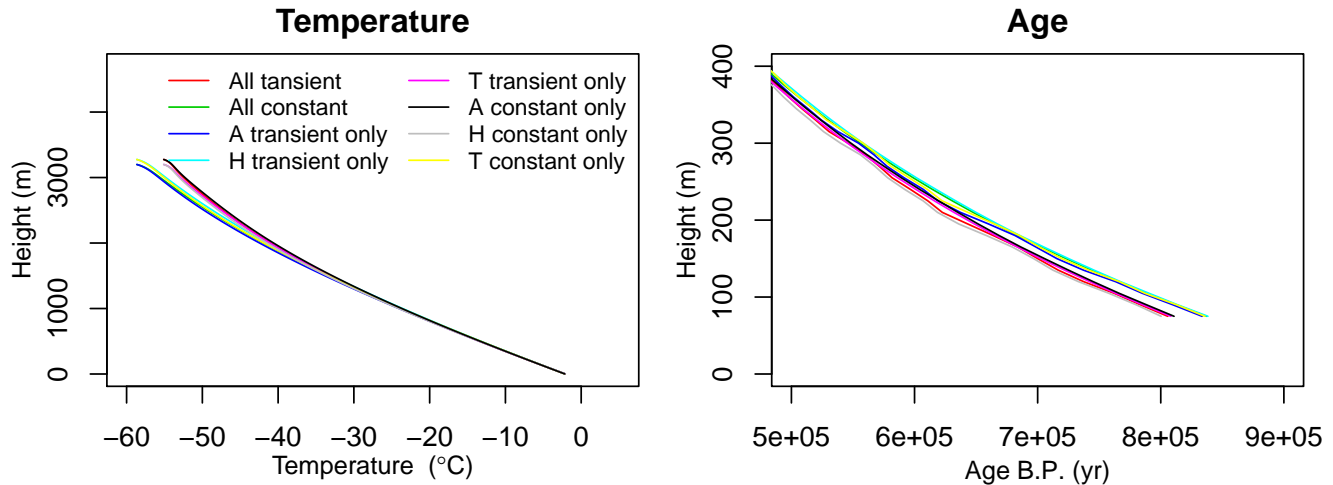
Figure 3.9:   Temperature (left panel) and age scale (right panel) for different runs with the boundary conditions for surface temperature, accumulation rate and ice thickness being the corrected LR04EDC transient values or the constant mean of corrected LR04EDC. Runs are performed with $Q_G = 53$ mWm^{-2}, m = 0.5, ΔT = 3°C, ΔA = +10%, ΔH = 100 m and L = 3000 m.

important parameter, explaining the difference shown in Figure 3.9 for age scale when a constant ice thickness is used.

In conclusion, steady state models give an output similar to the transient one for Dome C. At least, the difference is within the uncertainty range of the model. Moreover, the corrections used in the steady state [Fi] model also produce results similar to the LR04EDC corrected model (even if the age scale is slightly better for the transient model). Nevertheless, when the model enters some non-melting phases or when a longer time period is investigated, we believe that the transient model will be more accurate. This hypothesis is tested in the next section

3.2.4   Results of experiment 2

The three experiments done at Dome C have shown different aspects of the model:

1. The first run shows that the LR04EDC time series cannot reproduce the temperature profile for Dome C, despite the inclusion of the valley effect, the internal heat production and the firn conductivity correction. The age scale can be correctly reproduced but this requires a ground heat flux value greater than in the literature.

2. By changing the glacial temperature by 2.5 to 3.5°C and the accumulation rate by +5 to +15% both temperature and age scale can be nicely reproduced. The corresponding values for the free parameters are consistent with the literature.

3. When using mean values instead of transient boundary condition, the results are quite similar. Nevertheless, for runs over longer time periods we believe the transient model to be more reliable.

4. The reconstruction of age scale is slightly better than the result found in [Fi], whereas the temperature for the last hundreds meters above bedrock are similar (close to the surface [Fi] temperature is wrong due to the use of mean value).
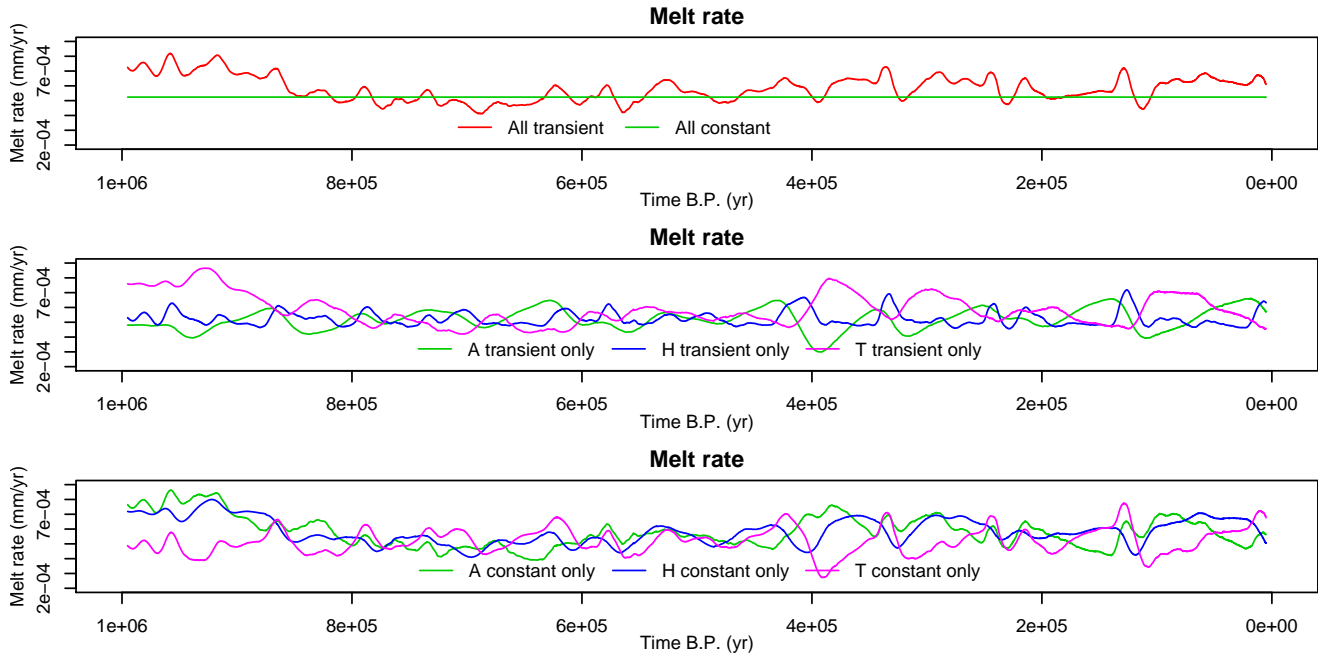
Figure 3.10: Melt rate for different runs with time series boundary condition for surface temperature, accumulation rate, and ice thickness being the corrected LR04EDC transient values or mean values. The upper panel shows run with all the boundary condition being transient or constant, the middle panel shows runs with only one boundary condition being transient whereas the last panel shows runs with only one boundary condition being kept constant to its mean value. Runs performed with $Q_G = 53$ mWm^{-2}, m = 0.5, ΔT = 3°C, ΔA = +10%, ΔH = 100 m, and L = 3000 m.

5. Constant [Fi] boundary conditions produce temperature profiles suffering from the same problem than the temperature profiles obtained with the transient model using the non-corrected LR04EDC time series: the bottom temperature is too cold and the vertical temperature gradient is wrong. Nevertheless [Fi] uses another way to solve this problem : c and K are computed using constant temperature ($\sim$ 270K), which gives a good temperature profile for the bottom part.

6. Both surface temperature, accumulation rate and ice thickness changes have an important influence on melt rate.

In conclusion, the results obtained for Dome C are mixed. Indeed, with the normal LR04EDC boundary conditions the model fails to produce a reasonable temperature profile. Since the main influence on the temperature profile arises from the last glacial period and the Holocene, and since temperature records for these two periods are quite accurate, a correction of order 2.5 to 3.5°C is quite unlikely. Nevertheless, the values found for the free parameters with the corrections on the boundary condition are consistent with the literature. Some additional remarks on this temperature issue are given in the Section Summary and additional considerations.

3.3   Experiment 3: Oldest ice

For this last experiment, the model is used to find a potential *oldest ice* site. This site is considered to have the same past condition as Dome C, i.e. the same time series for accumulation rate and surface temperature, but a smaller ice thickness. Nevertheless, the thickness variations over time are the same as at Dome C. The time series for thickness is then the LR04EDC time series minus a constant value ranging from 100 m to 1000 m. The free parameters m and Q_G are considered to be also the same as those at Dome C. For this whole experiment, unless otherwise is specified the free parameter values used are the ones obtained with the corrected LR04EDC time series at Dome C (see Section 3.2.2). The values of the free parameters are given in Tables 3.1 and 3.2. Finally, since the drill site should be chosen over a flat bedrock, no valley effect is taken into account. Such a site is supposed to exist not too far from Dome C.

Two different vision exist for the ideal oldest ice site. It can be argued that little to no melting would be beneficial to ensure a free-to-move ice sheet (not frozen to bedrock) and thus avoid breaks, folding or general stratigraphic disturbances in the ice core column as observed in some ice cores [Al]. This melting should be as small as possible to avoid excessive loss of basal old ice. However, basal ice at the melting temperature is not ideal for gases retrieval because of the diffusion processes. From this point of view, an ice sheet frozen to bedrock with a basal temperature at most at –10°C is recommended [Be, Po]. These two different basal conditions are discussed in this experiment.

The previous experiment has shown that the best output for Dome C is obtained by transient runs with some correction on the LR04EDC times series. Nevertheless, runs with corrected mean LR04EDC values and the [Fi] model with correction on c and K give perfectly acceptable results. For this experiment, the first runs are performed with the corrected LR04EDC transient time series, *i.e* what we believe to be the boundary condition at Dome C, and the corresponding values for the free parameters found. The free parameters values taken are the ones found with a 5000 m wide valley at Dome C (measurements suggest that a 5000 m wide valley is more likely than 3000 m one [Fo]). Note that the LR04EDC corrections for temperature are not expanded back in time (see footnote 2), because at ~ 1 Myr before present the glacial periods start to be shorter and with a smaller temperature variability. Applying the +2.5 to +3.5°C temperature correction will then almost cancel the glacial cycles signal. The +5 to +15% accumulation rate correction is, however, kept for the whole time.

The second part of this experiment consists of runs with the uncorrected LR04EDC time series and with the mean value of the corrected LR04EDC time series, to infer the influence of the time series and of the usage of a transient model in the definition of the ideal oldest ice site.

Finally, the results are compared to the [Fi] model.

For this whole experiment the running time of the model is set to 4 Myr.

3.3.1   Corrected LR04EDC time series and Dome C free parameters

Several runs are performed with the correction on boundary conditions and the free parameters obtained from the Dome C experiment. Temperature corrections of 2.5 and 3.5°C and accumulation rate corrections of +5 to +15% are applied. Two form factor values are used, m = 0.45 with the corresponding ground heat flux of 53 mWm^2, and m = 0.55 with $Q_G = 55$ mWm^2 (see Tables 3.1

and 3.2).

The ice thickness is decreased by steps of 100 m from −100 m to −1000 m. The obtained temperature, melt rate, ice age profile, and ice age at 75 and 25 m above bedrock are presented in Figure 3.11.
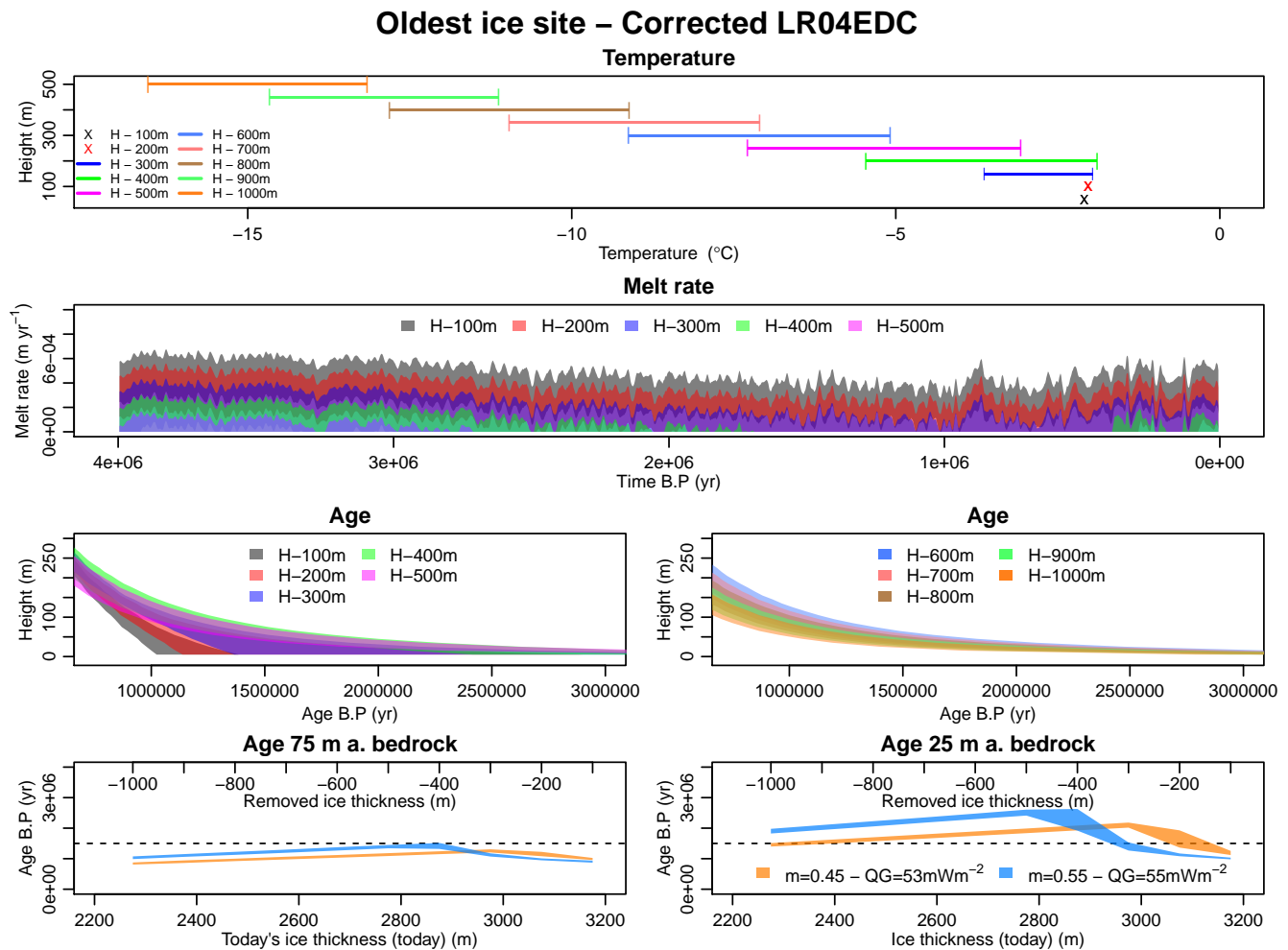
Figure 3.11: Output of the model for reduced ice sheet thickness, with boundary conditions and free parameters defined by Dome C experiment (see Section 3.2.2 and Tables 3.1 and 3.2). Top: Minimum and maximum basal temperature for various ice sheet thickness reduction (ice removed from the actual thickness value of 3275 m). Second line: Melt rate for various ice sheet thickness reduction. Only thickness reduction values giving some melting are shown. Third line: bottom of the age profile for ice thickness reduction from 100 to 500 m (left) and from 600 to 1000 m (right). Fourth line: Ice age at 75 m (left) and 25 m (right) above bedrock for the indicated couple of free parameters values for m and Q_G (which correspond to the boundaries of the accepted values for Dome C).

The first panel shows that for a thickness reduction of one or two hundred meters, the basal temperature for today is at melting point. Furthermore, for three and four hundreds meters removed, today's basal temperature might still be at the melting temperature but only for certain free parameters or boundary condition corrections values. For a removal of more than 400 m of ice, there is no chance for today's basal temperature to be at melting point. The first panel also shows the increase of the melting temperature as the ice thickness decreases due to pressure reduction.

The melt rate and age profiles show that from minus 200 m in ice sheet thickness compared to Dome C there is already a chance to have some non-melting periods in the last 2 Myr and that it

is unavoidable for a thickness reduction of 400 m and above. For minus 600 m and above, there is no melting at all for the last 4 Myr. The general decrease observed in melt rate between 4 Myr and 1 Myr before present is due to the decrease in mean surface temperature (see 1.8) whereas the increase in the last million of years is mainly due to the applied correction in glacial temperatures (see next Section for run without temperature correction).

The obtained age scale is shown in the last four panels of Figure 3.11. The two upper ones show that as soon as no melting is reached the bedrock ice becomes really old, whereas when still some melting is possible the bedrock ice age covers a large area of possible values. Nevertheless, when looking at some meters above bedrock (75 meters for bottom left panel and 25 meters for bottom right panel), this effect is less marked.

Some more details are important to understand the last two panels of Figure 3.11. For the first six panels, the values shown are always the interval between the minimum and maximum value obtained for the 8 runs (2 values for m[6], two values for ΔT and two values for ΔA, thus eight possible combinations). For the last two panels showing the ice age at respectively 75 and 25 meters above bedrock, the age for the two different values of m are shown separately, meaning that the area between the two curves represents also some possible values. The width of the lines features the influence of ΔT and ΔA on the age scale.

The dome shape of the curves is explained by the different phenomena contributing to reduce the ice age for a given depth. Since the ice sheet insulates the basal layers from the cold flux from the surface, a higher thickness induces an increase in the melt rate. This effect is reinforced by the decrease of the melting temperature as the basal pressure increases. As the thickness is reduced the melt rate decreases, which leads to an older ice age (right part of the peak), until reaching no melting (to be more precise: no melting over the whole time period corresponding to the basal ice age). This point is reached for an ice removal of $\sim 300 - 400$ m. When there is no melting at all (left part of the peak), the ice thickness by itself also explains the observed decrease in ice age because of the deformation of annual layers. Indeed, when comparing a thick and a thin ice sheet at a given height above bedrock, younger ice will be found in the thin ice sheet. The sum of these two contributions is minimal for an ice sheet thickness as close as possible to the thickness where some melting start to occur, explaining the position of the maximum observed in the figure.

The behavior of the blue and orange curves, corresponding to different values of m and Q_G, exhibit a difference on both sides of the maximum. For low thickness, as explained the dominant factor is the thinning. As shown in Figure 1.1, smaller values for the form factor produce a steeper velocity curve near bedrock and thus more compressed annual layers, which explains why the ice is younger for m = 0.45 than for m = 0.55. Note that at low thickness there is no melting at all, so Q_G has no influence. As the thickness increases, the age maximum is reached. This maximum does not correspond to the same thickness for the two curves. This is simply due to the different values of Q_G: for the blue curve Q_G is bigger, meaning that the melting will still occur at lower thickness than for the orange curve. On the right side of the peak, the higher ground heat flux values also explain why the blue curve falls below the orange one.

A last effect is the small widening of the curves that can be observed at 25 m above bedrock. The wider areas correspond to thicknesses at which both partial melting, melting all the time, and no melting can coexist depending on the value of ΔT and ΔP, leading to the observed difference on ice age for a given thickness reduction.

---

[6] Q_G depends on the m value, see Table 3.2.

The three effects mentioned above (presence of a maximum, behavior of the age depending on the values of Q_G and m, and widening of the curves) are more pronounced at 25 m than at 75 m above bedrock. This shows that when searching for old ice, thus drilling close to bedrock, there is a high sensitivity of the ice age to the different parameters describing the ice sheet. It is interesting to observe that the values of the free parameters has more influence than the uncertainty on the boundary condition time series for the ice age close to bedrock (difference between the two curves versus the width of the curves on the last two panels).

With the perspective of finding some 1.5 Myr old ice, important observations can be made from this experiment. First, at 75 m above bedrock, none of the outputs produce old enough ice. It is then needed to drill deeper. At 25 m above bedrock, an ice thickness reduction of 150 to 1000 m (depending on the value of the free parameters) compared to Dome C allows the retrieval of at least 1.5 Myr old ice, with the oldest ice obtained for an ice sheet with a thickness comprised between 2800 and 3000 m today. To ensure a permanent melting, the ice sheet should not be more than ~ 200 thinner than Dome C. Only few free parameter values are accepted to get 1.5 Myr old ice with this thickness. It can therefore be concluded that a site fulfilling the necessary conditions for having 1.5 Myr old ice at 25 m above bedrock along with an ice never frozen to bedrock in the last 1.5 Myr will likely not exist. If it is accepted to have an ice sheet that is, at least for some periods, frozen to bedrock, it would be advantageous to have a basal temperature at $\sim -10°C$ for a better gas conservation [Be, Po]. This could be achieved with an ice sheet ~ 750 m thinner than Dome C (see Figure 3.11 top panel), but in this case the ice would be just 1.5 Myr old at 25 m above bedrock depending on the free parameters values (Figure 3.11 bottom right panel).

The Figure shows that ice far older than 1.5 Myr would be found at such a site, with a maximum age of around 3 Myr. This maximum value is due to the increase of the melt rate between 2 and 3 Myr before present. However, 3 Myr old ice will likely not be usable for lab measurement. Indeed, between 75 and 25 m above bedrock, the ice age increases by ~ 1.5 Myr, meaning an annual layer thickness of ~ 0.01 mm for the layers at 25 m above bedrock and thus a temporal resolution of ~ 1 kyr with current laboratory equipment.

In conclusion, by using the boundary conditions corrected to fit to Dome C temperature and age scale record as well as the corresponding values for free parameters, a site with 1.5 Myr old ice between 75 and 25 m above bedrock will very likely exist. This site should ideally have an ice sheet thickness between 2800 and 3000 m. Nevertheless, such a site will likely not have the necessary conditions to have the ice never frozen to bedrock during the last 1.5 Myr, nor have basal ice at the ideal temperature for gas conservation. As seen in the previous experiments, the model is quite sensitive to the boundary condition and to the free parameters values. The robustness of these conclusions will therefore be tested in the next sections with runs using various boundary condition values and different parameterizations of the model.

3.3.2 Other time series and parametrization

3.3.2.1 Non-corrected LR04EDC conditions

In the second experiment of this thesis, is has been shown that the boundary condition time series have to be corrected to allow the model to reproduce the borehole temperature profile measured at Dome C. These corrections were considered as real changes on the boundary conditions and were therefore applied for the research of an oldest ice site in the first part of this experiment.

Nevertheless, these surface temperature and accumulation rate corrections can also be considered as artifact to reflect some unknown physical processes happening at Dome C and not included in the model[7]. In this case, one can imagine that the free parameters values found for Dome C are valid for the surrounding region, but that the time series correction may not apply because the un-described physical processes at Dome C do not exist for other sites. This is the hypothesis tested in this section; the model is run as in the previous section, but with the original LR04EDC time series.
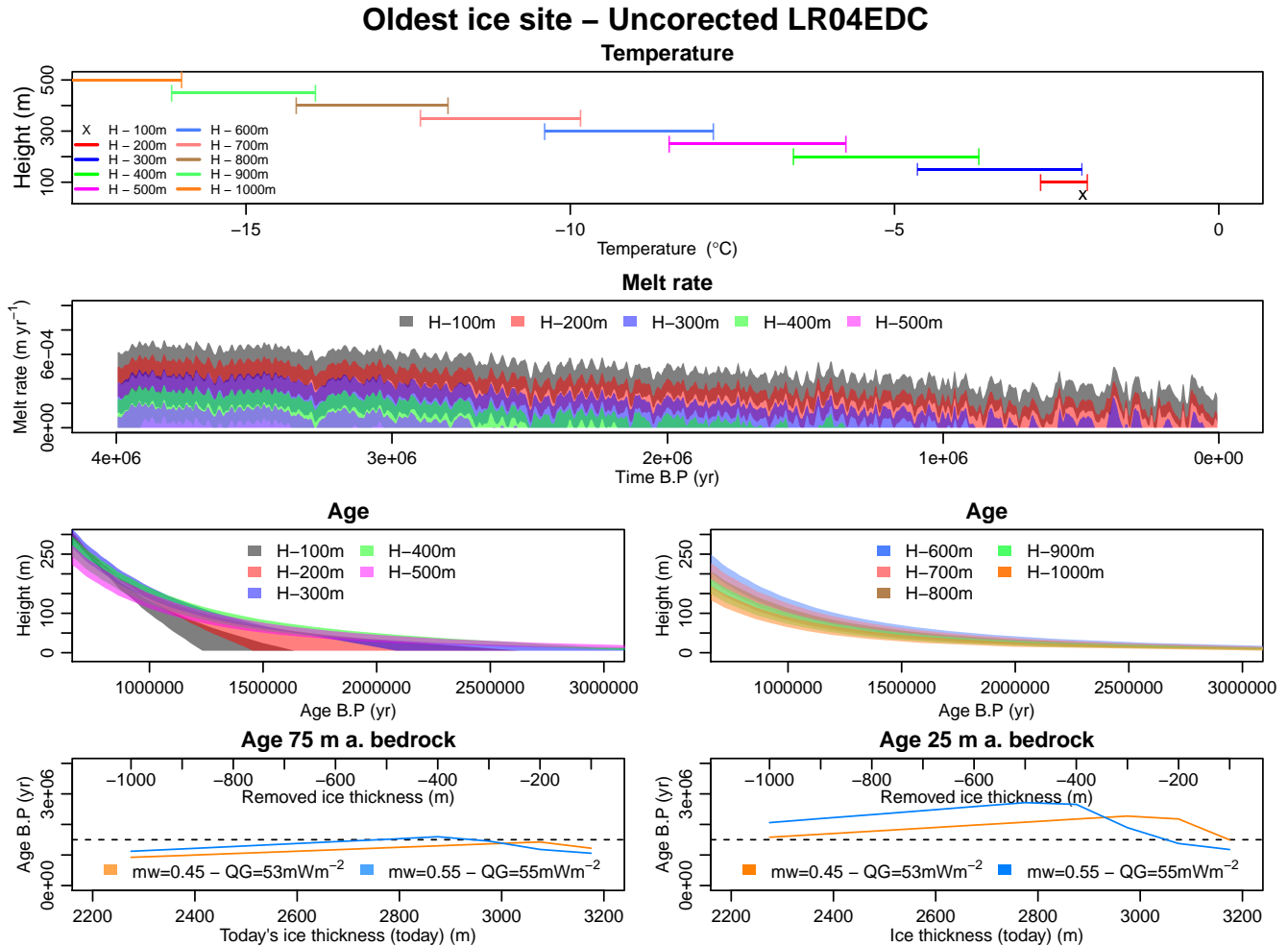
Figure 3.12: Same as Figure 3.11, but with the non corrected LR04EDC time series used for the boundary conditions.

The result is shown in Figure 3.12. By comparing it with the corrected LR04EDC run, it can clearly be seen that the correction on the surface temperature increases the melt rate in the last 1 Myr. Otherwise, this uncorrected run shows in general the same behavior as the corrected one. Due to the lower melt rate, the ice at 25 and 75 m above bedrock is a bit older and the bedrock ice is a bit colder. Moreover, with these boundary conditions, finding 1.5 Myr old ice at −10°C at 25 m above bedrock is more likely than with the corrected boundary conditions.

---

[7]Note that this model already includes valley effect and internal heat production that are usually neglected in other models, as [Fi, Pa1]. Moreover, extensive time has been spent to try to find any other processes that could have an influence on the temperature profile, without success.

I conclusion, the main features observed by using the LR04EDC corrected or uncorrected time series are similar, especially the ideal thickness value.

3.3.2.2   Sensitivity to free parameters and accumulation rate

Since the boundary conditions required for Dome C have finally little effect on the research of the requirement for an oldest ice site, another important question is the effect of the free parameters. Indeed, the free parameters values are fixed at Dome C with the correction on the time series. But as shown in Section 3.2.1, if the uncorrected LR04EDC times series is used without correction at Dome C, the required ground heat flux to have a reasonable age scale is higher (55 to 59 mWm^{-2}). Although these values are not really likely, because they are obtained from a temperature profile having a wrong gradient, they will still be tested for a potential oldest ice site. Indeed, the spatial variability of the ground heat flux is not well known [S.R] and thus the ground heat flux at the oldest ice drill site is *a priori* not precisely known.

Along the same line, the model is tested for various values of the form factor and accumulation rate correction. The runs are performed with the following default parameters: the uncorrected LR04EDC time series, m = 0.5 and Q$_G$ = 55 mWm^{-2}. For the first run, the values of Q$_G$ range from 51 to 59 mWm^{-2}, increased by steps of 2 mWm^{-2}. For the second run, m takes the values of 0.4, 0.5, and 0.6. For the last run, the accumulation rate is corrected with ΔP = $\pm$10 and ΔP = $\pm$20%.

The results can be see in Figure 3.13. As expected, the main influence arises from ground heat flux values. If the ground heat flux exceed $\sim$ 56 mWm^{-2}, the ideal thickness to find 1.5 Myr old ice defined before (between 2800 and 3000 m) does not hold anymore. Indeed, with high Q$_G$ values there is still some melting at such thickness. In this case, thinner ice sheet should be preferred. Regarding form factor, the effect described in Section 3.3.1 is well illustrated. The form factor has really low influence on the age when there is still important melting and the influence appears when the ice is most of the time frozen to bedrock. Note that the form factor itself, by governing downward cold flux, has an influence on the position of this transition. For thickness leading to ice sheet frozen to bedrock, higher form factor values lead to older ice for a given depth, because higher form factor values produce less compressed basal layers. Finally, for a change of order –10% to +20% in the accumulation rate time series, there is not a big influence on the required thickness to find 1.5 Myr old ice. An accumulation rate reduction of –20% and more might lead to too young ice at the targeted 2800 and 3000 m thickness. However, the second Dome C experiment suggests that the LR04EDC underestimates the accumulation rate (see Section 3.2.2), thus a reduction of –20% is really unlikely. In summary, it is not expected to have too much problems due to the accumulation rate correction for a potential oldest ice site determination, which is an important point since accumulation rate history is subject to non negligible uncertainty.

In conclusion, the parameters that could potentially be the most problematic, and should thus be known as precisely as possible, is the ground heat flux value. The first Dome C experiment shows that some corrections are needed for the temperature gradient at the bottom of the ice sheet (see Section 3.2.1). Unfortunately, melt rate and thus age are determined by both the temperature gradient and the ground heat flux. In consequence, this gradient issue directly influences the value obtained for Q$_G$ since it is determined by comparison with the age profile, meaning that there is not a high confidence in this result. Nevertheless, the values found in the literature for Q$_G$ range from 53 to 57 mWm^{-2} [Fi, Pa], perfectly in agreement with what is found with this model. To take
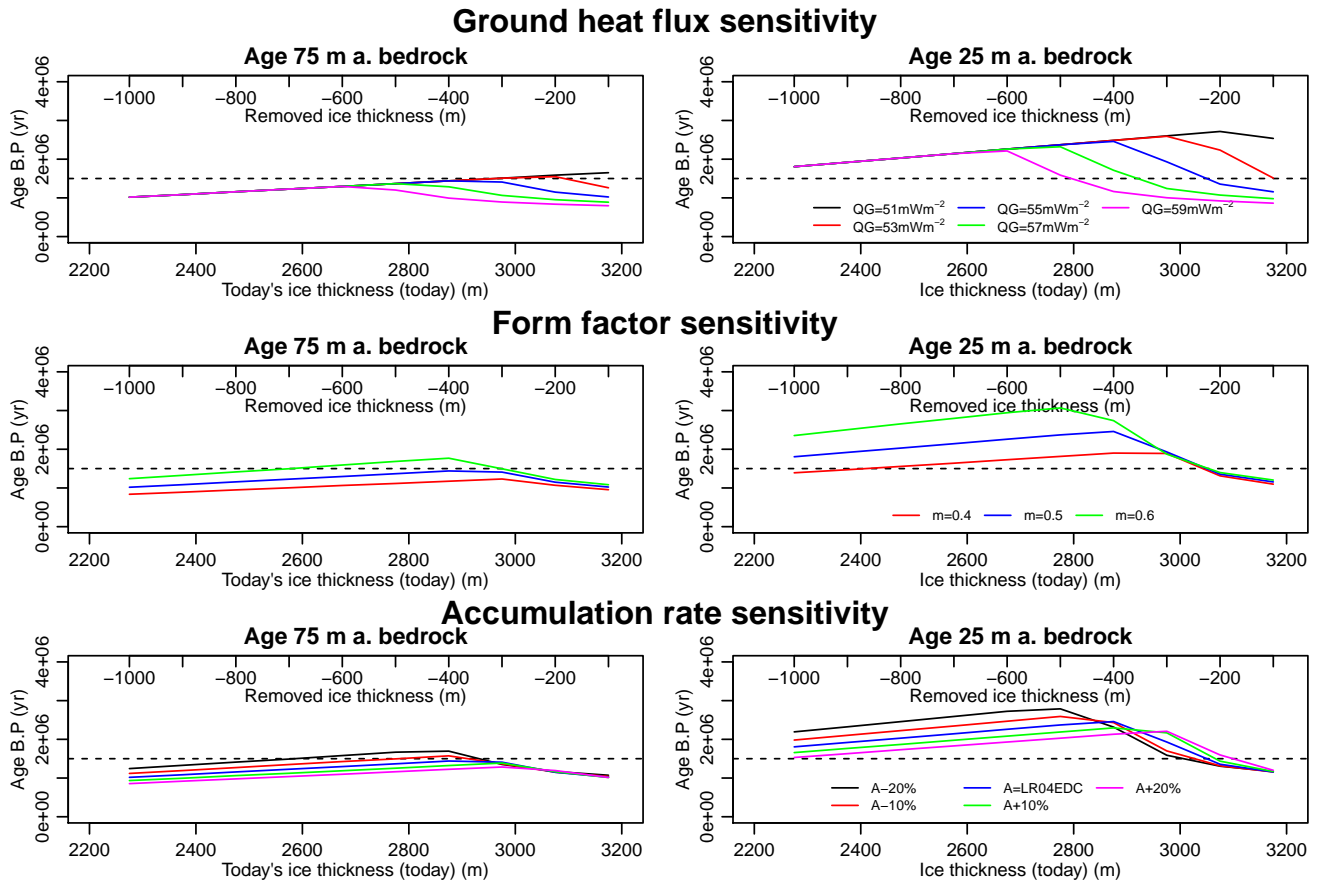
Figure 3.13: Ice age at 75 (left) and 25 (right) meters above bedrock for various ice sheet today thicknesses. Top: Age for different values of the ground heat flux Q_G. Middle: Age for different values of the form factor m. Bottom: Age for different correction of the accumulation rate time series. The default parameters are the uncorrected LR04EDC time series, m = 0.5 and Q_G = 55 mWm^{-2}.

Table 3.3: Mean values of the corrected LR04EDC time series (with $\Delta T = +3°C$ for recent glacial periods and $\Delta A = +10\%$) taken over 3 different time periods.

Mean last 1 Myr	Mean last 1.5 Myr	Mean last 2 Myr
$\bar{T}_s = 214.46°C$	$\bar{T}_s = 214.54°C$	$\bar{T}_s = 214.72°C$
$\bar{H} = 3198$ m	$\bar{H} = 3204$ m	$\bar{H} = 3209$ m
$\bar{A} = 0.0210 \, \mathrm{m \, yr^{-1}}$	$\bar{A} = 0.0218 \, \mathrm{m \, yr^{-1}}$	$\bar{A} = 0.0225 \, \mathrm{m \, yr^{-1}}$

into account this uncertainty on the ground heat flux, the ideal thickness is redefined to thicknesses between 2750 and 2950 m. This might lead to the loss of some resolution for the annual layers, but increases the likelihood of finding 1.5 Myr old ice.

3.3.3 Constant boundary condition runs

To conclude this research for an oldest ice drill site, runs are performed using constant boundary conditions instead of transient ones. For Dome C, the results obtained with steady state runs were acceptable. When reducing thickness, however, the model jumps between phases of positive or zero melting, and in this case steady state models might give wrong results. This is the question addressed in this Section.

Note that for this section, to allow a comparison with previous plots, all the age plots are made with respect to the thickness the ice would have today if the model were transient. Indeed, if the mean value is used for the thickness, its value is always ~ 100 m smaller than today's thickness for a transient time series with the same mean value. To make the age plots comparable with the ones from the previous sections, the thickness value plotted is set to 3275 minus the value subtracted to the thickness used in the run.

3.3.3.1 Mean LR04EDC

The first test is performed by using the mean value of the corrected LR04EDC time series boundary conditions. The time series is corrected with $\Delta T = +3°C$ for recent glacial periods and $\Delta A = +10\%$. The mean is taken over the last 1 Myr, 1.5 Myr and 2 Myr (see values in Table 3.3). The free parameters used are m = 0.5 and $Q_G = 54 \mathrm{mWm^{-2}}$. A transient run with the same correction on boundary conditions and free parameters values is performed to be compared with. The results are shown in Figure 3.14.

First of all, the time period chosen to take the mean of the boundary condition, ie between 1 and 2 Myr, has little influence (see line width in Figure 3.14) and this little uncertainty is far smaller than the one induced by the range of acceptable values for free parameters or the boundary condition corrections discussed above.

This run using constant values for boundary conditions exhibits less melting and thus older ice than the transient run. Moreover, since there is less melting, the transition to frozen ice sheet (peaks in bottom panels) is reached at higher thickness.

As already discussed in Section 3.2.3, there are two important features which disappear when using

a steady state model. Firstly, the influence of thickness change is lost. Despite the fact that the mean value of ice sheet thickness decreases during the last 2 Myr, today's value is higher than any value found between 1 and 2 Myr B.P (see Figure 1.11). There is thus a positive $\frac{\partial H}{\partial t}$ contribution in (1.2) for the transient model. Since increasing the value of $\frac{\partial H}{\partial t}$ has the same effect as lowering the accumulation rate (see (1.2)) and lowering the accumulation rate increases the melt rate (see Figure 3.13), the average effect of the disappearance of the thickness changes is a decrease in melt rate value. This partially explains why the steady state runs produce melting below the mean of the transient run (see Figure 3.14 top panel) and thus older ice (bottom panels).

The second effect is that when the transient model jumps between melting and non-melting phases, the steady state model can be *stuck* in a non-melting phase. This can be observed in the top panel of Figure 3.14 for a thickness reduction of 300 m. In this case, all the information from melt rate is lost and the ice age is overestimated.

The combination of these two effects leads to a general underestimation of the melt rate, explaining the difference seen in the bottom right panel of Figure 3.14 on the right part of the peak (i.e. the melting region). This will also change the thickness value at which the ice sheet is frozen to bedrock (peak position). An additional issue is the choice of the period taken for the mean values. It has been shown that taking the mean over the last 1, 1.5 or 2 Myr has not a great impact. Nevertheless, at 25 m above bedrock the ice might reach an age of 3 Myr and the LR04EDC time series values increase substantially between 2 and 3 Myr B.P.[8] (see Figure 1.11), making the determination of the period taken for the average a non-trivial question. Indeed, this period would be different for each thickness reduction value. A solution could be to use an iterative approach to determine the average periods to take.

In conclusion, even though the results obtained with a steady state model are not too far from what is obtained with a transient model, we would not recommend the usage of a steady state model for the purpose of defining an ideal location for an oldest ice drill site. Indeed, the usage of the steady state model adds an error of ~ 100 m on the upper acceptable thickness value. Moreover, the steady state model uses free parameter values defined by the transient model at Dome C. If the steady state model were used at Dome C, some additional error would arise from the definition of the free parameters values. Even though these errors might compensate (that seems to be the case here[9]), it is not recommended to accumulate errors. Finally, the choice of the period where the average of the boundary conditions should be taken starts to be problematic when searching for an oldest ice site. This could be tackled by the usage of an iterative approach, but in this case several successive runs of the model are required and thus the run time gained by the simplification of the model would mainly be lost.

3.3.3.2   Other steady state model

The results found so far for a potential oldest ice site – an ideal thickness between 2700 and 2900 m if the uncertainty on the ground heat flux value is taken into account and surface temperature and accumulation rate similar to Dome C conditions are used – are quite different to what is presented

---

[8]The mean values for the corrected LR04EDC over the last 3 Myr are: $\bar{T}_s = 215.49°C$, $\bar{H} = 3221$ m, and $\bar{A} = 0.0245$ m yr^{-1}

[9]Indeed, Figures 3.9 and 3.10 show that steady state runs also underestimate melt rate at Dome C. The value obtained for Q_G if a steady state model were used for the free parameters definition would then be slightly higher and thus partially compensate the melt rate underestimation for potential oldest ice site.
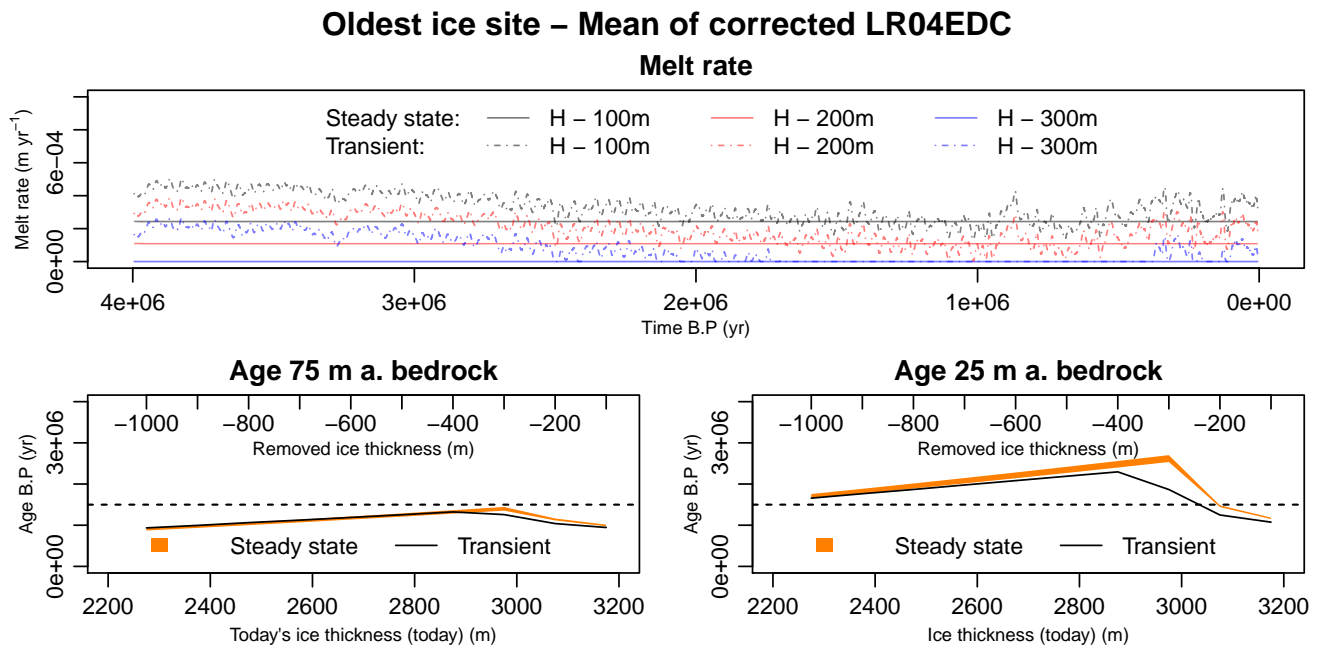
Figure 3.14: Melt rate and age profile at 75 and 25 m above bedrock for steady state runs and transient runs. The steady state runs use the mean values of the corrected LR04EDC time series as boundary condition and the transient ones use the corrected LR04EDC. The correction on the time series are $\Delta T = +3°C$ for recent glacial periods and $\Delta A = +10\%$. The free parameters used are m = 0.5 and $Q_G = 54 mWm^{-2}$. For the steady state runs, the intervals found for each value are the area spanned by three runs using mean value taken over different time period (see Table 3.3).

in [Fi]. Indeed, by using a steady state model [Fi] finds a peak position corresponding to a thickness of 2650 m (for $Q_G = 55$ mWm^{-2}, A = 0.2 mm yr^{-1}, and at 25 m above bedrock) and to ensure that no basal melting occurs recommend a thickness of 2500 m ice–equivalent. When the transient model is run in a steady state mode, the results are even further away from [Fi] result. In this last part it is explained why this difference occurs and why the model transient developed for this master, by having among other things a more reliable melt rate estimation, is an improvement with respect to the [Fi] model.

The model is set to [Fi] conditions (constant density, A = 0.0191 m ice-eq yr^{-1}, T_S = 213 K, H = 3151 m ice-eq and m = 0.5) and run with two values for the ground heat flux: $Q_G = 53.5$ and 55 mWm^{-2} ([Fi] finds 53.5 mWm^{-2} for Dome C but uses 55 mWm^{-2} for the oldest ice site). In addition, the model is ran with and without the correction on c and K. The output is shown in Figure 3.15.

The results for the corrected model are really similar to what is presented in [Fi]. Note that they might seem different but in [Fi] the plot are made using the mean value for the thickness (i.e. today thickness is 3151 m ice equivalent in [Fi]), whereas in this thesis the plots are made using the real thickness (3275 m). This explains the apparent ~ 125 m difference on the age plots with respect to the figures in [Fi]. The corrected [Fi] model gives clearly more melting, what was already observed for Dome C (see Figure 3.8). But when the ice sheet thickness is reduced, this effect becomes more important. If the correction on c and K is released (Figure 3.15 bottom panels), the melt rate clearly drops down and is slightly smaller to what is predicted by the transient model or the steady state model using the mean of the LR04EDC time series – again in agreement with the

results found by Dome C steady state experiment (see Section 3.2.3 and Figure 3.8) – leading to an overestimation on the ice age for high thickness values (see lower left panel).

For the [Fi] run without correction, the differences with the steady state model using the mean of the LR04EDC are due to the influence of the density profile. Indeed, the firn layer acts as an insulator and retains the cold from the surface to penetrate deeper in the ice sheet (see Section 2.2.1, in particular in Figure 2.2). By having no firn layer, the [Fi] model has a bigger cold flux and thus less melt rate, explaining the difference seen in the bottom panels of Figure 3.15 between uncorrected [Fi] model and mean LR04EDC model. Note that a part of the difference is also explained by the slight difference between the bondary conditions used by [Fi] and the mean of the uncorrected LR04EDC time series.

Regarding the corrected version of [Fi], the difference with regard to the transient model can also be explained. In the corrected [Fi] model using a constant value of 271 K to compute the thermal parameters, the value of the thermal conductivity K is smaller (see (1.8)) whereas the value of the specific heat capacity c is bigger (see (1.11)). Since the relation to temperature is exponential for K and linear for c, the dominant effect is expected to come from K. K being smaller over the entire ice column, the ice sheet will act as a thermal insulator. Close to bedrock, this will restrain the cold flux from the top. Since the melt rate is due to the difference between this cold flux and the ground heat flux, the melt rate is then bigger with the corrected K. For Dome C, this effect on the melt rate is similar to what is obtained by correcting the boundary conditions. But as we start to reduce thickness, the effects of the two different corrections diverge.

There are several arguments in favor of the correction used in this work with respect to [Fi] correction. The ice thermal conductivity dependence on temperature can be measured in laboratory [Sl] and is well known, there is thus no reason for the thermal conductivity to be computed with the melting temperature such as in [Fi]. On the other hand, the correction made to the LR04EDC time series, even though a $+3°C$ seems rather quite unlikely, are more acceptable. Moreover, when running the model for various thicknesses as in this experiment, releasing the correction on the boundary condition has not a too big impact on the result (see Figures 3.11 and 3.12) whereas the [Fi] correction has a huge impact (see Figure 3.15). Therefore, since the LR04EDC correction is less unlikely than the thermal conductivity one and since it has a lower impact on the model when changing the ice thickness, it can be concluded that this correction is more suited. Moreover, the good results found by our model at GRIP support its correctness. Finally, all the features arising from the usage of a transient model and the inclusion of a firn layer that is not present in [Fi] are additional reasons to support the results found by the transient model.

3.3.4　Results of experiment 3

This experiment, devoted to the research of some 1.5 Myr old ice, brings some important results:

1. A drill site allowing to retrieve 1.5 Myr old ice between 75 and 25 m above bedrock likely exists. Taking into account the uncertainty on the different parameters, such a site should have a similar climate history than Dome C, but a thickness comprised between 2750 and 2950 m today.

2. The requirements to have a basal temperature at around $-10°$ or to have some melting all the time, either to have as few gas diffusion as possible or to preserve the ice core stratigraphy, are hardly achievable if a reasonable security margin on age and on resolution wants to be
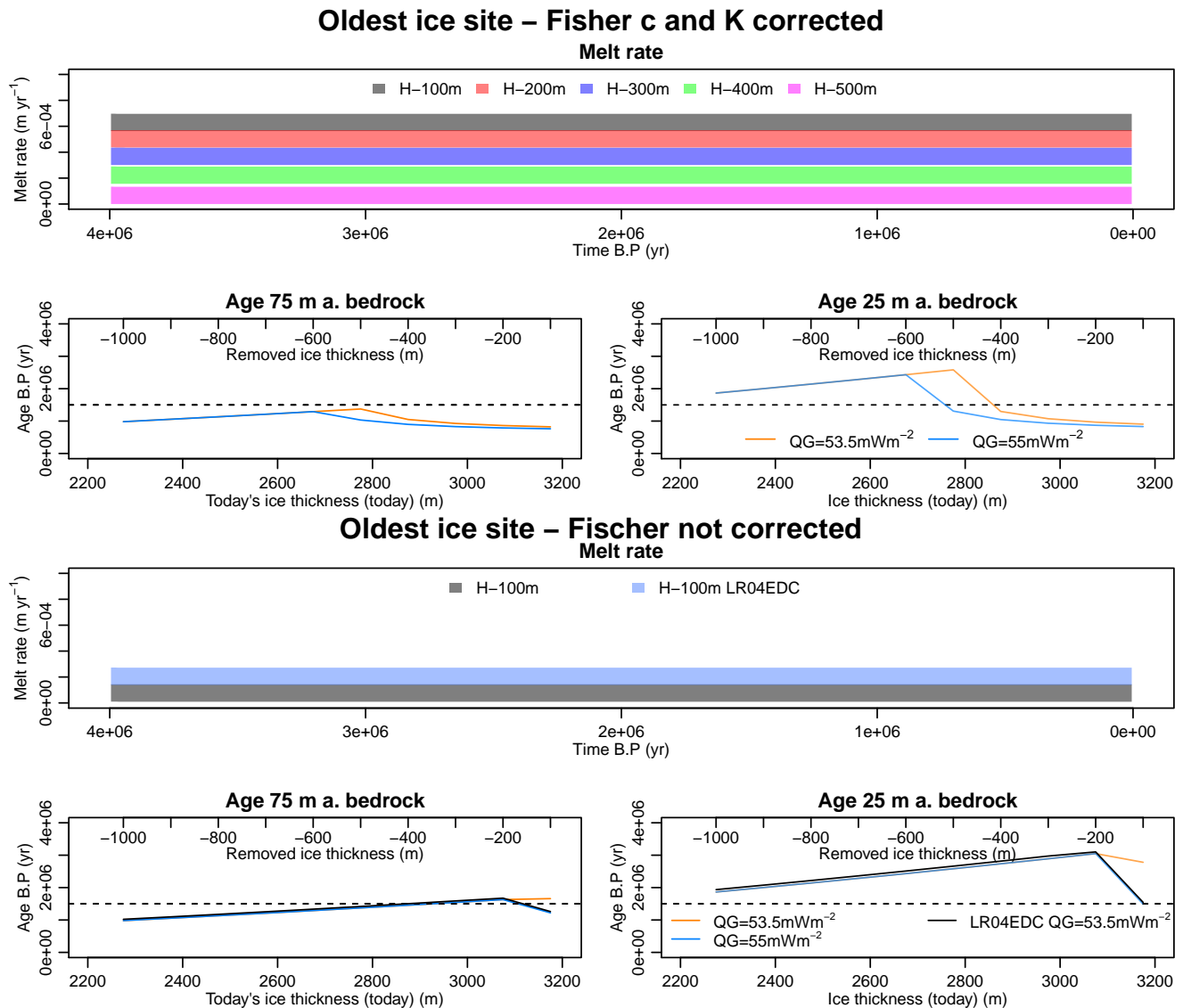
Figure 3.15: Melt rate and ice age at 75 and 25 above bedrock for [Fi] model with A = 0.0191 m ice-eq yr^{-1}, T_S = 213 K, H3151 m ice-eq, m = 0.5, and Q_G = 53.5 and 55 mWm^{-2}. Top panels: [Fi] model with c and K correction. Bottom panels: without correction. In the bottom panel, output of the model using mean of the uncorrected LR04EDC time series and the improved Heron-Langway density model is also shown for Q_G = 53.5 and 55 mWm^{-2} (melt plot) and Q_G = 53.5 mWm^{-2} (age plot), with in both cases m = 0.5 (the mean of uncorrected LR04EDC is taken over the last 1.5 Myr). Attention is drawn that in the last two panels the black line should be compared to the orange one, not to the blue.

kept. The recommended thickness range corresponds to a situation where no melting will very likely occur at least for some period if not always, and with a basal ice temperature between the melting point and −8°C.

3. The model predicts the possible existence of 3 Myr old ice at 25 m above bedrock. However, in addition to the technical difficulties to retrieve such a deep ice, the thinning of annual layers would make such an ice not usable to retrieve accurate information on climate history.

4. This result is not too sensitive to changes in the boundary conditions, but valid only if the ground heat flux value does not exceed the value found for Dome C by more than +5% (reduction of ground heat flux is less problematic).

5. The use of a transient model is more suitable than a steady state model. Indeed, when using the model in a steady state mode with mean values of past climatic conditions and ice thickness the results are similar to the transient result, but with a non-negligible difference (∼ 100 m for the ideal thickness definition). Moreover, the uncertainty would be bigger if the steady state model were already used at Dome C to define the free parameters value. There is a way to partially reduce the uncertainty when using a steady state model for the research of oldest ice (iterative approach to define the average period to use), but it would make the run time similar to the transient model.

6. Results found are quite different to the ideal thickness prescribed in [Fi] (defined in a secure no melting region), showing the improvement offered by the transient model.

However, some major sources of uncertainty remain and should be taken in consideration. They are discussed in the next part of this study.

Summary and additional considerations

In the first chapter, the different processes taking place in an ice dome were described. In particular, the Herron-Langway density model was improved to take temperature and pressure contributions into account, and the chapter also discussed in detail the thermal conductivity of the firn layer along with the basal melting process. In addition, 4 Myr long time series for surface temperature, accumulation rate, and ice sheet thickness were established for Dome C based on the correlation between the existing 800 kyr time series [Baz, Jou, P3, Ve] and a 4 Myr oceanic time series for $\delta^{18}O$ [L.R]. This time series was shown to be more accurate than the ones used (for temperature) and modelled (for accumulation rate and ice thickness) in the 3D model developed in [P.DC]. Furthermore, the chapter introduced age scale and borehole temperature measurements and explained in depth the difference between existing borehole records for Dome C, due to partial extrapolation of the records. Similar time series for GRIP were established, based on an inverse temperature reconstruction [D-J3, Joh]. At the end of the chapter, two different algorithms were presented to solve the heat equation and the Crank-Nicholson scheme was shown to be, by far, the fastest. To conclude the first chapter, technical details were given on the usage of processor tasks splitting for reducing the run time of the model.

The second chapter was devoted to several tests of the model. The necessity of a 150 kyr spin up was shown. Throughout the sensitivity tests performed, the model showed a correct behavior and a large field of validity regarding the different parameters. The firn density parameterization and thermal conductivity correction were also highlighted as major concerns for modeling the temperature and age profiles. Moreover, this chapter demonstrates that bedrock topography can have a non-negligible influence on the temperature profile and therefore an important impact on the melt rate value. The explicit and Crank-Nicolson scheme were compared and the gain of accuracy due to a second pass in the C-N scheme was shown. Finally, the study of internal heat production, based on a steady state ice divide model, was shown to have a small influence on the temperature profile. In the last part of the second chapter, the correlation of the model for certain conditions with a simple steady state model [Fi] was shown.

In the third chapter, three experiments were conducted with the model. The first experiment – consisting of a comparison between the model predictions and the measurement and other models existing at GRIP [D-J2, D-J3, Gu, Gu2, Joh, Ra, Se] – was a robust validation of the model. Despite the uncertainty on past boundary conditions, the results are in good agreement with the literature [Joh, D-J3]. This experiment also showed that the simple flux shape function described in [Fi] gives slightly better results than the more complicated [Pa] formulation for this site. The second experiment made for Dome C conditions showed mixed results. With the normal LR04EDC

boundary conditions, the model failed to produce a reasonable temperature profile (see additional discussion below). Nevertheless, the values found for the form factor and the ground heat flux when the boundary condition time series is corrected are consistent with the literature [Fi, Pa]. This experiment has also shown that the results are quite similar when using mean values instead of transient boundary conditions. The difference observed is attributed to the absence of thickness changes in the steady states model and its influence on the melt rate. The temperature profiles obtained are slightly different to the ones found by [Fi] steady state model because of the correction used in [Fi] model (c and K constant).

The last experiment has been dedicated to the research on an oldest ice site. It has been shown that a drill site allowing to retrieve 1.5 Myr old ice between 75 and 25 m above bedrock likely exists and that this site should have a similar climate conditions as Dome C, but a thickness of only 2750 to 2950 m today. This result has been shown to be not too sensitive to changes in the boundary conditions, but valid only if the ground heat flux value does not exceed the value found for Dome C by more than +5%. Although the model predicts the presence of ice older than 1.5 Myr, it is explained that the layer compression would probably make this ice of lower importance for laboratory measurements. Finally, this chapter discusses several reasons why a transient model is more suitable than a steady state model for such a study and the difference with respect to [Fi] results is also explained. Moreover, it is shown why the results found by this study are more accurate than the values given in [Fi]. However, there is a non-negligible uncertainty around this result that will be discussed below.

Dome C temperature issue

Although reasonably good results are obtained for GRIP, the model fails to reproduce a correct temperature profile for Dome C. This is in spite of the inclusion of an enhanced density model, the valley effect, and a simple parameterization of the internal heat production which are generally not present in similar models. Moreover, scheme comparison and iterative tests have excluded computational error as an explanation of Dome C temperature profile issue.

To overcome this issue, the boundary condition time series was modified. Although the correction on accumulation rate (between +5 and +15%) is acceptable given the poor knowledge about the history of this value and because the assumption that the accumulation rate is only determined by temperature is probably over-simplistic [Jou3], the temperature correction of +2.5 to +3.5°C applied during the glacial periods is more problematic.

The surface temperature reconstruction used in this work [Jou, Pa3] is based on deuterium thermometry. This method uses a calibration of the deuterium and atmospheric inversion layer temperature relationship established in [Jou3], where a non-negligible uncertainty is recognized. Moreover, other studies suggest that additional error may arise from thickness variation, changes in the evaporation conditions and moisture source, changes in the strength of the inversion layer, and changes in the seasonality pattern of precipitation [Jou4, M-D, We]. In [M-D] it is suggested that the [Jou] temperature time series is in fact a "fixed elevation" temperature (the information cannot be found in [Jou]), and that this "fixed elevation" correction leads to a $\sim$ 2°C colder LGM and an overall $\sim$ 1°C colder glacial periods [M-D]. This would mean that these values should be added to the temperature time series to have the real surface temperature at Dome C, which would explain a part of the correction needed in the model. Moreover, an uncertainty of ± 2°C for the glacial temperature retrieved by deuterium excess is recognized in [M.D]. An independent thermometry

method, based on water isotope diffusion, points to to a slightly colder temperature for Greenland during the Younger Dryas compared to the temperature obtained with the usual deuterium excess method [Simo]. In conclusion, the temperature shift between warm and cold periods is still an open question and, even if a +2.5 to +3.5°C seems quite unlikely, a correction of up to +2°C during glacial periods is coherent with the known uncertainty of the thermometry method used [Jou3, M-D]. Moreover, this raises the question of the thickness time series and shows that a more accurate thickness reconstruction along with a better parameterization in the model of how the ice sheet elevation at the time of precipitation influences the deuterium surface temperature reconstruction would be beneficial.

Some other direction can be explored to explain this 2°C difference observed between Dome C modeled and measured temperature profile. In the second chapter, sensitivity tests showed that the inclusion of a firn layer results to an increase in temperature of about 0.5°C along the whole profile (see Figure 2.2), mainly due to the influence of the firn on the thermal conductivity. The model uses a simple steady state firn layer model, whereas some more refined models and dynamical models exists [Go, Sp]. The inclusion of a better density model might thus explain a non-negligible part but not all of the observed 2°C difference. In Section 2.2.1, it has been demonstrated that the choice of the parameterization of the thermal conductivity through firn can also change the values of the temperature profile by up to 0.2°C. Nowadays, the precise thermal conductivity of snow and firn is still an open question [Go], but a more accurate parameterization would lead to a better temperature profile modeling in Dome C.

Nevertheless, since the model produces an output in agreement with measurements for GRIP conditions, the thermal description of firn seems to be not too inaccurate and thus a large correction is not expected from the firn thermal conductivity parameterization. Note that this argument might not be totally valid when talking about the density parameterization. Indeed, it is possible for Dome C to be out of the validity range of the Herron-Langway model, although it is not really likely since Herron-Langway has been tested for Vostok conditions [H.L].

Two other candidates that could potentially explain the temperature difference observed between the model and the measurements are topography and internal energy production. The topography is shown to be possibly significant. Actual available topography measurements [Fo] and the description of the effect of the topography developed for this model suggest that the influence on temperature is not larger than ∼ 0.2°C, but a high resolution survey of the topography close to Dome C drill site would be fundamental to really address this question. In addition, only the heat conduction induced by topography has been discussed, whereas the heat advection by lateral ice movement is not considered. Although lateral ice advection would not exist for a dome, the Dome itself was likely at another position in the past and the dome migration might have been quite fast [Ne]. This means that the ice retrieved at Dome C has not always been below a dome in the last hundreds of thousands of years and therefore some lateral ice flow was present. For this effect to be able to explain the warmer temperature observed in the borehole measurement with respect to the model output, some warm ice inflow is needed. This might come from uplift of ground ice driven by the basal topography [Ri] or from inflow from an upstream position with a thickness at least 300 m lower than today. Moreover, if the ice is not frozen to bedrock some basal slip might occur [Ri] producing friction that acts as a higher ground heat flux (see Section 1.1.6).

The internal energy production has been simply parameterized using a model developed of an ice divide. Despite the demonstration that it could be used to approximate the situation at Dome C (see Section 1.1.6), some differences between dome and ice divide dynamics exist. Moreover,

the model used is a steady state model. To infer the influence of an increased deformation on the energy production, some tests with the internal energy value increased during transition between glacial and interglacial periods[10] were performed (see Section 2.2.1.3). It has shown that an increase by an unrealistic factor 100 of energy production during these transition periods leads to a significant effect. Here some additional runs are performed with a slightly different setup. The ice sheet thinning is also taken into account for the definition of thickness rapid variation periods (see footnote 10). Figure 3.16 left panel shows the result for an increase of a factor 100 and 1000 of the internal energy due to ice deformation. Whereas for a factor 100, there is not a large effect from it being applied only during fast thickness variation periods or during all the time, the difference becomes more significant for an increase of a factor 1000. This figure and the values given in Figure 1.4 show that an internal energy density production between 10^{-5} and 10^{-4} $\mathrm{W\,m^{-3}}$ would be enough to explain the temperature difference between the model and the borehole record. The right panel shows the temperature profile difference with respect to the berehole temperature if the model run duration is extended (today's boundary conditions are used for the additional time). It can be seen that the model is not yet at equilibrium with the surface temperature and accumulation rate of the Holocene. Indeed, for additional run time the temperature continue to increase and seems to converge to its equilibrium profile (close to the gray line), which appears to be quite close the measured borehole temperature. However, the necessary time is several tens of thousands of years (and the basal gradient will still not be exactly the same than for the measurements). In other words, if the model was converging faster to its equilibrium temperature, today's temperature profile would be closer to the measurements. As shown in the left panel, really high internal energy (but unrealistic with current models) would bring today's modeled borehole temperature closer to its equilibrium profile and thus to the measurements.

The development of a full 3D thermo-mechanical model with a high spatial resolution seems to be the only solution to get a better estimate of internal heat production. Such a model would also include a more accurate topography effect and dome migration description, but it would require an accurate past accumulation rate time series. Two other effects contributing to the internal heat production have been studied: the internal radioactivity and cosmic rays. By computing the radioactivity using the dust concentration given in [La] (an approximation of a constant value of $\sim 400\ \mu\mathrm{g\,kg^{-1}}$ is used) and a mean activity of $\sim 10^{-11}\mathrm{W\,kg^{-1}}$ [T.S] (dust is approximated to have the same composition as the Earth's crust), the heat production is of order 10^{-14} to $10^{-13}\mathrm{W\,m^{-3}}$. Regarding cosmic rays, the energy deposition can be roughly considered as constant over the ice sheet depth[11] and represent an energy density of 10^{-12} to $10^{-11}\mathrm{W\,m^{-3}}$ [Javier Bilbao, personal communication]. Both of them are too small by several order of magnitude to have a significant impact on the temperature profile.

Unlike firn and density parameterization, a different basal topography, dome migration history, or internal mechanics between Dome C and GRIP are totally acceptable and can explain why the model reproduces satisfactorily the temperature profile at GRIP but not at Dome C.

Finally, more constraints on past boundary conditions and a better understanding of the geology – allowing some constraints on the ground heat flux values and eventual variation over time – would surely be beneficial.

---

[10] These periods were defined as period where the thickness change is positive and exceed 30 cm per century. This is fulfilled during $\sim 17\%$ of the time in the last 1 Myr and during $\sim 16\%$ of the time in the last 2 Myr. Taking into account also negative thickness variation gives more or less the double.

[11] On the top part the dominant contribution is the muon interaction whereas in the lower part electrons produced by neutrino decay dominate.
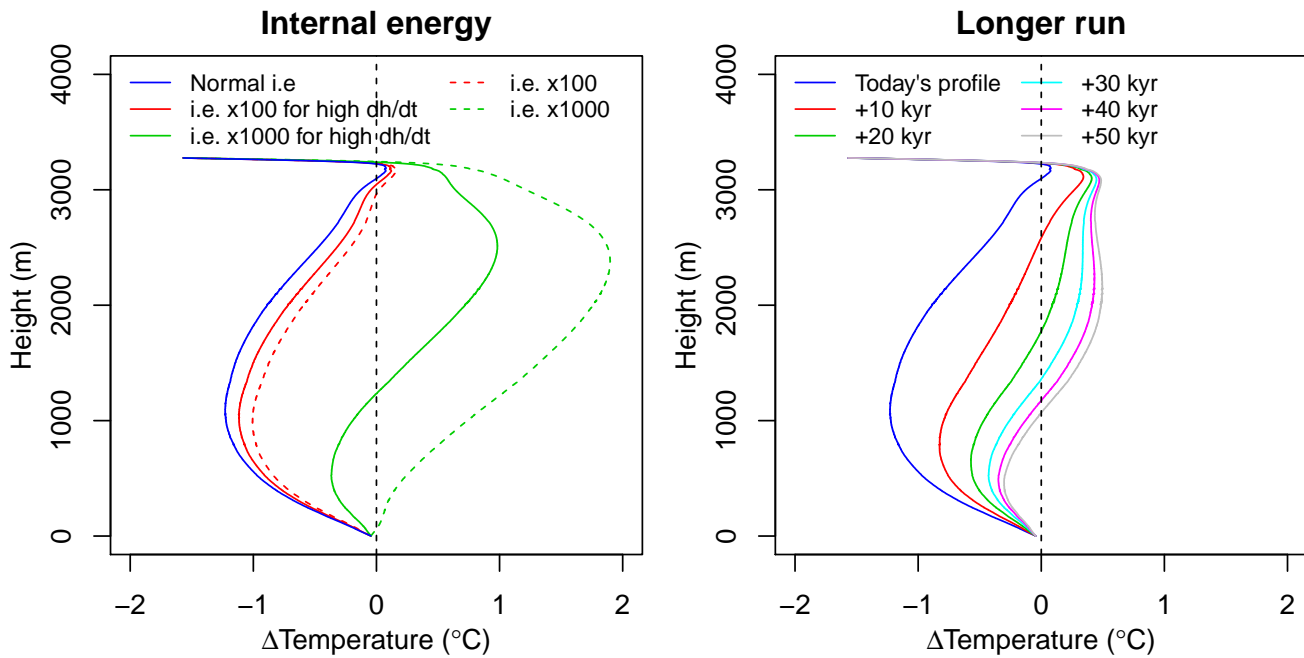
Figure 3.16: Left: temperature difference with respect to the borehole temperature for runs where the internal energy due to deformation is increased by a factor 100 or 1000 over the periods of high thickness variation (solid lines) or during all the time (dashed lines). Right: temperature difference with respect to the borehole temperature for a run with an additional time added at the end (up to 50 kyr). For the additional time, the boundary conditions used are today's values.

Oldest ice site determination

The result found for the oldest ice site is an ideal thickness comprised between 2750 and 2950 m, which corresponds to a situation where no melting will very likely occur at least for some period if not always and with a basal ice temperature between the melting point and –8°C. This result is valid if the real accumulation rate history lies in a –10 to +20% range around the LR04EDC values, if the ground heat flux is comprised between 52 and 57 mWm^2, and if the form factor is between 0.45 and 0.55. All of these values are considered as constant over time, but there is no reason to believe that they are. However, it is delicate to estimate variation of these values in the past. Indeed, without a 3D thermo-mechanical model there is no possibility to infer any hypothetical evolution of the flux shape function. It is only known that the ice sheet dynamics for a given location has likely varied over time; for example because of the dome migration effect discussed above. Regarding the ground heat flux, it is not excluded that its value has changed over time. Indeed, even if geological processes time scales are usually of several million of years, the isostatic rebounds which come along the numerous glacial/interglacial cycles or the basal drag of some different rocks may have an influence of the ground heat flux value. Moreover, some additional sources of heat were perhaps present in the past, for example because of basal friction or because of sub-glacial water flow.

An additional effect – which has not been included in the model because it is not relevant for Dome C – might have some importance when exploring regions where no melting phases occur. This effect is the process that happens when there is no basal melting. Indeed, in the model, when the heat flux balance is negative at the bottom of the ice sheet, the necessary energy to bring back the balance to zero is taken by cooling the basal ice. Nevertheless, the cooling of the bedrock itself

might also be considered (as in [Pa]). For this purpose, some layers of rock should be included, with the temperature or a heat flux fixed at the bottom of these rocky layers. This would slow down the cooling and heating of basal ice when there is no melting and keep the basal ice a bit warmer, but not change the overall energy balance if the bottom boundary condition remains fixed by a heat flux. Thus, there is not a significant impact expected on melt rate and age profile. A measurable effect would be the change in basal temperature for a site where there is no melting, for example GRIP, but this would not be distinguishable from a slight increase of the ground heat flux value. The second hypothesis would be the presence of available water for freezing. In this case, the water would be frozen when no melting occurs and thus keep the temperature at the melting point. This would make it easier for the melting process to restart and the overall effect would be a larger mean melt rate because of shorter periods of no-melting. Nevertheless, the question of where this ice would go should be included in the model and the quantity and periods of availability of the water should be parameterized.

The last point is the thickness time series; indeed, the thickness variation is simply parameterized using the surface temperature and a given age lag. The influence of eventual corrections on this thickness variation time series has not been discussed, in spite of the fact that the non-negligible influence of the thickness variation on the melt rate value has been proven. However, since no more information than the used time series are available, no test could have been conducted. As for the form factor, a comprehensive 3D model would give a better idea of thickness changes back in time.

This discussion adds some arguments to claim that the basal melting and age scale should really be treated with care. In sum, the recommended thickness value obtained is based on assumptions that are hard to fulfill (similarity to Dome C conditions, constancy of the form factor and ground heat flux, no sublacial water, etc.). However, that does not mean that the result found is not valid. First of all, the good agreement found at GRIP shows that the model is effective for non-melting description. Moreover, the effect (described above) of water refreezing, which is not included in the model, can only have a limited impact. Indeed, the availability of water would not be infinite. Regarding the form factor and the mechanical behavior of the ice sheet, the good results found for GRIP, and to a small extent for Dome C, show that a one-dimensional simplified parameterization remains robust. Moreover, comparable studies also find good results by using a simple 1D model [Go, Pa]. In addition, the results are quite resilient to small boundary condition corrections. It is true that the corrections on the surface temperature history needed to reproduce the correct temperature profile for Dome C are hardly explainable and are probably an artifact to represent some topographic effect of internal energy production missing in the model (see discussion above). However, this correction by addition of heat from the surface is probably better than the correction of the ice thermal conductivity used in [Fi]. Moreover it has clearly been shown that the influence of the time series corrections on ice age decreases for thinner ice sheets.

In conclusion, the value of 2750 to 2950 meters of ice for an ideal drill site should be considered as indicative and, for all the reasons given above, the related basal age cannot be predicted without a substantial uncertainty. Moreover, it has been shown that the drill site should be carefully chosen, particularly with regard to its ground topography. Nevertheless, the important information from this study is that 1.5 Myr old ice is very likely to exist and that it should be found at sites few hundreds of meters thicker than the thickness indicated in [Fi], and that a transient model – among other things by a transient computation of the melt rate – is a real improvement with respect to steady state models for exploring the field of old ice retrieval.

Conclusion and outlook

The 4 Myr long LR04EDC time series obtained by parameterization of the Lisiecki and Raymo [L.R] benthic time series and based on the existing EDC07 [Jou, Pa3] and AICC2012 [Baz, Ve] time series for Dome C can be considered as an acceptable representation of the past condition, despite the fact that the influence of the surface elevation on the temperature remains unclear [M-D]. It shows a reasonable agreement with a time series established from a large-scale Antarctica model [P.DC]. This study has shown the importance of using well constrained time series for modeling the borehole temperature and the age profile.

The influence of various parameters on the temperature profile and age scale, which can be obtained by this type of 1D model, have been discussed. It is concluded that the thermal influence of a firn layer, through density and thermal conductivity, and the inclusion of basal topography thermal effects are non-negligible, whereas the internal heat production seems to be negligible, at least with the actual knowledge [D-J]. However, the different tests performed show that these three effects should be studied in more detail to improve the accuracy and reliability of such models. For parameters such as form factor and ground heat flux, the results confirm the discussion already existing in the literature [D-J3, Fi, Joh, Pa].

In general, the model developed shows a high level of agreement with the literature and can be considered as robust. Nevertheless, its usage at Dome C shows some discrepancies and highlights the lack of parameterization of some physical processes. The best candidates are the various effects of the topography and the three dimensional mechanical behavior of the ice sheet.

The value obtained for the ideal ice sheet thickness, which would allow the retrieval of ice as old as possible for surface temperature and accumulation rate history similar to Dome C, is 2750 to 2950 m. For such a site, today's ground ice temperature is between –8°C and the melting point. This result takes into consideration the uncertainty found for free parameters values and boundary conditions corrections, but an unquantifiable uncertainty comes from all the effects not included in the model (described in the previous section). However, the result of the various sensitivity tests shows that many of these effects should not have a too large of an influence on this value. The important information is that the ideal thickness value differs to the one currently admitted [Fi], and strong arguments have been given for the higher thickness value found in this thesis. Moreover, this study gives some information on the impact of topography that were not present in the previous previous studies.

Model improvements

Several fundamental improvements have been cited above. The transformation to a full 3D model would require to essentially restart from scratch and the spatial and correspondingly, temporal resolution would be reduced to keep a reasonable run time. However, there are some other improvements that would require less work and fewer fundamental changes in the model.

The inclusion of basal rock layers would be quite easy. It has not been done because it is believed to have a negligible influence on melt rate. The inclusion of some basal refreezing process, although a bit more complicated, would also be possible. This requires to parameterize the quantity of available water and a fraction of ice produced, which would remain exactly below the ice column (the rest would spread around due to pressure). Having the ground heat flux and form factor changing over time would be a trivial inclusion in the source code. Nevertheless, to be relevant some information about the rate of change of these values on the past are necessary.

From a more technical point of view, some possible improvements to the model remain to increase the model efficiency. Indeed, the basic time unit used in the model is the second. This small time unit leads to some small values to work with, especially when talking about melt rate and accumulation rate. This requires the usage of double precision variable, slowing the computation and increasing the memory demand. The usage of 1 yr as the time unit would require a recomputation of all the physical constants but allow to use float instead of double precision variables and, as a consequence, slightly reduce the processor and memory usage. A non-negligible time is spent to compute the density profile. Some sensitivity studies on the influence of the temperature and pressure profile on density would be useful to determine if a more simple approximation of the density, based on linear piecewise approximation of the Herron-Langway output (as done for the internal energy computation) with a temperature correction, would be enough to get a reasonable accuracy. The same idea applies for the valley effect. Indeed, the current version requires this to compute a second temperature profile for every time steps. Nevertheless a statistical analysis of several runs could perhaps lead to a simpler parameterization of this effect.

Other possible usage of the model

It would not be difficult to run the model with a Monte Carlo approach [M.U] to retrieve past boundary conditions for various sites where borehole temperature records are available, as already done by other models [D-J3, D-J4]. If some age scale exists, it could be used as an additional constraint on the acceptable results. However, the implementation of few of the improvements described above would be beneficial in order to keep a reasonable time for the thousands and thousands of runs needed by a Monte-Carlo approach without reducing the complexity of the model.

In its current form, the model can be used to approximate the temperature profile for sites where past boundary conditions are known. This could be useful for ice core gas studies. Note that if solely the temperature profile is important and not the age scale, boundary conditions need to be known only for the Holocene and last glacial periods. Indeed, all temperature events from the Eemian and before are washed out by thermal diffusion. For the spin up, considering the temperature at equilibrium in the last glacial period is a valid approximation. An approximation of the ground heat flux value is also needed. By enhancing the density profile with more recent and dynamical models [Sp], the model could also be used for the computation of the close off depth

[Go]. Moreover, the model offers the possibility to have a full transient temperature record (see Figure 3.17), which could allow us, amongst other things, to explore the temperature diffusion time during glacial/inter-glacial transitions or the time needed to reach the equilibrium after any modification of the boundary conditions.

Finally, this transient model can be used as a piece of a larger 2D and 3D model. In particular, due to the detailed model representation of the melt rate process, density influence on heat conductivity, and to a small extent firn model and topography impact, the complexity of this model makes it particularly suited to perform sensitivity tests and thus to infer which processes can be discarded in a larger model for optimization purposes.
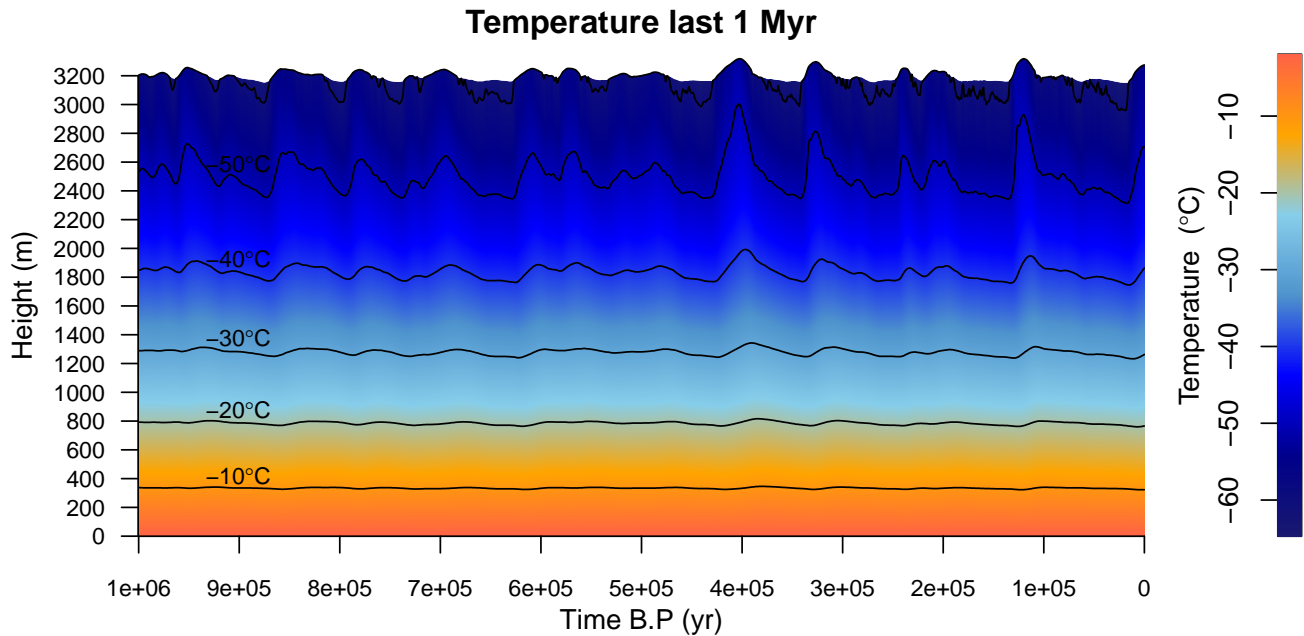
Figure 3.17: Ice temperature at Dome C over the last million of years. Obtained with the LR04EDC time series for the boundary conditions, m = 0.5 and $Q_G = 55 \text{mWm}^{-2}$. Black lines indicate isotherms.

Acknowledgments

References

[Al] R.B. Alley, A.J. Gow, D.A. Meese, J.J. Fitzpatrick, E.T. Waddington, and J.F. Bolzan, 1997: *Grain-scale processes, folding, and stratigraphic disturbance in the GISP2 ice core.* Journal of Geophysical Research: Oceans, **102**, 26819–26830.

[Bar] J.-M. Barnola, P. Pimienta, D. Raynaud, and Y.S. Korotkevich, 1991: *CO_2-climate relationship as deduced from the Vostok ice core: a re-examination based on new measurements and on a re-evaluation of the air dating.* Tellus B, **43**, 83–90.

[Baz] L. Bazin, A. Landais, B. Lemieux-Dudon, H. Toye Mahamadou Kele, D. Veres, F. Parrenin, P. Martinerie, C. Ritz, E. Capron, V. Lipenkov, M.-F. Loutre, D. Raynaud, B. Vinther, A. Svensson, S. Rasmussen, M. Severi, T. Blunier, M. Leuenberger, H. Fischer, V. Masson-Delmotte, J. Chappellaz, and E. Wolff, 2013: *An optimized multi-proxies, multi-site Antarctic ice and gas orbital chronology (AICC2012): 120-800 ka.* Climate of the Past, **9**, 1715–1731.

[Be] B. Bereiter, H. Fischer, J. Schwander, and T.F. Stocker, 2014: *Diffusive equilibration of N_2, O_2 and CO_2 mixing ratios in a 1.5 million years old ice core.* The Cryosphere, **8**, 245–256.

[Bo] J.F. Bolzan, 1985: *Ice flow at the Dome C ice divide based on a deep temperature profile.* J. Geophys. Res., **90**, 8111–8124.

[C.B] S.D. Conte and C. de Boor, 1980: *Elementary numerical analysis, an algorithmic approach, 2nd edition.* International Series in Pure and Applied Mathematics, Springer, 432 pp.

[Ch] J.G. Charney, R. Fjørtoft, and J. von Neumann, 1950: *Numerical Integration of the Barotropic Vorticity Equation.* Tellus, **2**, 27–254.

[C.N] J. Crank and E. Nicolson, 1947: *A practical method for numerical evaluation of solutions of partial differential equations of the heat-conduction type.* Proc. Camb. Phil. Soc., **43**, 50–67.

[C.P] K.M. Cuffey and W.S.B. Paterson, 2010: *The physics of glaciers, 4th edition.* Elsevier, 693 pp.

[Cl] P.U. Clark, R.B. Alley, and D. Pollard, 1999: *Northern Hemisphere Ice-Sheet Influences on Global Climate Change.* Science, **286**, 1104–1111.

[Da] W. Dansgaard, S.J. Johnsen, H.B. Clausen, D. Dahl-Jensen, N.S. Gundestrup, C.U. Hammer, C.S. Hvidberg, J.P. Steffensen, A.E. Sveinbjörnsdottir, J. Jouzel, and G. Bond, 1993: *Evidence for general instability of past climate from a 250-kyr ice-core record.* Nature, **364**, 218–220.

[D-J] D. Dahl-Jensen, 1989: *Steady thermomechanical flow along two-dimensional flow lines in large grounded ice sheets.* J. Geophys. Res., **94**, 10355–10362.

[D-J2] D. Dahl-Jensen, 1993: *Reconstruction of palaeo climate from temperature measurements in bore holes on the Greenland ice sheet.* In Proceedings of the Interdisciplinary Inversion Workshop 2, Edition K. Mosegaard, University of Copenhagen, Copenhagen, 11–14.

[D-J3] D. Dahl-Jensen, K. Mosegaard, N. Gundestrup, G.D. Clow, S.J. Johnsen, A.W. Hansen, and N. Balling, 1998: *Past Temperatures Directly from the Greenland Ice Sheet.* Science, **282**, 268–271 .

[D-J4] D. Dahl-Jensen, I.M. Vin, and A. Elcheikh, 1999: *Monte Carlo inverse modelling of the Law Dome (Antarctica) temperature profile.* Annals of Glaciology, **29**, 145–150.

[El] H. Elderfield, P. Ferretti, M. Greaves, S. Crowhurst, I.N. McCave, D. Hodell, and A.M. Piotrowski, 2012: *Evolution of Ocean Temperature and Ice Volume Through the Mid-Pleistocene Climate Transition.* Science, **337**, 704–709.

[EPICA] EPICA Community Members, 2004: *Eight glacial cycles from an Antarctic ice core.* Nature, **429**, 623–628.

[Fi] H. Fischer, J. Severinghaus, E. Brook, E. Wolff, M. Albert, O. Alemany, R. Arthern, C. Bentley, D. Blankenship, J. Chappellaz, T. Creyts, D. Dahl-Jensen, M. Dinn, M. Frezzotti, S. Fujita, H. Gallee, R. Hindmarsh, D. Hudspeth, G. Jugie, K. Kawamura, V. Lipenkov, H. Miller, R. Mulvaney, F. Parrenin, F. Pattyn, C. Ritz, J. Schwander, D. Steinhage, T. van Ommen, and F. Wilhelms, 2013: *Where to find 1.5 million yr old ice for the IPICS Oldest-Ice ice core.* Clim. Past, **9**, 2489–2505.

[Fi2] H. Fischer, M. Wahlen, J. Smith, D. Mastroianni, and B. Deck, 1999: *Ice Core Records of Atmospheric CO_2 Around the Last Three Glacial Terminations*, Science, **283**, 1712–1714.

[Fo] A. Forieri, L. Zuccoli, A. Bini, A. Zirizzotti, F. Remy, and I. E. Tabacco, 2013: *New bedrock map of Dome C, Antarctica, and morphostructural interpretation of the area.* Annals of Glaciology, **39**, 321–325.

[Go] A.J. Gow, D.A. Meese, R.B. Alley, J.J. Fitzpatrick, S. Anandakrishnan, G.A. Woods, and B.C. Elder, 1997: *Physical and structural properties of the Greenland Ice Sheet Project 2 ice core: A review.* J. Geophys. Res., **102**, 26559–26575.

[Gr] S.L. Graham, P.B. Kessler, and M.K. McKusick, 1982: *Gprof: A call graph execution profiler.* SIGPLAN '82 Proceedings of the 1982 SIGPLAN symposium on Compiler construction, New-York, USA, 120–126.

[GRIP] Greenland Ice-Core Project (GRIP) Members, 1993: *Climate instability during the last interglacial period recorded in the GRIP ice core.* Nature, **364**, 203–207.

[Gu] N.S. Gundestrup, D. Dahl-Jensen, S.J. Johnsen, and A. Rossi, 1993: *Borehole survey at dome GRIP 1991.* Cold Regions Science and Technology, **21**, 399–402.

[Gu2] N.S. Gundestrup, H.B. Clausen, and B.L. Hansen, 1994: *The UCPH borehole logger.* National Institute Polar Research, Special issue, **49**, 224–233.

[Hi] N.J. Higham, 2002: *Accuracy and Stability of Numerical Algorithms: Second Edition.* Society for Industrial and Applied Mathematics Philadelphia, 680 pp.

[H.L] M.M. Herron and C.C. Langway, 1980: *Firn densification: an empirical model.* Journal of Glaciology, **25**, 373–385.

[H.McC] Y. Huang and W.F. McColl, 1997: *Analytical inversion of general tridiagonal matrices.* J. Phys. A: Math. Gen., **30**, 7919–7933.

[H.O] P. Huybrechts and J. Oerlemans, 1988: *Evolution of the East Antarctic ice sheet: a numerical study of thermo-mechanical response patterns with changing climate.* Annals of Glaciology, **11**, 52–59.

[Hu] P. Huybrechts, 1998: *Report of the Third EISMINT Workshop on Model Intercomparison.* European Science Foundation, 120 pp.

[Im] J. Imbrie, A. Berger, E.A. Boyle, S.C. Clemens, A. Duffy, W.R. Howard, G. Kukla, J. Kutzbach, D.G. Martinson, A. McIntyre, A.C. Mix, B. Molfino, J.J. Morley, L.C. Peterson, N.G. Pisias, W.L. Prell, M.E. Raymo, N.J. Shackleton, J.R. Toggweiler, 1993: *On the structure and origin of major glaciation cycles. 2. The 100,000-year cycle.* Paleoceanography, **8**, 699–735.

[IPCC] V. Masson-Delmotte, M. Schulz, A. Abe-Ouchi, J. Beer, A. Ganopolski, J.F. González Rouco, E. Jansen, K. Lambeck, J. Luterbacher, T. Naish, T. Osborn, B. Otto-Bliesner, T. Quinn, R. Ramesh, M. Rojas, X. Shao and A. Timmermann, 2013: *Information from Paleoclimate Archives. In: Climate Change 2013: The Physical Science Basis. Contribution of Working Group I to the Fifth Assessment Report of the Intergovernmental Panel on Climate Change [T.F. Stocker, D. Qin, G.-K. Plattner, M. Tignor, S.K. Allen, J. Boschung, A. Nauels, Y. Xia, V. Bex, and P.M. Midgley (eds.)].* Cambridge University Press, Cambridge, United Kingdom and New York, NY, USA, 384–465.

[Ja] E. Javierre, C. Vuik, F.J. Vermolen, and S. van der Zwaag, 2006: *A comparison of numerical models for one-dimensional Stefan problems.* Journal of Computational and Applied Mathematics, **192**, 445–459.

[Jou] J. Jouzel, V. Masson-Delmotte, O. Cattani, G. Dreyfus, S. Falourd, G. Hoffmann, B. Minster, J. Nouet, J.M. Barnola, J. Chappellaz, H. Fischer, J.C. Gallet, S. Johnsen, M. Leuenberger, L. Loulergue, D. Luethi, H. Oerter, F. Parrenin, G. Raisbeck, D. Raynaud, A. Schilt, J. Schwander, E. Selmo, R. Souchez, R. Spahni, B. Stauffer, J.P. Steffensen, B. Stenni, T.F. Stocker, J.L. Tison, M. Werner, and E.W. Wolff, 2007: *Orbital and Millennial Antarctic Climate Variability over the Past 800,000 Years.* Science, **317**, 793–797.

[Jou2] J. Jouzel, V. Masson, O. Cattani, S. Falourd, M. Stievenard, B. Stenni, A. Longinelli, S.J. Johnsen, J.P. Steffenssen, J.R. Petit, J. Schwander, R. Souchez, N.I. Barkov, 2001: *A new 27 ky high resolution East Antarctic climate record.* Geophysical Research Letters, **28**, 3199–3202.

[Jou3] J. Jouzel, F. Vimeux, N. Caillon, G. Delaygue, G. Hoffmann, V. Masso-Delmotte, and F. Parrenin, 2003: *Magnitude of isotope/temperature scaling for interpretation of central Antarctic ice cores.* Journal of Geophysical Research: Atmospheres, **108**, 4361.

[Jou4] J. Jouzel, R.B. Alley, K.M. Cuffey, W. Dansgaard, P. Grootes, G. Hoffmann, S.J. Johnsen, R.D. Koster, D. Peel, C.A. Shuman, M. Stievenard, M. Stuiver, and J. White, 1997: *Validity of the temperature reconstruction from water isotopes in ice cores.* Journal of Geophysical Research, **102**, 26471–26487.

[Joh] S. J. Johnsen, D. Dahl-Jensen, W. Dansgaard, and N. Gundestrup, 1995: *Greenland palaeotemperatures derived from GRIP bore hole temperature and ice core isotope profiles.* Tellus B, **47**, 624–629.

[Joh2] S.J Johnsen, H.B. Clausen, W. Dansgaard, N.S. Gundestrup, C.U. Hammer, U. Andersen, K.K. Andersen, C.S. Hvidberg, D. Dahl-Jensen, J.P. Steffensen, H. Shoji, A.E. Sveinbjörns-dóttir, J. White, J. Jouzel, and D. Fisher, 1997: *The $\delta^{18}O$ record along the Greenland Ice Core Project deep ice core and the problem of possible Eemian climatic instability.* Journal of Geophysical Research: Oceans, **102**, 26397–26410.

[La] F. Lambert, B. Delmonte, J.R. Petit, M. Bigler, P.R. Kaufmann, M.A. Hutterli, T.F. Stocker, U. Ruth, J.P. Steffensen, and V. Maggi, 2008: *Dust-climate couplings over the past 800,000 years from the EPICA Dome C ice core.* Nature, **452**, 616–619.

[L.D] L. Lliboutry and P. Duval, 1985: *Various isotropic and anisotropic ices found in glacier and polar ice caps and their corresponding rheologies*, Ann. Geophys., **3**, 207–224.

[Lo] C. Lorius, L. Merlivat, J. Jouzel, and M. Pourchet, 1979: *A 30,000-yr isotope climatic record from Antarctic ice.* Nature, **280**, 644–648.

[L.R] L.E. Lisiecki and M.E. Raymo, 2005: *A Pliocene-Pleistocene stack of 57 globally distributed benthic d18O records.* Paleoceanography, **20**, PA1003.

[Ma] N. Mattor, T.J. Williams and D.W. Hewett, 1995: *Algorithm for solving tridiagonal matrix problems in parallel.* Parallel Computing, **21**, 1769–1782.

[M-D] V. Masson-Delmotte, B. Stenni, K. Pol, P. Braconnot, O. Cattani, S. Falourd, M. Kageyama, J. Jouzel, A. Landais, B. Minster, J.M. Barnola, J. Chappellaz, G. Krinner, S. Johnsen, R. Rothlisberger, J. Hansen, U. Mikolajewicz, and B. Otto-Bliesner, 2010: *EPICA Dome C record of glacial and interglacial intensities.* Quaternary Science Reviews, **29**, 113–128.

[Ne] N.A. Nereson, R.C.A. Hindmarsh, and C.F. Raymond, 1998: *Sensitivity of the divide position at Siple Dome, West Antarctica to boundary forcing.* Annals of Glaciology, **27**, 207–214.

[N.U] N. Metropolis and S. Ulam, 1949: *The monte carlo method.* Journal of the American statistical association, **44**, 335–341.

[P.DC] D. Pollard and R.M. DeConto, 2009: *Modelling West Antarctic ice sheet growth and collapse through the past five million years.* Nature, **458**, 329–332.

[Pa] F. Parrenin, G. Dreyfus, G. Durand, S. Fujita, O. Gagliardini, F. Gillet, J. Jouzel, K. Kawamura, N. Lhomme, V. Masson-Delmotte, C. Ritz, J. Schwander, H. Shoji, R. Uemura, O. Watanabe, and N. Yoshida, 2007:*1-D-ice flow modelling at EPICA Dome C and Dome Fuji, East Antarctica.* Clim. Past, **3**, 243-259.

[Pa2] F. Parrenin, R. Hindmarsh, and F. Remy, 2006: *Analytical solutions for the effect of topography, accumulation rate and lateral flow divergence on isochrone layer geometry.* J. Glaciol., **52**, 191–202.

[Pa3] F. Parrenin, J.-M. Barnola, J. Beer, T. Blunier, E. Castellano, J. Chappellaz, G. Dreyfus, H. Fischer, S. Fujita, J. Jouzel, K. Kawamura, B. Lemieux-Dudon, L. Loulergue, V. Masson-Delmotte, B. Narcisi, J.-R. Petit, G. Raisbeck, D. Raynaud, U. Ruth, J. Schwander, M. Severi, R. Spahni, J.P. Steffensen, A. Svensson, R. Udisti, C. Waelbroeck, and E. Wolff, 2007: *The EDC3 chronology for the EPICA Dome C ice core.* Climate of the Past, **3**, 485–497.

[Pe] J.R. Petit, J. Jouzel, D. Raynaud, N.I. Barkov, J.-M. Barnola, I. Basile, M. Bender, J. Chappellaz, M. Davisk, G. Delaygue, M. Delmotte, V.M. Kotlyakov, M. Legrand, V.Y. Lipenkov, C. Lorius, L. Pépin, C. Ritz, E. Saltzmank, and M. Stievenar, 1999: *Climate and atmospheric history of the past 420,000 years from the Vostok ice core, Antarctica.* Nature, **399**, 429–436

[Po] K. Pol, V. Masson-Delmotte, S. Johnsen, M. Bigler, O. Cattani, G. Durand, S. Falourd, J. Jouzel, B. Minster, F. Parrenin, C. Ritz, H.C. Steen-Larsen, and B. Stenni, 2010: *New MIS 19 EPICA Dome C high resolution deuterium data: Hints for a problematic preservation of climate variability at sub-millennial scale in the "oldest ice".* Earth and Planetary Science Letters, **298**, 95–103.

[Ra] S.O. Rasmussen, M. Bigler, S.P. Blockley, T. Blunier, S.L. Buchardt, H.B. Clausen, I. Cvijanovic, D. Dahl-Jensen, S.J. Johnsen, H. Fischer, V. Gkinis, M. Guillevic, W.Z. Hoek, J. John Lowe, J.B. Pedro, T. Popp, I.K. Seierstad, J. Peder Steffensen, A.M. Svensson, P. Vallelonga, B.M. Vinther, M.J.C. Walker, J.J. Wheatley, and M. Winstrup, 2014: *A stratigraphic framework for abrupt climatic changes during the Last Glacial period based on three synchronized Greenland ice-core records: refining and extending the INTIMATE event stratigraphy.* Quaternary Science Reviews, **106**, 14–28.

[R.T] F. Remy and I.E. Tabacco, 2000: *Bedrock features and ice flow near the EPICA Ice Core Site (Dome C, Antarctica).* Geophysical Research Letters, **27**, 405–408.

[Ri] E. Rignot, J. Mouginot, and B. Scheuchl, 2011: *Ice flow of the Antarctic ice sheet.* Science, **333**, 1427–1430.

[Sa] A.N. Salamatin, V.Y. Lipenkov, N.I. Barkov, J. Jouzel, J.R. Petit, and D. Raynaud, 1998: *Ice core age dating and paleothermometer calibration based on isotope and temperature profiles from deep boreholes.* Journal of Geophysical Research, **103**, 8963–8977.

[Sc] J. Schwander, T. Sowers, J.-M. Barnola, T. Blunier, A. Fuchs, and B. Malaize, 1997:*Age scale of the air in the summit ice: Implication for glacial-interglacial temperature change.* Journal of Geophysical Research, **102**, 19483–19493.

[S.D-J] J. Schwander and D. Dahl-Jensen, 2005: *European Project for Ice Coring in Antarctica (EPICA), Concordia Station, Chief Scientist's Report 2004/05.* Prepared for the EPICA Steering bodies and the participating scientists, 13 pp.

[Se] I.K. Seierstad, P.M. Abbott, M. Bigler, T. Blunier, A.J. Bourne, E. Brook, S.L. Buchardt, C. Buizert, H.B. Clausen, E. Cook, D. Dahl-Jensen, S.M. Davies, M. Guillevic, S.J. Johnsen, D.S. Pedersen, T.J. Popp, S.O. Rasmussen, J.P. Severinghaus, A. Svensson, and B.M. Vinther, 2014: *Consistently dated records from the Greenland GRIP, GISP2 and NGRIP ice cores for the past 104 ka reveal regional millennial-scale delta O-18 gradients with possible Heinrich event imprint.* Quaternary Science Reviews, **106**, 29–46.

[Sh] M. Shahskov, 1996: *Conservative Finite-Difference Methods on General Grids.* CRC Press, Florida, USA, 359 pp.

[Sime] L.C. Sime, E.W. Wolff, K.I.C. Oliver, and J.C. Tindall, 2009: *Evidence for warmer interglacials in East Antarctic ice cores.* Nature, **462**, 342–345.

[Simo] S.B. Simonsen, S.J. Johnsen, T.J. Popp, B.M. Vinther, V. Gkinis, and H.C. Steen-Larsen, 2011: *Past surface temperatures at the NorthGRIP drill site from the difference in firn diffusion of water isotopes.* Climate of the Past, **7**, 1327–1335.

[Sl] G.A. Slack, 1980: *Thermal conductivity of ice.* Physical Review B, **22**, 3065–3071.

[Sp] M.K. Spencer, R.B. Alley, and T.T. Creyts, 2001: *Preliminary firn-densification model with 38-site dataset.* Journal of Glaciology, **47**, 671–676.

[S.R] N.M. Shapiro and M.H. Ritzwoller, 2004: *Inferring surface heat flux distributions guided by a global seismic model: particular application to Antarctica.* Earth and Planetary Science Letters, **223**, 213–224.

[Ta] K.C. Taylor, G.W. Lamorey, G.A. Doyle, R.B. Alley, P.M. Grootes, P.A. Mayewski, J.W.C. White, and L.K. Barlow, 1993: *The 'flickering switch' of late Pleistocene climate change.* Nature, **361**, 432–436.

[T.S] D.L. Turcotte and G. Schubert, 2014: *Geodynamics.* Cambridge University Press, Cambridge, U.K., 636 pp.

[Ve] D. Veres, L. Bazin, A. Landais, H. Toye Mahamadou Kele, B. Lemieux-Dudon, F. Parrenin, P. Martinerie, E. Blayo, T. Blunier, E. Capron, J. Chappellaz, S. Rasmussen, M. Severi, A. Svensson, B. Vinther, and E. Wolff, 2013: *The Antarctic ice core chronology (AICC2012): an optimized multi-parameter and multi-site dating approach for the last 120 thousand years.* Climate of the Past, **9**, 1733–1748.

[Vit] L. Vittuari, C. Vincent, M. Frezzotti, F. Mancini, S. Gandolfi, G. Bitelli, and A. Capra, 2004: *Space geodesy as a tool for measuring ice surface velocity in the Dome C region and along the ITASE traverse.* Annals of Glaciology, **39**, 402–408.

[Vin] B.M. Vinther, S.L. Buchardt, H.B. Clausen, D. Dahl-Jensen, S.J. Johnsen, D.A. Fisher, R.M. Koerner, D. Raynaud, V. Lipenkov, K.K. Andersen, T. Blunier, S.O. Rasmussen, J.P. Steffensen, and A.M. Svensson, 2004: *Holocene thinning of the Greenland ice sheet.* Nature, **461**, 385–388.

[We] M. Werner, U. Mikolajewicz, M. Heimann, and G. Hoffmann, 2000: *Borehole versus isotope temperatures on Greenland: Seasonality does matter.* Geophysical Research Letters, **27**, 723–726.

Appendices

Appendix A

Boundary condition R code

A.1   EDC

```
 1 setwd("~/Documents/C/simple_melt_EDC/R_script/EDC_time_series")
 2 library(ncdf)
 3
 4 ###########Pollard Time Series Loading and processing#########
 5
 6 #Load Pollard's data
 7 nc1 <- open.ncdf("fort.92_1f_ts.nc");
 8 nc2 <- open.ncdf("fort.92_2f_ts.nc");
 9 nc3 <- open.ncdf("fort.92_3f_ts.nc");
10 nc4 <- open.ncdf("fort.92_4f_ts.nc");
11 nc5 <- open.ncdf("fort.92_5f_ts.nc");
12
13 #Extract latitude and longitude
14 lat<-get.var.ncdf(nc1,"alatd")
15 lon<-get.var.ncdf(nc1,"alond")
16 #Find the closest point to Dome C
17 bestDist=100;
18 bestx<-0;
19 besty<-0;
20 dcx<--75.1
21 dcy<-123.33
22 dist<-rep(0,141*141)
23 i<-1
24 for (x in 1:141){
25   for(y in 1:141){
26     xp<-lat[x,y];
27     yp<-lon[x,y];
28     dist[i]<-sqrt((xp-dcx)^2+(yp-dcy)^2);
29     if(dist[i]<bestDist){
30       bestx<-x;
31       besty<-y;
32       bestDist<-dist[i]
33     }
34     i=i+1
35   }
36 }
37 #Extract height and temperature
38 h1<-get.var.ncdf(nc1,"h")
39 h2<-get.var.ncdf(nc2,"h")
40 h3<-get.var.ncdf(nc3,"h")
41 h4<-get.var.ncdf(nc4,"h")
42 h5<-get.var.ncdf(nc5,"h")
43 t1<-get.var.ncdf(nc1,"ts")
44 t2<-get.var.ncdf(nc2,"ts")
45 t3<-get.var.ncdf(nc3,"ts")
```

```
46 t4<-get.var.ncdf(nc4,"ts")
47 t5<-get.var.ncdf(nc5,"ts")
48 #Extract the height and temperature at dome C
49 htot<-c(h5[bestx,besty,3:221],h4[bestx,besty,22:221],h3[bestx,besty,22:221],h2[bestx,besty
        ,22:221],h1[bestx,besty,22:203])
50 ttot<-c(t5[bestx,besty,3:221],t4[bestx,besty,22:221],t3[bestx,besty,22:221],t2[bestx,besty
        ,22:221],t1[bestx,besty,22:203])
51 #Create a linear spline with one point every 100yr for temperature and height
52 x_100h<-seq(-5*10^6,0,100)
53 spl_height<-spline(htot,n=length(x_100h),method="natural")
54 spl_temp<-spline(ttot,n=length(x_100h),method="natural")
55 #Creat variable containing temperature and height for the last 4Myr
56 Pol_temp<-as.data.frame(cbind(seq(-4000000,0,by=100),spl_temp[[2]][10001:50001]))
57 Pol_height<-as.data.frame(cbind(seq(-4000000,0,by=100),spl_height[[2]][10001:50001]))
58 colnames(Pol_temp)<-c("time","val")
59 colnames(Pol_height)<-c("time","val")
60 #Reverse the time series to have present on first position
61 Pol_temp$time<-rev(Pol_temp$time)
62 Pol_temp$val<-rev(Pol_temp$val)
63 Pol_height$time<-rev(Pol_height$time)
64 Pol_height$val<-rev(Pol_height$val)
65
66 ###########Lisiecki and Raymo time series Loading#########
67 #Load LR time serie
68 LR04_full<-as.matrix(read.table("LR04stack.txt",header=FALSE, sep="\t"))
69 #Create a linear spline with one point every 100 hr
70 LR_spl<-spline(LR04_full[,c(1,2)],n=4855/5*50+1,method="natural")
71 #Creat variable containing LR value for the last 4Myr
72 LR04<-as.data.frame(cbind(seq(-4000000,0,by=100),rev(LR_spl[[2]][c(1:40001)])))
73 colnames(LR04)<-c("time","val")
74 #Reverse the time series to have present on first position
75 LR04$time<-rev(LR04$time)
76 LR04$val<--rev(LR04$val)
77
78 ###########Dome C time series Loading#########
79 #Load Dome C time series
80 DomeC_full<-as.matrix(read.table("EDC_AICC2012_official.csv",header=TRUE, sep="\t"))
81 #Create linear splines for depth, accumulation rate and thining with 1 point every 100yr
82 DomeC_depth<-as.data.frame(spline(DomeC_full[,c(1,2)],xout=seq(0,3190,by=1),method="natural"))
83 DomeC_acc<-as.data.frame(spline(DomeC_full[,c(2,6)],xout=seq(0,807900,by=100),method="natural"
        ))
84 DomeC_thining<-as.data.frame(spline(DomeC_full[,c(2,7)],xout=seq(0,807900,by=100),method="
        natural"))
85 colnames(DomeC_depth)<-c("depth","Time")
86 colnames(DomeC_acc)<-c("time","val")
87 colnames(DomeC_thining)<-c("time","val")
88 #Reverse time axis
89 DomeC_acc$time<--DomeC_acc$time
90 DomeC_thining$time<--DomeC_thining$time
91
92 ###########Jouzel time series Loading#########
93 #Load Jouzel time series
94 Jouzel_full<-as.matrix(read.table("jouzel07sci.txt",header=TRUE,fill=TRUE))
95 #Create linear splines for accumulation rate with 1 point every 100yr and the EDC3 depth-Time
        relation
96 Jouzel_depth<-as.data.frame(spline(Jouzel_full[,c(2,3)],xout=seq(0,3190,by=1),method="natural"
        ))
97 Jouzel_temp<-as.data.frame(spline(Jouzel_full[,c(2,5)],xout=seq(0,3190,by=1),method="natural")
        )
98 colnames(Jouzel_depth)<-c("depth","Time")
99 colnames(Jouzel_temp)<-c("depth","temp")
100 #Change the Time scale to AICC2012, create a spline with a point every 100yr and reverse the
        time axis
101 Jouzel_temp$depth<-DomeC_depth$Time
102 Jouzel_temp<-as.data.frame(spline(Jouzel_temp,xout=seq(0,807900,by=100),method="natural"))
103 Jouzel_temp[1,2]<-0.4
104 colnames(Jouzel_temp)<-c("time","val")
105 Jouzel_temp$time<--Jouzel_temp$time
106
107 ###########EDC2007 time series Loading#########
108 #Load EDC2007 time series
109 EDC2007_full<-as.matrix(read.table("edc2007accum.txt",header=TRUE,fill=TRUE))
```

```r
110  head(EDC2007_full)
111  #Create linear splines for depth and accumulation rate with 1 point every 100yr
112  EDC2007_acc<-as.data.frame(spline(EDC2007_full[,c(2,3)],xout=seq(0,3190,by=1),method="natural"
       ))
113  EDC2007_thining<-as.data.frame(spline(EDC2007_full[,c(2,4)],xout=seq(0,3190,by=1),method="
       natural"))
114  EDC2007_height<-as.data.frame(spline(EDC2007_full[,c(2,5)],xout=seq(0,3190,by=1),method="
       natural"))
115  colnames(EDC2007_acc)<-c("time","val")
116  #plot(Jouzel_depth$Time[1:200],Jouzel_temp$val[1:200],ylim=c(-6,3))
117  colnames(EDC2007_height)<-c("time","val")
118  #Change the Time scale to AICC2012, create a spline with a point every 100yr and reverse the
       time axis
119  EDC2007_acc$time<-DomeC_depth$Time
120  EDC2007_thining$time<-DomeC_depth$Time
121  EDC2007_height$time<-DomeC_depth$Time
122  EDC2007_acc<-as.data.frame(spline(EDC2007_acc,xout=seq(0,807900,by=100),method="natural"))
123  EDC2007_thining<-as.data.frame(spline(EDC2007_thining,xout=seq(0,807900,by=100),method="
       natural"))
124  EDC2007_height<-as.data.frame(spline(EDC2007_height,xout=seq(0,807900,by=100),method="natural"
       ))
125  colnames(EDC2007_acc)<-c("time","val")
126  colnames(EDC2007_thining)<-c("time","val")
127  colnames(EDC2007_height)<-c("time","val")
128  EDC2007_acc$time<--EDC2007_acc$time
129  EDC2007_thining$time<--EDC2007_thining$time
130  EDC2007_height$time<--EDC2007_height$time
131
132  ###### Plots for Time scale######
133  pdf("age_depth_models.pdf",width=8,height=4.5)
134  par(mfrow=c(2,1))
135  par(mar=c(3.5,3,2,1))
136  plot(Jouzel_depth$Time,(Jouzel_depth$Time-DomeC_depth$Time),xlim=c(8e5,0),type="l",col="black"
       ,main="EDC2007 minus AICC 2012 time scale",ylab="",xlab="")
137  mtext(side = 2, text =expression(paste(Delta,"Time (yr)")), line = 1.9)
138  mtext(side = 1, text = "AICC 2012 Time B.P (yr)", line = 2.2)
139
140  plot(Jouzel_full[,3],Jouzel_full[,5],type="l",col="blue",xlim=c(8e5,0),main="EDC2007
       temperature with EDC2007 and AICC 2012 timescale",xlab="",ylab="")
141  lines(-Jouzel_temp[,1],Jouzel_temp[,2],col="red")
142  legend("topleft", legend = c("EDC2007 Time-depth model", "AICC2012 Time-depth model"),col=c("
       blue","red"),bty = "n",lwd=c(1,1))
143  mtext(side = 2, text ="Temperature (K)", line = 1.9)
144  mtext(side = 1, text = "AICC 2012 Time B.P (yr)", line = 2.2)
145  dev.off()
146
147  ########MODELS#######
148  #Crate shorter time series for LR and Pollard to match with other time series
149  LR04_short<-LR04[c(1:8080),]
150  Pol_temp_short<-Pol_temp[c(1:8080),]
151  Pol_height_short<-Pol_height[c(1:8080),]
152
153  ####Temperature model####
154  #Find the time lag between LR04 and Jouzel temp, firt the multiplication factor
155  best<-array(0,100)
156  for (i in 1:100){
157    LR04_spl<-as.data.frame(spline(LR04_short$time*(1.05+i/1000),LR04_short$val,xout=seq
         (0,-807900,by=-100),method="natural"))
158    colnames(LR04_spl)<-c("time","val")
159    a=ccf(as.vector(scale(LR04_spl$val)),as.vector(scale(Jouzel_temp$val)),lag.max=30,plot=FALSE
         )
160    best[i]=max(a[[1]]);
161  }
162  best_i_t<-which(best==max(best))
163  #Then the lag
164  LR04_spl<-as.data.frame(spline(LR04_short$time*(1.05+best_i_t/1000),LR04_short$val,xout=seq
       (0,-807900,by=-100),method="natural"))
165  colnames(LR04_spl)<-c("time","val")
166  a=ccf(as.vector(scale(LR04_spl$val)),as.vector(scale(Jouzel_temp$val)),lag.max=50,plot=FALSE)
167  best_lag<-which(a[[1]]==max(a[[1]]))-50
168  Time_lag_LR<-best_lag*100
169  a=ccf(as.vector(scale(Pol_temp_short$val)),as.vector(scale(Jouzel_temp$val)),lag.max=100,plot=
```

```
          FALSE)
170  LR04_spl<-as.data.frame(spline(LR04_short$time*(1.05+best_i_t/1000)+Time_lag_LR,LR04_short$val
          ,xout=seq(0,-807900,by=-100),method="natural"))
171  colnames(LR04_spl)<-c("time","val")
172
173  ###MEASURES AND LR
174  LR04_long<-as.data.frame(spline(LR04$time*(1.05+best_i_t/1000)+Time_lag_LR,LR04$val,xout=seq
          (0,-4010000,by=-100),method="natural"))
175  colnames(LR04_long)<-c("time","val")
176  LR04EDC_short<-LR04_spl
177  LR04EDC_long<-LR04_long
178  LR04EDC_short$val<-scale(LR04_spl$val)*var(Jouzel_temp$val)^0.5+mean(Jouzel_temp$val)-55
179  LR04EDC_long$val<-(LR04_long$val-mean(LR04_spl$val))*(var(Jouzel_temp$val)/var(LR04_spl$val))
          ^0.5+mean(Jouzel_temp$val)-55
180
181  ####Accumulation model####
182  LR04EDC_short$acc<--0.005+1.5*2^((LR04EDC_short$val)/10)
183  LR04EDC_long$acc<--0.005+1.5*2^((LR04EDC_long$val)/10)
184
185  ####Thickness Model####
186  #Find the best time lag
187  a<-ccf(as.vector(scale(EDC2007_height$val)),as.vector(scale(Jouzel_temp$val+218.65)),lag.max
          =50,plot=FALSE)
188  best_i<-which(a[[1]]==max(a[[1]]))-50
189  Time_lag_thick<-best_i*100
190  LR04EDC_short_lag<-as.data.frame(spline(LR04_spl$time-Time_lag_thick,LR04_spl$val,xout=seq
          (0,-807900,by=-100),method="natural"))
191  colnames(LR04EDC_short_lag)<-c("time","val")
192  LR04EDC_long_lag<-as.data.frame(spline(LR04_long$time-Time_lag_thick,LR04_long$val,xout=seq
          (0,-4010000,by=-100),method="natural"))
193  colnames(LR04EDC_long_lag)<-c("time","val")
194  LR04EDC_long_lag$val<-(LR04EDC_long_lag$val-mean(LR04EDC_short_lag$val))*(var(EDC2007_height$
          val)/var(LR04EDC_short_lag$val))^0.5+mean(EDC2007_height$val)+3270.3
195  LR04EDC_short_lag$val<-scale(LR04EDC_short_lag$val)*var(EDC2007_height$val)^0.5+mean(EDC2007_
          height$val)+3270.3
196  LR04EDC_short_lag_smooth<-LR04EDC_short_lag
197  sp<-100
198  for (i in (1+sp):(length(LR04EDC_short_lag[,1])-sp)){
199    LR04EDC_short_lag_smooth$val[i+sp/2]=sum(LR04EDC_short_lag$val[(i):(i+sp)])/(sp+1)
200  }
201  LR04EDC_long_lag_smooth<-LR04EDC_long_lag
202  sp<-100
203  for (i in (1+sp):(length(LR04EDC_long_lag[,1])-sp)){
204    LR04EDC_long_lag_smooth$val[i+sp/2]=sum(LR04EDC_long_lag$val[(i):(i+sp)])/(sp+1)
205  }
206  LR04EDC_short$thick<-LR04EDC_short_lag_smooth$val
207  LR04EDC_long$thick<-LR04EDC_long_lag_smooth$val
208
209  ###Paste the time series together###
210  LR04EDC<-LR04EDC_long
211  LR04EDC$val[1:length(Jouzel_temp$val)]<-Jouzel_temp$val-55
212  LR04EDC$acc[1:length(DomeC_acc$val)]<-DomeC_acc$val
213  LR04EDC$thick[1:length(EDC2007_height$val)]<-EDC2007_height$val+3275.3
214
215  ##Correction for the pasting point (transition smoothing)####
216  LR04EDC_cor<-LR04EDC
217  sp<-50
218  for (i in (1):(100)){
219    LR04EDC_cor$thick[8000+i+sp/2]=sum(LR04EDC$thick[(8000+i):(8000+i+sp)])/(sp+1)
220  }
221  LR04EDC$thick<-LR04EDC_cor$thick
222
223
224
225  ###Export data###
226  write.table(rev(Jouzel_temp$val[1:1501]-55+273.15), "LR04-EDC_temp_150kyr.dat", sep = "\t",
          row.names = FALSE,col.names = FALSE)
227  write.table(rev(DomeC_acc$val[1:1501]/3600/24/365), "LR04-EDC_acc_150kyr.dat", sep = "\t", row
          .names = FALSE,col.names = FALSE)
228  write.table(rev(EDC2007_height$val[1:1501]+3309), "LR04-EDC_thickness_150kyr.dat", sep = "\t",
          row.names = FALSE,col.names = FALSE)
229
```

```
230  write.table(rev(LR04EDC$val[1:10001]+273.15), "LR04-EDC_temp_1Myr.dat", sep = "\t", row.names
         = FALSE,col.names = FALSE)
231  write.table(rev(LR04EDC$acc[1:10001]/3600/24/365), "LR04-EDC_acc_1Myr.dat", sep = "\t", row.
         names = FALSE,col.names = FALSE)
232  write.table(rev(LR04EDC$thick[1:10001]), "LR04-EDC_thickness_1Myr.dat", sep = "\t", row.names
         = FALSE,col.names = FALSE)
233
234  write.table(rev(LR04EDC$val[1:40001]+273.15), "LR04-EDC_temp_4Myr.dat", sep = "\t", row.names
         = FALSE,col.names = FALSE)
235  write.table(rev(LR04EDC$acc[1:40001]/3600/24/365), "LR04-EDC_acc_4Myr.dat", sep = "\t", row.
         names = FALSE,col.names = FALSE)
236  write.table(rev(LR04EDC$thick[1:40001]), "LR04-EDC_thickness_4Myr.dat", sep = "\t", row.names
         = FALSE,col.names = FALSE)
237
238  ### Borehoel record ans age scale
239
240  EDCt<-as.matrix(read.table("temperature-sampled-1m-EpicaRome.dat",header=FALSE, sep=" "))
241  EDCt2<-as.matrix(read.table("EDC temp profile.csv",header=FALSE, sep="\t"))
242  EDCt2
243  EDCt[,1]<--EDCt[,1]
244  EDCt[,2]<-rev(EDCt[,2])
245  EDCt2[,2]<-3255+EDCt2[,2]
246
247  EDCTime<-as.matrix(read.table("EDC_AICC2012_official.csv",header=TRUE, sep="\t"))
248  EDCTime<-EDCTime[,c(1,2)]
249  head(EDCTime)
250  tail(EDCTime)
251  EDCTime[,1]<-3275-EDCTime[,1]
252  EDCTime[,2]<-EDCTime[,2]+55
253  Time_EDC<-as.data.frame(spline(EDCTime,xout=seq(75,3255,by=15),method="natural"))
254
255  write.table(EDCt[,2]+273.15, "EDC_temp_forC.dat", sep = "\t", row.names = FALSE,col.names =
         FALSE)
256  write.table(Time_EDC[,2], "EDC_Time_forC.dat", sep = "\t", row.names = FALSE,col.names = FALSE
         )
```

code/EDC_time_series.r

A.2   GRIP

```
 1  setwd("~/Documents/C/simple_melt_EDC/R_script/greenland_time_series")
 2
 3  pdf("Greenland_time_series.pdf",width=8,height=4)
 4
 5  par(mfrow=c(1,3))
 6  par(mar=c(4,4,3,1))
 7
 8  #####PART 1 Surface temperature and ice thickness #########
 9  #Load the temperature reconstruction by Dahl-Jensen,1998
10  #Extrapolate it to have one point every 100ka
11  #Reconstruct the ice thickness changes and accumulation rate according to Dahl-Jensen,1998
         footnotes 9 and 11
12  #Export these 3 times series with one point every 100ka to be used in the model
13  temp_raw<-as.matrix(read.table("data/ddjtemp.txt",header=TRUE,sep="\t"))
14  #Shift the time scal by 2kyr to have 0 in 2000
15  temp_raw[,1]<--(temp_raw[,1]-2000)
16  temp_raw
17  #Extrapolate 1 point every 100yr
18  temp_spl<-as.data.frame(spline(temp_raw,xout=seq(32000,0,by=-100),method="natural"))
19  #Create a complementary time series between 32000 yr B.P. and 100000 yr B.P.
20  #unsing values from Dahl-Jensen, 1998
21  temp_compl<-matrix(c
         (-100000,-86000,-71500,-64000,-58000,-52000,-39000,-37000,-33500,-32000,-42,-48,-52,-52,-54,-53,-56,-5
         ,ncol=2,nrow=10)
22  temp_sup<-matrix(c
         (-100000,-86000,-71500,-64000,-58000,-52000,-39000,-37000,-33500,-32000,-25000,-20000,-15000,-10000,-80
         ,ncol=2,nrow=18)
23  temp_inf<-matrix(c
```

```
         (-100000,-86000,-71500,-64000,-58000,-52000,-39000,-37000,-33500,-32000,-25000,-20000,-15000,-10000,-80
         ,ncol=2,nrow=18)
24  temp_inf[,1]<--temp_inf[,1]
25  temp_sup[,1]<--temp_sup[,1]
26  temp_compl[,1]<--temp_compl[,1]
27  #temp_compl<-matrix(c
         (-100000,-86000,-71500,-64000,-58000,-52000,-39000,-37000,-33500,-32000,-42,-46,-50,-50,-52,-51,-54,-5
         ,ncol=2,nrow=10)
28  #Add points linearly interpolated to gett a better smoothed spline
29  temp_compl_approx<-as.data.frame(approx(temp_compl,xout=seq(100000,32100,by=-100), method = "
         linear"))
30  temp_sup<-as.data.frame(approx(temp_sup,xout=seq(100000,0,by=-100), method = "linear"))
31  temp_inf<-as.data.frame(approx(temp_inf,xout=seq(100000,0,by=-100), method = "linear"))
32  #Combine the 2 time series to have one surface temperature record from -100000 to today
33  temp_grip<-rbind(temp_compl_approx,temp_spl)
34  #Reconstruction of the ice thickness using values from JOHNSEN, DAHL-JENSEN, DANSGAARD and
         NIELS,1995
35  #and Dahl-Jensen,1998
36  thickness_points<-matrix(c(100000,75000,50000,20000,10000,0,3010,2995,2980,2980,3230,3030),
         ncol=2,nrow=6)
37  #Add points linearly extrapolated in between to get a better smoothed extrpolation
38  thickness_approx<-approx(thickness_points,xout=seq(100000,0,by=-3000), method = "linear")
39  thickness_spl<-as.data.frame(spline(thickness_approx,xout=seq(100000,0,by=-100),method="
         natural"))
40  thickness_grip<-thickness_spl
41
42
43  ########PART 2 Borehole temperature and age model#########
44  temp_borehole<-as.matrix(read.table("data/griptemp.txt",header=TRUE,sep="\t"))
45  temp_grip_bore<-as.data.frame(spline(temp_borehole,xout=seq(0,floor(thickness_grip[1001,2]),by
         =1),method="natural"))
46  #Create an extrapolation with a point 25 meters of age record to be able to compare to model
         outpute
47  age_borehole<-as.matrix(read.table("data/GRIP_age.txt",header=TRUE,sep="\t"))
48  age_borehole[,1]<-(3025-age_borehole[,1])
49  age_grip<-as.data.frame(spline(age_borehole,xout=seq(300,2960,by=10),method="natural"))
50
51
52  ########PART 2 Accumulation rate#########
53
54  #Reconstruction of the accumulation rate following Dah-Jensen,1998:
55  #L(T)=L0*exp[0.0467(T,ÄiT0),Äi0.000227(T,ÄiT0)^2], where L(T) is the accumulation
56  #rate at the surface temperature T, T0 is the present
57  #ice accumulation rate, which is 0.23 m/year at GRIP
58  #and 0.49 m/year at Dye 3, and T0 is the present
59  #surface temperatures at the sites: ,Äi31.7 C at GRIP
60  #and ,Äi20.1 C at Dye 3, respectively (9)
61  acc_0=0.23
62  T_0=-31.7
63  acc_grip<-temp_grip
64  acc_sup<-temp_sup
65  acc_inf<-temp_inf
66  acc_grip[,2]<-acc_0*exp(0.0467*(temp_grip[,2]-T_0)-0.00027*(temp_grip[,2]-T_0)^2)
67  acc_sup[,2]<-acc_0*exp(0.0467*(temp_sup[,2]-T_0)-0.00027*(temp_sup[,2]-T_0)^2)
68  acc_inf[,2]<-acc_0*exp(0.0467*(temp_inf[,2]-T_0)-0.00027*(temp_inf[,2]-T_0)^2)
69
70  ###Accumulation from inverse age model###
71
72  wdef<-function(z,thickness,m){
73    return ((z/ thickness)^(m+1))
74  }
75  wdefp<-function(z,thickness,p){
76    return (1-(p+2)/(p+1)*(1-(z/ thickness))+1/(p+1)*(1-(z/ thickness))^(p+2))
77  }
78  age_SPLC<-as.data.frame(spline(age_borehole[seq(1,10000,by=500),],xout=seq(274,3025,by=1),
         method="natural"))
79  age_SPLC2<-as.data.frame(spline(age_borehole[,c(2,1)],xout=seq(0,100000,by=100),method="
         natural"))
80  dadzC<-age_SPLC
81  age_SPLC
82  for (i in c(2:2751)){
83    dadzC[i,3]<-(age_SPLC[i-1,2]-age_SPLC[i+1,2])/2
```

```
84  }
85  dadzC [1 ,3] < -( age_SPLC [1 ,2] - age_SPLC [2 ,2])
86  dadzC [2752 ,3] < -( age_SPLC [2751 ,2] - age_SPLC [2752 ,2])
87  dadz_SPLC < -as.data.frame(spline(dadzC[,c(2,3)],xout=seq(0,100000,by=100),method="natural"))
88  dhdtC < -dadz_SPLC
89  for (i in c(2:1001)){
90      dhdtC [i ,2] < -( rev ( thickness_grip [ ,2])[i -1] - rev ( thickness_grip [ ,2])[ i +1])/200
91  }
92  dhdtC [1 ,2] < -( rev ( thickness_grip [ ,2])[1] - rev ( thickness_grip [ ,2])[2])/100
93  dhdtC [1001 ,2] < -( rev ( thickness_grip [ ,2])[1000] - rev ( thickness_grip [ ,2])[1001])/100
94
95  acc1 =1/( wdef ( rev ( age_SPLC2 [1:1001 ,2]) , thickness_grip [ ,2][1:1001] ,0.4)* rev ( dadz_SPLC [1:1001 ,2])
        )- rev ( dhdtC [1:1001 ,2])
96  acc2 =1/( wdef ( rev ( age_SPLC2 [1:1001 ,2]) , thickness_grip [ ,2][1:1001] ,0.6)* rev ( dadz_SPLC [1:1001 ,2])
        )- rev ( dhdtC [1:1001 ,2])
97  acc3 =1/( wdef ( rev ( age_SPLC2 [1:1001 ,2]) , thickness_grip [ ,2][1:1001] ,0.8)* rev ( dadz_SPLC [1:1001 ,2])
        )- rev ( dhdtC [1:1001 ,2])
98  acc4 =1/( wdefp ( rev ( age_SPLC2 [1:1001 ,2]) , thickness_grip [ ,2][1:1001] ,0.5)* rev ( dadz_SPLC
        [1:1001 ,2]))- rev ( dhdtC [1:1001 ,2])
99  acc5 =1/( wdefp ( rev ( age_SPLC2 [1:1001 ,2]) , thickness_grip [ ,2][1:1001] ,2)* rev ( dadz_SPLC [1:1001 ,2]))
        - rev ( dhdtC [1:1001 ,2])
100 acc6 =1/( wdefp ( rev ( age_SPLC2 [1:1001 ,2]) , thickness_grip [ ,2][1:1001] ,3)* rev ( dadz_SPLC [1:1001 ,2]))
        - rev ( dhdtC [1:1001 ,2])
101
102 ### Export time series #####
103 write.table(temp_grip[,2]+273.15, "GRIP_temp_100kyr.dat", sep = "\t", row.names = FALSE,col.
        names = FALSE)
104 write.table((acc_grip[,2])/3600/24/365, "GRIP_acc_100kyr.dat", sep = "\t", row.names = FALSE,
        col.names = FALSE)
105 write.table(thickness_grip[,2], "GRIP_thick_100kyr.dat", sep = "\t", row.names = FALSE,col.
        names = FALSE)
106 write.table(age_grip[,2], "GRIP_age_forC.dat", sep = "\t", row.names = FALSE,col.names = FALSE
        )
107 write.table(rev(temp_grip_bore[,2]+273.15), "GRIP_temp_forC.dat", sep = "\t", row.names =
        FALSE,col.names = FALSE)
108
109 write.table(rev(age_SPLC2[1:1001,2]), "GRIP_age_depth_forC_100kyr.dat", sep = "\t", row.names
        = FALSE,col.names = FALSE)
110 write.table(rev(dadz_SPLC[1:1001,2]), "GRIP_dadz_forC_100kyr.dat", sep = "\t", row.names =
        FALSE,col.names = FALSE)
111 write.table(rev(dhdtC[1:1001,2]), "GRIP_dhdt_forC_100kyr.dat", sep = "\t", row.names = FALSE,
        col.names = FALSE)
```

<div align="center">code/greenland_time_serie.r</div>

Appendix B

Deformation energy: technical details

The two terms leading to internal heat production included in the model are:

$$\dot{\mathrm{E}}_{\mathrm{I}}^{\mathrm{def}}(z,t) = \dot{\epsilon}_{\mathrm{xx}}\sigma_{\mathrm{xx}} + \dot{\epsilon}_{\mathrm{yy}}\sigma_{\mathrm{yy}} + \dot{\epsilon}_{\mathrm{zz}}\sigma_{\mathrm{zz}} + 2(\dot{\epsilon}_{\mathrm{xy}}\sigma_{\mathrm{xy}} + \dot{\epsilon}_{\mathrm{xz}}\sigma_{\mathrm{xz}} + \dot{\epsilon}_{\mathrm{yz}}\sigma_{\mathrm{yz}}) \tag{B.1}$$

$$\dot{\mathrm{E}}_{\mathrm{I}}^{\mathrm{comp}}(z,t) = \frac{\mathrm{w}(z,t)\mathrm{P}(z,t)}{\rho(z,t)}\frac{\partial \rho(z,t)}{\partial z} \tag{B.2}$$

Where (1.19) can be expressed as (see 1.1.6):

$$\dot{\mathrm{E}}_{\mathrm{I}}^{\mathrm{def}}(z,t) = 2\left[\left(\frac{\partial \mathrm{w}}{\partial z}\right)^2 + \left(\frac{\partial \mathrm{u}}{\partial z}\right)^2\right]^{\frac{2}{3}}\mathrm{A(T)}^{-\frac{1}{3}} \tag{B.3}$$

The equation (B.2) can directly be implemented. Indeed, ω and ρ are already computed in the model, P is obtained by summing ρ over the depth and $\frac{\partial \rho(z,t)}{\partial z}$ can be obtained by a numerical derivative of the density (using a central difference, except for the edges).

Regarding (B.3), the term $\frac{\partial \mathrm{w}}{\partial z}$ can easily be computed analytically from (1.3) or (1.4) or numerically. The values of u(z) are given in [D-J] as a function the reduced depth z/H and the surface horizontal speed $\mathrm{u_S}$ and for various values of the distance from the dome summit. The values used are $\mathrm{u_S} = 0.015\,\mathrm{m\,yr^{-1}}$ [Vit] (considered as constant over time) and a distance of 6 Km from the dome summit [Vit].

Data are graphically read from Fig. 3 of [D-J] – 14 points are read and the curve is interpolated and numerically derived in R. It is possible have a good fit of the derivative with a power of 6 polynomial, but due to the slow computation of power function in C, the curve is approximated by 7 pieces of linear models[1] shown in Figure B.1 left panel.

---

[1]Including a power of six computation double the run time of the model
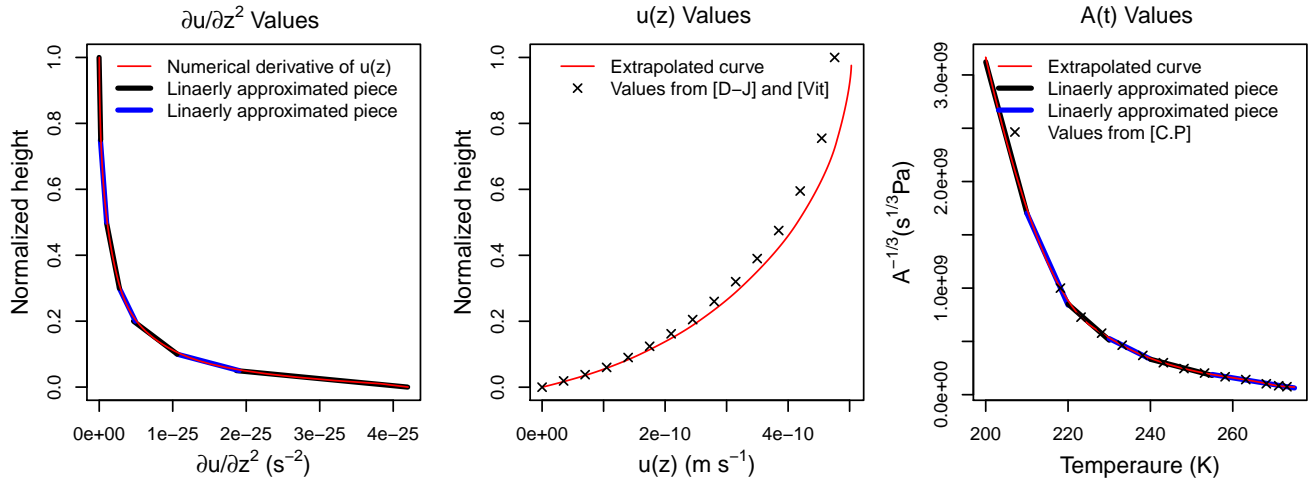
Figure B.1: Left: Values of $\frac{\partial u}{\partial z}^2$ obtained from numerical derivative of u(z) (red line) and approximation by pieces of linear model (red and black lines). Center: Values of u(z) read from [D-J] with position and surface velocity from [Vit] (black crosses) and numerical extrapolation of these values (red lines). Right: Values of A(t) red from [C.P] (to the power $-1/3$, black crosses), extrapolation of these values (red line) and approximation by pieces of linear model (red and black lines).

Typical values for A(T) are given in [C.P]. All the values in [C.P] Table are taken (with a value of $1 \cdot 10^{-27} \mathrm{s}^{-1} \mathrm{Pa}{-3}$ added for $-55°C$), elevated to the power $-\frac{1}{3}$ and interpolated in R (the interpolation is made until $-55°C$). As for $\frac{\partial u}{\partial z}$, the curve is approximated by piece of linear model (six in this case). The result is shown in Figure B.1 right panel.

These two approximations by pieces explain the small discontinuities of values and derivative on internal energy shown on Figure 1.4 of Section 1.1.6.

Appendix C

Changing boundary conditions at EDC: details

As discussed in Section 3.2.2, the time series can be corrected in different manner. The temperature can be corrected by a constant value during glacial periods (defined in 2 on page 53) or linearly corrected to adjust the LGM value to as chosen value:

$$T(t) = (T(t) - T(today)) \cdot \frac{T(LGM) - T(today)}{T(LGM) - T(today) + \Delta T} + T(today)$$

Where ΔT is the correction of the last glacial glacial maximum/Holocene temperature difference. The accumulation rate can be either taken directly from the LR04EDC time series or computed with (1.25) and the corrected temperature profile.

The results for the four combination of corrections and the free parameters value corresponding to the best result are shown in Figures C.1 to C.4 and in Tables C.1 and C.2. The result found in Section 3.2.2 are repeated here for comparison.

It can be observed that a re-computation of the accumulation rate leads to a slightly less good age scale and a warmer profile on the top. This temperature difference comes from the higher accumulation rate during the Holocene when (1.25) is used instead of the EDC07 time series (which is used for the first part of the LR04EDC time series), as shown in Figure 1.9. Moreover, the re-computed accumulation rate requires a slightly higher ground heat flux ($+1$ mWm^{-2}).

Table C.1: Range of cold period temperature correction ΔT, accumulation rate correction ΔA and valley width L giving acceptable output for Dome C with values for form factor and ground heat flux as in Table C.2.

ΔT (K)	ΔA (%) LR04EDC	ΔA (%) From (1.25)	L (m)
$\in (+2.5, +3.5)$	$\in (+5, +15)$	$\in (-5, -15)$	$\in (3000, 5000)$

Table C.2:   Value of the ground heat flux Q_G for the different accepted values of the form factor m and valley width L. Run 1: Temperature corrected only during glacial periods by a constant value and accumulation rate from the LR04EDC time series. Run 2 : Temperature corrected by linear squeezing and accumulation rate from the LR04EDC time series. Run 3: Temperature corrected only during glacial periods by a constant value, and accumulation rate computed from (1.25) and the corrected temperature time series. Run 4 : Temperature corrected by linear squeezing, and accumulation rate computed from (1.25) and the corrected temperature time series.

m	L	Q_G (mWm^{-2}) Run 1	Q_G (mWm^{-2}) Run 2	Q_G (mWm^{-2}) Run 3	Q_G (mWm^{-2}) Run 4
0.45	3000	52	52	53	53
0.45	5000	53	53	54	54
0.50	3000	53	53	54	54
0.50	5000	54	54	55	55
0.55	3000	54	54	55	55
0.55	5000	55	55	56	56
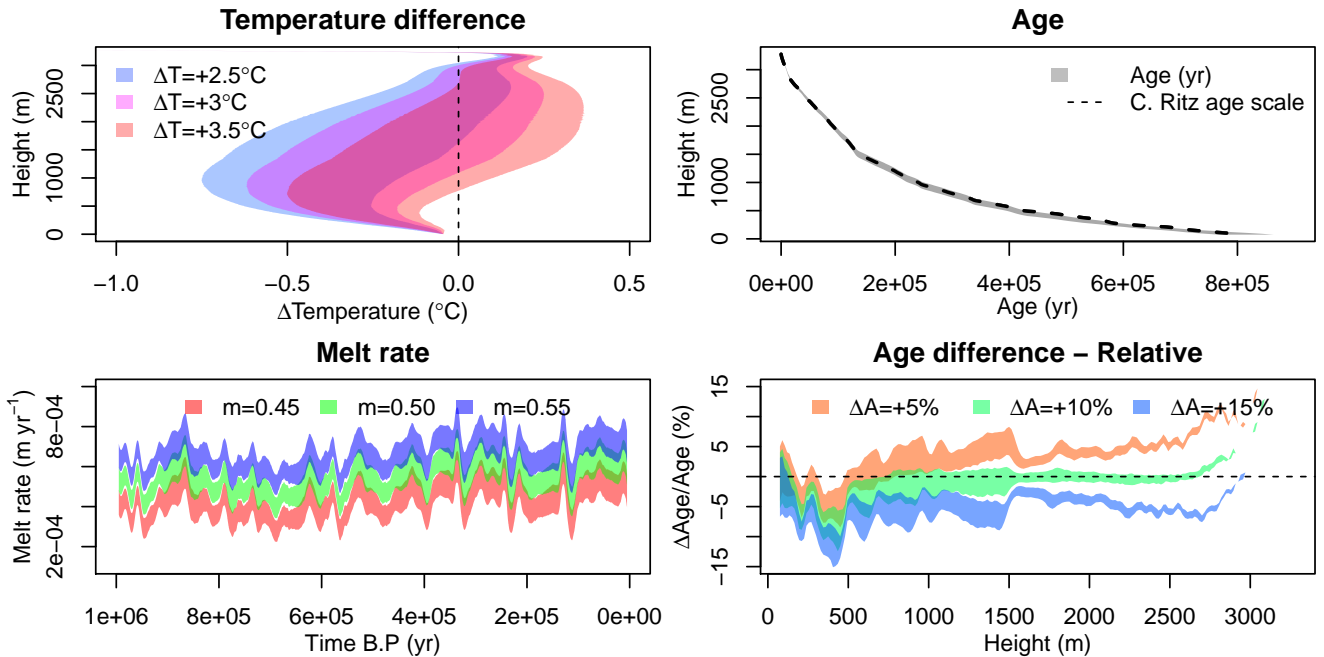
Figure C.1: Run 1: Temperature corrected only during glacial periods by a constant value, and accumulation rate from the LR04EDC time series. Top left: Temperature difference with the borehole measure. Top right: Age scale. Bottom left: Melt rate. Bottom right: Age difference with the AICC 2012 time scale. Corresponding free parameters are given in Tables C.1 and C.2.
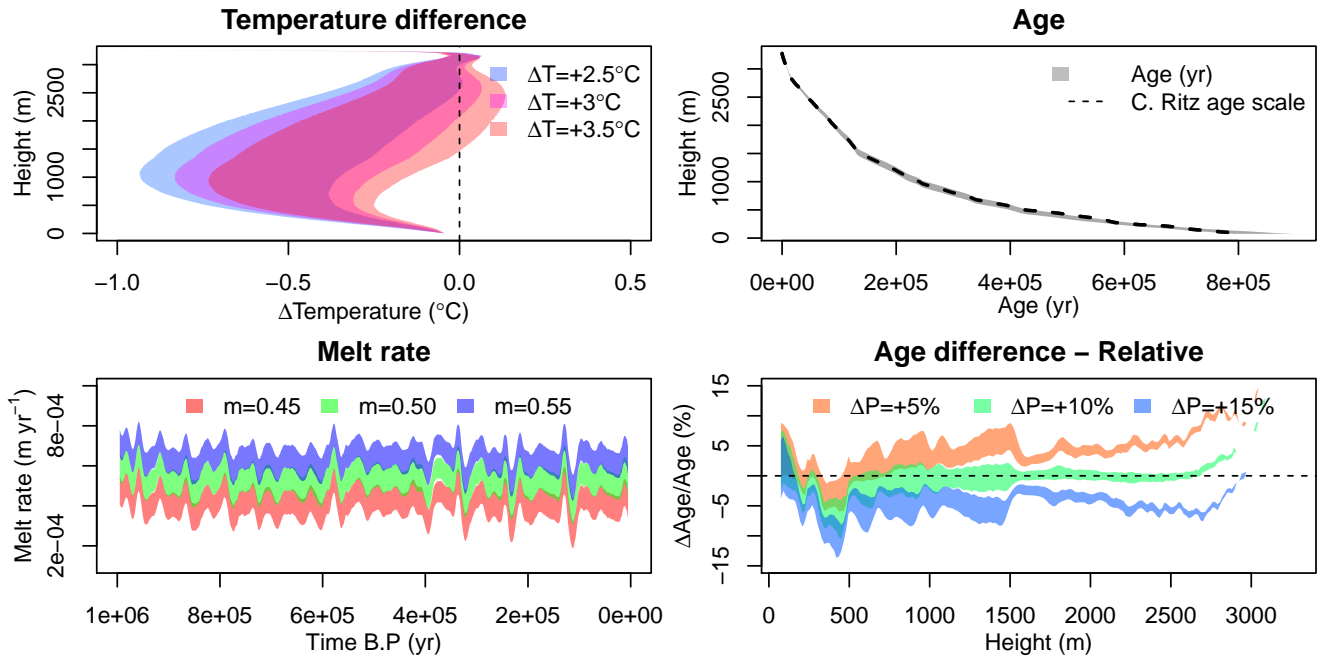
Figure C.2: Run 2 : Temperature corrected by linear squeezing and accumulation rate from the LR04EDC time series. Top left: Temperature difference with the borehole measure. Top right: Age scale. Bottom left: Melt rate. Bottom right: Age difference with the AICC 2012 time scale. Corresponding free parameters are given in Tables C.1 and C.2.
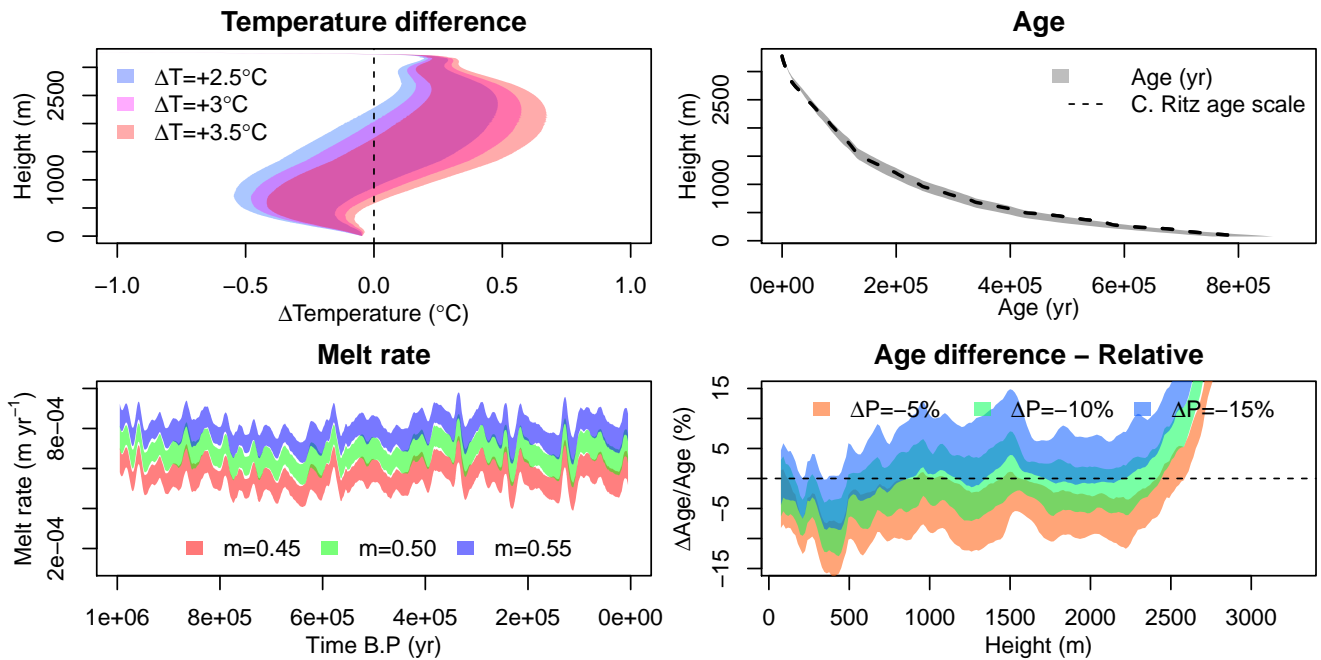
Figure C.3: Run 3: Temperature corrected only during glacial periods by a constant value, and accumulation rate computed from (1.25) and the corrected temperature time series. Top left: Temperature difference with the borehole measure. Top right: Age scale. Bottom left: Melt rate. Bottom right: Age difference with the AICC 2012 time scale. Corresponding free parameters are given in Tables C.1 and C.2.
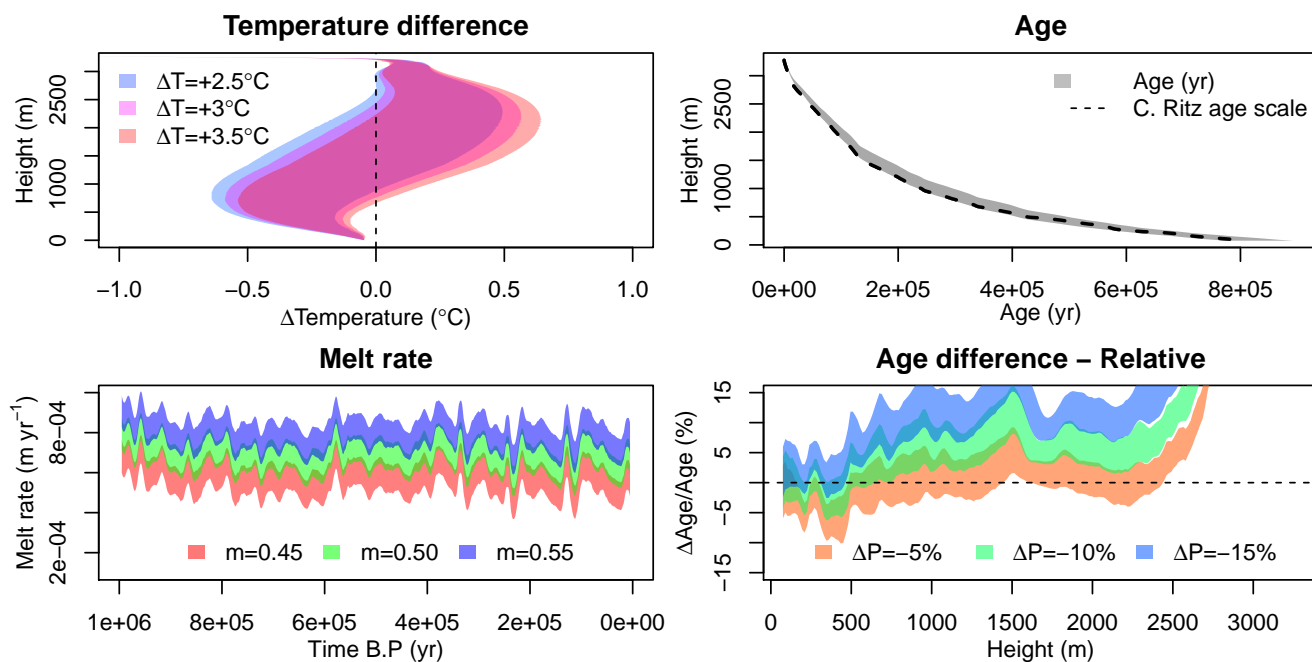
Figure C.4: Run 4 : Temperature corrected by linear squeezing, and accumulation rate computed from (1.25) and the corrected temperature time series. Top left: Temperature difference with the borehole measure. Top right: Age scale. Bottom left: Melt rate. Bottom right: Age difference with the AICC 2012 time scale. Corresponding free parameters are given in Tables C.1 and C.2.

Appendix D

C code

The code presented here is the general version fo the model applicable for Dome C. When ran for GRIP, for the oldest ice research and for the various sensitivity tests, the model has been slightly modified. The values for the free parameters are entered at the beginning of the *main.c* file whereas some general parameters are defined as preprocessor variable at the beginning of the *main.h* file. See comments on the code for details.

The has been compiled with gcc on two different linux systems: on Ubuntu 14.04.2 LTS (kernel version 3.13.0-43-generic), and on Ubuntu 15.04 (kernel version 3.19.0-15-generic). The -*Wall* (security), -*fopenmp* (link to multi-processing library, Open MP should be installed) and -*lm* (link to math library) flags are used. The -*pg* flag can be added to get a profile of the execution.

D.1   Main.c

```
 1  // Written by Adrien Michel
 2  // adrien.michel@no-log.org
 3  // For the purpose of a Master thesis at the
 4  // Climate and Environmental Group
 5  // And
 6  // Oeschger Center for Climate Change Research
 7  // University of Bern
 8  // February 2016
 9
10  // This code is developed to run on Linux machine, but should run on Windows or Mac OS
11
12  //The only parameters defined in main.c are the free parameters of the model, the correction
        to the boundary condition time series,
13  //and the initial temperature profile for spin up
14  //For any other modification see the main.h file
15
16  //Include the header file main.h, containing all the key functions and parameters.
17  #include "main.h"
18
19  int main()
20  {
21      //Set internal timer
22      double begin = omp_get_wtime();
23
24      //Tables to load data
25      double surfaceTempLoad[T],iceThicknessLoad[T],accLoad[T]= {0};
26      double ageGRIP[Z],tGRIP[Z]= {0};
27      int i=0;
```

```
28
29      //DEfine a table to store a summary of the various runs performed
30      double** summary;
31      summary = malloc( 15000  * sizeof(*summary));
32      for (i = 0; i < 15000; i++)
33      {
34          summary[i] = malloc(11*sizeof(summary));
35      }
36
37      //Load boundary condition LR04EDC time series. Data file exist for 1Myr of 4Myr
38      readTable(surfaceTempLoad,"time_series/LR04-EDC_temp_1Myr.dat");
39      readTable(iceThicknessLoad,"time_series/LR04-EDC_thickness_1Myr.dat");
40      readTable(accLoad,"time_series/LR04-EDC_acc_1Myr.dat");
41
42      //Load borehole temperature and age profile for comparison
43      readTable(ageGRIP,"time_series/EDC_age_forC.dat");
44      readTable(tGRIP,"time_series/EDC_temp_forC.dat");
45
46      //The following array contain the value of the different free parameters
47      double mwArr[] = {0.5}; //Form factor
48      int mwN=sizeof(mwArr) / sizeof(mwArr[0]);
49      int mwL=0;
50      double QGArr[] = {0.054}; //Ground heat flux
51      int QGN=sizeof(QGArr) / sizeof(QGArr[0]);
52      double TcorArr[] = {1}; //Correction for temperature between 6000 and 2000 BP in K
53      int TcorN=sizeof(TcorArr) / sizeof(TcorArr[0]);
54      double TcorArr2[] = {3}; //Correction for cold periods temperature in K
55      int TcorN2=sizeof(TcorArr2) / sizeof(TcorArr2[0]);
56      double PcorArr[] = {10}; //Correction of accumulation time series in %
57      int PcorN=sizeof(PcorArr) / sizeof(PcorArr[0]);
58      double deltaHArr[] = {100}; //Depth of the valley
59      int deltaHN=sizeof(deltaHArr) / sizeof(deltaHArr[0]);
60      double lenArr[] = {5000}; //Width of the valley
61      int lenN=sizeof(lenArr) / sizeof(lenArr[0]);
62      double flatArr[] = {500}; //Flat arrea at the bottom of the valley
63      int flatN=sizeof(flatArr) / sizeof(flatArr[0]);
64
65      int tot=mwN*QGN*TcorN*PcorN*deltaHN*lenN*flatN*TcorN2; //Number of run, the size of the
            summary table should be bigger
66
67      // Loops for the values of the free parameter
68      int count=0;
69      #pragma omp parallel for //Initialize the core splitting, should be placed in front of a
            loop having if possible a number of elements corresponding to a multiple of the core
            numbers
70      for (mwL=0; mwL<mwN; mwL++)
71      {
72      double mw=mwArr[mwL];
73      int QGL=0;
74      for (QGL=0; QGL<QGN; QGL++)
75      {
76      double QG=QGArr[QGL];
77      int TcorL=0;
78      for (TcorL=0; TcorL<TcorN; TcorL++)
79      {
80      double tCor=TcorArr[TcorL];
81      int TcorL2=0;
82      for (TcorL2=0; TcorL2<TcorN2; TcorL2++)
83      {
84      double tCor2=TcorArr2[TcorL2];
85      int PcorL=0;
86      for (PcorL=0; PcorL<PcorN; PcorL++)
87      {
88      double pCor=PcorArr[PcorL];
89      int deltaHL=0;
90      for (deltaHL=0; deltaHL<deltaHN; deltaHL++)
91      {
92      double deltaH=deltaHArr[deltaHL];
93      int lenL=0;
94      for (lenL=0; lenL<lenN; lenL++)
95      {
96      double len=lenArr[lenL];
```

```
97      int flatL=0;
98      for (flatL=0; flatL<flatN; flatL++)
99      {
100     double flat=flatArr[flatL];
101
102         double surfaceTemp[T],iceThickness[T],acc[T],melt[T]= {0};
103         double spin_up_temp[Z],spin_up_temp2[Z],temperatureBorder[Z],tnew[Z]= {0};
104
105         //Dynamically allow the memory for the temperature matrix
106         double** temperature;
107         int li,co=0;
108         temperature = malloc( Z  * sizeof(*temperature));
109         for (li = 0; li < Z; li++)
110         {
111             temperature[li] = malloc(T*sizeof(temperature));
112         }
113         for (li = 0; li < Z; li++)
114         {
115             for (co=0; co<T; co++)
116             {
117                 temperature[li][co] = 0;
118             }
119         }
120
121         //Loop over the time steps to implement the correction on the time series
122         for(li=0; li<T; li++)
123         {
124             surfaceTemp[li]=surfaceTempLoad[li];
125             iceThickness[li]=iceThicknessLoad[li];
126             acc[li]=accLoad[li]*3600*24*365/31556926;
127
128             if((li>38900 && li<39850) ( li< 38650 && li > 38100) ( li< 37800 && li > 37650)
129                 ( li< 37500 && li > 36800) ( li< 36600 && li > 36100) ( li< 35700 && li >
                    35200) ( li< 34700 && li > 34400) ( li< 33700 && li > 33300) ( li< 32600 && li
                     > 32400) ( li< 32050 && li > 31900)  ( li< 31300 && li > 3700) )
129             {
130                 surfaceTemp[li]+=tCor2;
131             }
132             else
133             {
134                 if (li>39980 && li<40001)
135                 {
136                     surfaceTemp[li]=surfaceTemp[li]-tCor;
137                 }
138             }
139             acc[li]+=acc[li]*pCor/100.;
140         }
141
142         // set the initial temperature profile
143         double Tmelt=273.16-9.8*7.42*1E-8*921*iceThickness[0];
144         double Tmelt2=273.16-9.8*7.42*1E-8*921*(iceThickness[0]-deltaH);
145         double Tsurf=surfaceTemp[0];
146
147         //Spin up the second profile used for the valley effect
148         if(deltaH!=0)
149         {
150             for(li=0; li <=(int)(iceThickness[0]-deltaH); li++)
151             {
152                 spin_up_temp2[li]=Tmelt2+(Tsurf-Tmelt2)*pow(li/(iceThickness[0]-deltaH),1);
153             }
154             spin_up(spin_up_temp2,iceThickness[0]-deltaH,surfaceTemp[0],acc[0],QG,mw,
                    temperatureBorder,deltaH,1,len,flat);
155             for(li=0; li <=(int)(iceThickness[0]-deltaH); li++)
156             {
157                 temperatureBorder[li]=spin_up_temp2[li];
158             }
159
160         }
161
162         //Spin up the main profile first without the valley effect and a second time if the
                valley effect is enables
163         for(li=0; li <=(int)iceThickness[0]; li++)
```

```
164             {
165                     spin_up_temp[li]=Tmelt+(Tsurf-Tmelt)*pow(li/iceThickness[0],1);
166             }
167         spin_up(spin_up_temp,iceThickness[0],surfaceTemp[0],acc[0],QG,mw,temperatureBorder,
                deltaH,1,len,flat);
168
169         if(deltaH!=0){
170             spin_up(spin_up_temp,iceThickness[0],surfaceTemp[0],acc[0],QG,mw,temperatureBorder
                    ,deltaH,0,len,flat);
171         }
172
173         for(li=0; li<Z; li++)
174         {
175             temperature[li][0]=spin_up_temp[li];
176             tnew[li]=spin_up_temp[li];
177         }
178
179         //Loop over all the time steps
180         int time=1;
181         float time_for_loop=0;
182         for (time=1; time<T; time++)
183         {
184             double begin2=omp_get_wtime();
185
186             for(li=0; li <Z; li++)
187             {
188                 tnew[li]=0;
189             }
190             for(li=0; li <=(int)iceThickness[time-1]; li++)
191             {
192                 tnew[li]=temperature[li][time-1];
193             }
194             if(deltaH!=0)
195             {
196                 t_solve(temperatureBorder,time-1, iceThickness[time-1]-deltaH, iceThickness[
                        time]-deltaH, surfaceTemp[time],acc[time],melt,QG,mw,temperatureBorder,
                        deltaH,1,len,flat);
197             }
198
199             t_solve(tnew,time-1, iceThickness[time-1], iceThickness[time], surfaceTemp[time],
                    acc[time],melt,QG,mw,temperatureBorder,deltaH,0,len,flat);
200
201             tempScale(tnew,  iceThickness[time-1], iceThickness[time], surfaceTemp[time]);
202
203             if(deltaH!=0)
204             {
205                 tempScale(temperatureBorder,iceThickness[time-1]-deltaH, iceThickness[time]-
                        deltaH, surfaceTemp[time]);
206             }
207
208             for(li=0; li <=(int)iceThickness[time]; li++)
209             {
210                 temperature[li][time]=tnew[li];
211             }
212             time_for_loop+=(double)(omp_get_wtime() - begin2); //Store the loop time
213         }
214         //Print the time for the run and the individual loop mean time
215         printf("\nIntegration ok in: %f secondes  ",time_for_loop);
216         printf("Mean run time: %f miliseconds\n",time_for_loop/(T-1.)*1000.);
217
218
219         //Compute the difference with the age profile for 213 points and compute the mean of
                the difference
220         double** ageRel;
221         ageRel = malloc( 213  * sizeof(*ageRel));
222         for (i = 0; i < 213; i++)
223         {
224             ageRel[i] = malloc(2*sizeof(ageRel));
225         }
226         double ageDiff=0;
227         for(li=0; li<213; li++)
228         {
```

```
229                    float height=li*15+75;
230                    int age=T-1;
231                    while (height<iceThickness[age] && age>0)
232                    {
233                        height+=((acc[age]*31556926*100-melt[age]*100-(iceThickness[age]-iceThickness[
                                age-1]))*wDef((double)height,iceThickness[age],mw)+melt[age]*100);
234                        age--;
235                    }
236                    ageRel[li][0]=li*75+15;
237                    ageRel[li][1]=(T-1-age)*100;
238                    ageDiff+=fabs(ageRel[li][1]-ageGRIP[li]);
239                }
240            ageDiff/=213;
241
242            //Compute the difference with the borehole  temperature profile below 600 m deep (
                    because upper part of the measurements are affected by seasonality)
243            double tempDiff=0;
244            double tnew2[Z]= {0};
245            for(li=0; li<=(int)iceThickness[T-1]-7; li++)
246            {
247                tnew2[li]=temperature[li][T-1];
248                if(li<((int)iceThickness[T-1]-600))
249                {
250                    tempDiff+=fabs(tnew2[li]-tGRIP[li]);
251                }
252            }
253            tempDiff/=(iceThickness[T-1]);
254
255            // Generate a file name with the free parameters
256            char fileName[120]="";
257            char sufix[120]="";
258            sprintf(sufix, "%s_m_%.3f_Q_%.2f_Pcor_%.0f_Tcor_%.1f_Tcor2_%.1f_dH_%.0f_len_%.0f_flat_
                    %.0f","_EDC",mw,QG*1000,pCor,tCor,tCor2,deltaH,len,flat);
259            // Save the temperature profile, the melt rate and the age scale
260            sprintf(fileName, "%s%s","temp_profile",sufix);
261            saveTable(tnew,fileName,Z);
262            sprintf(fileName, "%s%s","meltRate",sufix);
263            saveTable(melt,fileName,T);
264            sprintf(fileName, "%s%s","ageRel",sufix);
265            save2DTable(ageRel,fileName,340,2);
266
267            //Create a summary table for all the runs
268            summary[count][0]=mw;
269            summary[count][1]=QG;
270            summary[count][2]=pCor;
271            summary[count][3]=tCor;
272            summary[count][4]=tCor2;
273            summary[count][5]=deltaH;
274            summary[count][6]=len;
275            summary[count][7]=flat;
276            summary[count][8]=tempDiff;
277            summary[count][9]=ageDiff;
278            summary[count][10]=tnew2[0]-273.15;
279            #pragma omp atomic
280            count++;
281            #pragma omp flush (count)
282            printf("END LOOP : %d/%d\n\n",count,tot);
283
284            //Uncomment the line below to save the whole temperature matrix
285            //saveTemp(temperature);
286
287            for (li = 0; li < Z; li++)
288            {
289                double* currentIntPtr = temperature[li];
290                free(currentIntPtr);
291            }
292            fflush(stdout);
293            count++;
294 }}}}}}}}
295
296    //Save the summary table
297    save2DTable(summary,"Summary",15000,11);
```

```
298
299      printf("Run OK -- in %f seconds\n",(double)(omp_get_wtime() - begin));
300
301      return 0;
302 }
```

<div align="center">code/main.c</div>

D.2   Main.h

```
 1 // Written by Adrien Michel
 2 // adrien.michel@no-log.org
 3 // For the purpose of a Master thesis at the
 4 // Climate and Environmental Group
 5 // And
 6 // Oeschger Center for Climate Change Research
 7 // University of Bern
 8 // February 2016
 9
10 // This code is developed to run on Linux machine, but should run on Windows or Mac OS
11
12 //*******LIBRARY**********
13 // Open MP should be installed (http://openmp.org/wp/)
14 // -lm and -fopenmp flags must be used for compilation
15 #include <stdio.h>
16 #include <stdlib.h>
17 #include <string.h>
18 #include <math.h>
19 #include <time.h>
20 #include <omp.h>
21
22 //*******Pre processor variables**********
23 // The preprocessor variables allow to change parameters of the model. If non accepted values
        are entered a fatal error may occur, values are not verified.
24 #define Z 3400//height of the table
25 #define T 40001//10001 //width of the table
26 #define S 1500 //Length of the spin up in hYr
27 #define TYPE "CN"//Scheme used, values can be CN or expl
28 #define rhoSnow 350 //Value of the snow density used in the computation of the density profile
29 #define THERMAL "CP" // Correction for the thermal parameters, can be CP,SC or FI
30 #define RHO "FIRN" // Set the density profile to realistic (FIRN) or constant (CONST)
31 #define VERTICAL "FI" // Set the flux shape function to FI or PA
32
33
34 //*******Definition the  main variables defined in main.h***********
35
36
37 //*************File management functions*************
38
39 // char* name= --> Used to store the name of the created file
40 // char fileName[120] --> Used to combine the relative path and the file name of the created
        file
41
42
43 //*************Computational function*************
44
45 //int thickness --> Ice thickness obtained from main.c, transformed to an integer
46 //double tnew[Z] --> Table used to store the new temperature computed
47 //double told[Z] --> Table used to store the temperature at the begining of the time step
        obtained from main.c
48 //int i,li --> Variables used in loops
49 //double L =333500 --> Latent heat of ice in J/kg
50 //double rho[Z] --> Table used to store the computed density profile
51 //double rhoIce[Z] --> Table used to compute the pure ice density profile (for actual
        temperature and pressure)
52 //double a[Z],b[Z] -->
53 //double a2[Z],b2[Z] -->
54 //double m --> Melt rate
```

```
55 //double tground --> Ground temperature
56 //double K[Z]  --> Ice thermal conductivity
57 //double cp[Z] --> Ice specific heat capacity
58 //double w[Z] --> Table used to store the velocity profile
59 //double w_def[Z] --> Table used to store the flux shape function values
60 //double delt=31556926.*100 --> Time step (100kyr)
61 //double delz=1 -->  Height Step
62 //double tmelt --> Melt temperature computed with the bottom pressure
63 //double dhdt  --> Thickness time derivative
64 //double se[Z]  --> Internal heat (valley effect + internal heat production) power density
65
66 //double rhoIceConst=917  -->  Pure ice density for a first approximation of the density
      profile
67 //double rhoSnowConst  --> Snow density (value defined in header)
68 //double R=8.3144  --> Gaz constant
69 //double k0  --> Value computed in the H-L density model
70 //double k1  --> Value computed in the H-L density model
71 //double z55  --> Value computed in the H-L density model
72 //double z0[Z]  --> Values computed in the H-L density model
73
74 //double c1[Z]  --> Sub-diagonal matrix element computed in the explicit scheme
75 //double c2[Z]  --> Diagonal matrix element computed in the explicit scheme
76 //double c3[Z]  --> Sub-diagonal matrix element computed in the explicit scheme
77
78 //double l[Z]  --> Sub-diagonal matrix element computed in the C-N scheme
79 //double d[Z]  --> Diagonal matrix element computed in the C-N scheme
80 //double r[Z]  --> Sub-diagonal matrix element computed in the C-N scheme
81 //double b[Z]  --> Vector to be multiplied with he inverse matrix in the C-N scheme (explicit
      part)
82
83
84
85 //*******Functions prototype************
86
87 //*************File management functions**************
88
89 void readTable(double* table,char* fileName);
90 // Read the indicated data file and store it to the given table. Size is not controlled, to
      avoid error the table should be large enough
91
92 void saveTemp(double **table);
93 // Save temperature profile for the last time step of the model
94
95 void saveTable(double *table, char *name, int tabSize);
96 // Save general 1D table containing doubles.
97
98 void save2DTable(double **table, char *name, int nRow, int nCol);
99 // Save general 2D table containing doubles
100
101
102
103 //*************Computational functions*************
104
105 void spin_up(double *temperature, double thick, double tsurf,double acc, double QG, double mw,
      double* tborder, double deltaH,int border,double len, double flat);
106 //Perform the spin_up of the model for the given time using the CN scheme
107
108 void t_solve(double *temperature, int time, double thickness, double thicknessFuture, double
      tsurf,double acc,double* melt, double QG, double mw, double* tborder,double deltaH, int
      border,double len, double flat);
109 //Getting the 1D array temperature a t-1, return the temperature at T.
110 //This function calls various function to compute all the needed parameters
111 //Finally, this function calls the defined algorithm to compute the temperature
112
113 void setRho(double* rho, double *rhoIce, double* temp, int thickness,double acc);
114 //Compute the density profile
115
116 void setHeatVar(double *K,double *cp,double *told,int thickness,double *rho, double* rhoIce);
117 //Compute the values of the K and c thermal variables, called by spin_up() and t_solve()
118
119 void computeMelt(double* m,double* tground,double* rho,double L,double K0,double cp0, double
      told1,double told0,double thickness,double delz,double QG);
```

```
120 // Compute the melt rate , called by spin_up () and t_solve ()
121
122 double wDef ( double z, double thickness , double mw );
123 // Compute the flux shape function values , called by spin_up () and t_solve ()
124
125 void setABW ( double * a, double * b, double * w, double * cp , double * K, double * rho , double delt , double
        delz , double acc , double m, double dhdt , double * w_def , int thickness );
126 // Compute the vertical velocity and the a,b ( explicit scheme ) or alpha , beta (CN scheme ) values ,
        called by spin_up () and t_solve ()
127
128 void setSe ( double *se , double * rho , double *w, double *cp , double *K, double delt , int thickness ,
        double * told , double deltaH , double dhdt , double * tborder , int border , double len , double
        flat );
129 // Compute the internal energy production and the lateral heat flux ( valley effect )
130
131 double getDwdz ( double *w, int z, int thickness );
132 // Compute the vertical derivative of the vertical velocity profile , called by setSe ()
133
134 double getA ( double t );
135 // Compute the creep factor A values from piecewise linear approximation , called by setSe ()
136
137 double getDudz ( double zh );
138 // Compute the vertical derivative of horizontal velocity profile from piecewise linear
        approximation , called by setSe ()
139
140 void integrate_CN ( double * tint , double * told , double * alpha , double * beta , double * alpha1 , double *
        beta1 , double tground , double tsurf , int thickness , int step , double * se );//, double * se );
141 // Compute the temperature using the CN scheme , called by spin_up () and t_solve ()
142
143 void integrate_expl ( double * told , double * a, double * b, double tground , double tsurf , double
        tsurf_old , int thickness , double * se );
144 // Compute the temperature using the explicit scheme , called by  t_solve ()
145
146 void tempScale ( double * told , double thickness , double thicknessFuture , double tsurf );
147 // Scale the temperature profile to the thickness value of the next step
148
149
150
151 //*************Definition of the functions*************
152
153 //*************File management functions*************
154
155 void readTable ( double * table , char * fileName )
156 {
157     // Read a table from the file called "filename" and store it into the double table called
            "table". Table should be 1D. "filename" can contain directory path.
158     FILE *fp;
159     int li =0;
160     double a =0;
161     if (( fp = fopen ( fileName , "r" ))== NULL )
162     {
163         printf ( "Cannot open file: %s\n", fileName );
164     }
165     else
166     {
167         printf ( "File: %s opened in reading mode\n", fileName );
168         while ( fscanf (fp ,"%lf",&a )==1)
169         {
170             table [li ]= a;
171             li ++;
172         }
173         if ( fclose ( fp )==0)
174         {
175             printf ( "File imported successfully (%d data) and closed: %s \n\n", li -1, fileName );
176         }
177         else
178         {
179             printf ( "Not able to close: %s \n\n", fileName );
180         }
181     }
182 }
183
```

```c
184  void saveTemp(double **table)
185  {
186      // Read the 2D double table containing the temperature profiles history and store it a
             file. The default path is a folder called "export".
187      FILE *fp;
188      int li,co=0;
189      char* name="Temperature_";
190      char fileName[120]="";
191      strcat(fileName,name);
192      strcat(fileName,TYPE);
193      strcat(fileName,".dat");
194      char path[120]="";
195      strcat(path,"export/");
196      strcat(path,fileName);
197      if((fp=fopen(path, "w+"))==NULL)
198      {
199          printf("Cannot open file.\n");
200      }
201      else
202      {
203          printf("File opened: %s\n...writing...\n",fileName);
204          for (li=0; li<Z; li++)
205          {
206              for (co=0; co<T; co+=10)
207              {
208                  if(table[li][co]>0)
209                  {
210                      fprintf(fp,"%f \t",table[li][co]);
211                  }
212                  else
213                  {
214                      fprintf(fp,"NaN \t");
215                  }
216              }
217              fprintf(fp,"\n");
218          }
219          fclose(fp);
220          printf("File closed: %s \n\n",fileName);
221      }
222  }
223
224  void saveTable(double *table,char *name,int tabSize)
225  {
226      // Read the 1D double table called "table" and store it a file called "filename".  Table
             should be tab delimited. "filename" can contain directory path. The default path is a
             folder called "export". The table size should be passed as parameter.
227      FILE *fp;
228      int li=0;
229      char fileName[120]="";
230      strcat(fileName,name);
231      strcat(fileName,"_");
232      strcat(fileName,TYPE);
233      strcat(fileName,".dat");
234      char path[120]="";
235      strcat(path,"export/");
236      strcat(path,fileName);
237      if((fp=fopen(path, "w+"))==NULL)
238      {
239          printf("Cannot open file: %s\n",fileName);
240      }
241      else
242      {
243          printf("File oppened:%s\n...writing...\n",fileName);
244          for (li=0; li<tabSize; li++)
245          {
246              fprintf(fp,"%f \n",table[li]);
247          }
248          fclose(fp);
249          printf("File closed: %s \n\n",fileName);
250      }
251  }
252
```

```
253  void save2DTable(double **table,char *name,int nRow,int nCol)
254  {
255      // Read the 2D double table called "table" and store it a tab delimited file called "
             filename". The default path is a folder called "export". The table dimensions should
             be passed as parameter.
256      FILE *fp;
257      int li=0;
258      int co=0;
259      char fileName[120]="";
260      strcat(fileName,name);
261      strcat(fileName,"_");
262      strcat(fileName,TYPE);
263      strcat(fileName,".dat");
264      char path[120]="";
265      strcat(path,"export/");
266      strcat(path,fileName);
267      if((fp=fopen(path, "w+"))==NULL)
268      {
269          printf("Cannot open file: %s\n",fileName);
270      }
271      else
272      {
273          printf("File oppened:%s\n...writing...\n",fileName);
274          for (li=0; li<nRow; li++)
275          {
276              for (co=0; co<nCol; co++)
277              {
278                  if(co!=0)
279                  {
280                      fprintf(fp,"\t");
281                  }
282                  fprintf(fp,"%f",table[li][co]);
283              }
284              fprintf(fp,"\n");
285          }
286          fclose(fp);
287          printf("File closed: %s \n\n",fileName);
288      }
289  }
290
291
292
293  //*************Computational functions*************
294
295  void spin_up(double *told, double thick, double tsurf,double acc,double QG,double mw,double*
         tborder, double deltaH,int border,double len, double flat)
296  {
297      // Perform a spin up for the time indicated in header (time in hyr). The spin up is done
             with a 2-passes implicit scheme.
298      double begin3=omp_get_wtime();
299      int thickness=(int)thick;
300      int i,li=0;
301      double L=333500;
302      double rho[Z],rhoIce[Z]= {[0 ... Z-1] = 921};
303      double a[Z],b[Z],a2[Z],b2[Z]= {0};
304      double m,tground=0;
305      double K[Z],cp[Z], w[Z], w_def[Z]= {0};
306      double delt=31556926.*100.;
307      double delz=1.;
308      double dhdt=0;
309      double se[Z]= {0};
310      for(li=0; li <=thickness; li++)
311      {
312          w_def[li]=wDef ((double) li, (double) thickness,mw);
313      }
314      for(i=0; i<S; i++)
315      {
316          double tint[Z],rho_first[Z],se_first[Z]= {0};
317          setRho(rho,rhoIce, told, thickness, acc);
318          setHeatVar(K, cp, told, thickness,rho,rhoIce);
319          computeMelt(&m,&tground,rho,L,K[1],cp[0],told[1],told[0],thick,delz,QG);
320          told[0]=tground;
```

```
321              setABW(a,b,w,cp,K,rho,delt,delz,acc,m,dhdt,w_def,thickness);
322              setSe(se,rho,w,cp,K,delt,thickness,told,deltaH,dhdt,tborder, border,len,flat);
323              integrate_CN(tint,told, a, b, a, b, tground, tsurf, thickness, 1,se);
324              for(li=0; li <=thickness; li++)
325              {
326                  rho_first[li]=rho[li];
327              }
328              // Second pass
329              setRho(rho,rhoIce, tint, thickness, acc);
330              setHeatVar(K, cp, tint, thickness,rho,rhoIce);
331              computeMelt(&m,&tground,rho_first,L,K[1],cp[0],tint[1],tint[0],thick,delz,QG);
332              tint[0]=tground;
333              setABW(a2,b2,w,cp,K,rho,delt,delz,acc,m,dhdt,w_def,thickness);
334              setSe(se,rho,w,cp,K,delt,thickness,told,deltaH,dhdt,tborder, border,len,flat);
335              for(li=0; li <=thickness; li++)
336                  {
337                      if(se[li]>0)
338                      {
339                          se[li]=(se[li]+se_first[li])/2;
340                      }
341                  }
342              integrate_CN(tint,told, a, b, a2, b2, tground,tsurf, thickness, 1,se);
343              for(li=0; li <=thickness; li++)
344              {
345                  told[li]=tint[li];
346              }
347          }
348      printf("Spin off OK -- in %f seconds\n",(double)(omp_get_wtime() - begin3));
349 }
350
351
352 void t_solve(double *temperature, int time, double thick, double thickFuture, double tsurf,
        double acc, double* melt, double QG, double mw,double* tborder,double deltaH,int border,
        double len, double flat)
353 {
354
355      int thickness=(int)thick;
356      double told[Z]= {0};
357      int i,li=0;
358      double L=333500;
359      double rho[Z],rhoIce[Z]= {[0 ... Z-1] = 921};
360      double a[Z],b[Z],a2[Z],b2[Z]= {0};
361      double m,tground=0;
362      double K[Z],cp[Z], w[Z], w_def[Z]= {0};
363      double delt=31556926.*100.;
364      double delz=1.;
365      double dhdt=(thickFuture-thick)/delt;
366      double se[Z]= {0};
367
368      for(li=0; li <=thickness; li++)
369      {
370          told[li]=temperature[li];
371          w_def[li]=wDef ((double) li, (double) thick,mw);
372      }
373      double tsurf_old=told[thickness];
374
375      if(strcmp(TYPE,"CN")==0)//C-N scheme
376      {
377          double rep=1; //Define the number of passes -1 in the C-N scheme
378          double tint[Z],rho_first[Z],rho_mean[Z],se_first[Z]= {0};
379          double cp0,K1=0;
380
381          setRho(rho,rhoIce, told, thickness, acc);
382          setHeatVar(K, cp, told, thickness,rho,rhoIce);
383          computeMelt(&m,&tground,rho,L,K[1],cp[0],told[1],told[0],thick,delz,QG);
384          setABW(a,b,w,cp,K,rho,delt,delz,acc,m,dhdt,w_def,thickness);
385          setSe(se,rho,w,cp,K,delt,thickness,told,deltaH,dhdt,tborder, border,len,flat);
386          integrate_CN(tint,told, a, b, a, b, tground, tsurf, thickness, 1,se);
387          for(li=0; li <=thickness; li++)
388          {
389              rho_first[li]=rho[li];
390          }
```

```
391            cp0=cp[0];
392            K1=K[1];
393            melt[time]=m*31556926.;
394
395            for (i=0; i<(int)rep; i++)
396            {
397                setRho(rho,rhoIce, tint, thickness, acc);
398                setHeatVar(K, cp, tint, thickness,rho,rhoIce);
399                for(li=0; li <=thickness; li++)
400                {
401                    rho_mean[li]=(rho[li]+rho_first[li])/2;
402                }
403                computeMelt(&m,&tground,rho_mean,L,(K[1]+K1)/2,(cp[0]+cp0)/2,(tint[1]+told[1])/2,(
                        tint[0]+told[0])/2,thick,delz,QG);
404                tint[0]=tground;
405                setABW(a2,b2,w,cp,K,rho,delt,delz,acc,m,dhdt,w_def,thickness);
406                setSe(se,rho,w,cp,K,delt,thickness,tint,deltaH,dhdt,tborder, border,len,flat);
407                for(li=0; li <=thickness; li++)
408                {
409                    if(se[li]>0)
410                    {
411                        se[li]=(se[li]+se_first[li])/2;
412                    }
413                }
414                integrate_CN(tint,told, a, b, a2, b2, tground, tsurf, thickness, 1,se);
415            }
416            for(li=0; li <=thickness; li++)
417            {
418                told[li]=tint[li];
419            }
420            melt[time]+=m*31556926;
421            melt[time]/=2;
422        }
423        else if(strcmp(TYPE,"EXPL")==0) // Explicit scheme
424        {
425            setRho(rho,rhoIce, told, thickness, acc);
426            setHeatVar(K, cp, told, thickness,rho,rhoIce);
427            computeMelt(&m,&tground,rho,L,K[1],cp[0],told[1],told[0],thick,delz,QG);
428            setABW(a,b,w,cp,K,rho,delt,delz,acc,m,dhdt,w_def,thickness);
429            setSe(se,rho,w,cp,K,delt,thickness,told,deltaH,dhdt,tborder, border,len,flat);
430            integrate_expl(told, a,b, tground, tsurf,  tsurf_old, thickness, se);
431            melt[time]+=m*31556926;
432        }
433        for(li=0; li <=thickness; li++)
434        {
435            temperature[li]=told[li];
436        }
437 }
438
439 void setRho(double* rho, double *rhoIce,double* temp, int thickness,double acc)
440 {
441     int li=0;
442     double rhoIceConst=917;
443     double rhoSnowConst=350;
444     double R=8.3144;
445     double k0=11*exp(-10160/(R*temp[thickness]));
446     double k1=575*exp(-21400/(R*temp[thickness]));
447     acc=acc*31556926.;
448     double z55 = 1/(rhoIceConst/1000*k0)*(log(0.55/(rhoIceConst/1000-0.55))-log(rhoSnowConst/(
            rhoIceConst-rhoSnowConst)));
449     double z0[Z]= {0};
450     for (li=0; li<=thickness; li++)
451     {
452         if(strcmp(RHO,"FIRN")==0){
453             rhoIce[li]=916.5-0.14438*(temp[li]-271.16)-0.00015175*(temp[li]-273.16)*(temp[li
                    ]-273.16);
454             if(thickness-li<z55)
455             {
456                 z0[li]=exp(rhoIce[li]/1000*k0*(thickness-li))*rhoSnowConst/(rhoIce[li]-
                        rhoSnowConst);
457                 rho[li]=rhoIce[li]*z0[li]/(1+z0[li]);
458             }
```

```
459                 else if (li>2000)
460                 {
461                         z0[li]=exp(rhoIce[li]/1000*k1*(thickness-li-z55)/sqrt(acc))*0.55/(rhoIce[li]/
                                1000-0.55);
462                         rho[li]=rhoIce[li]*z0[li]/(1+z0[li]);
463                 }
464                 else
465                 {
466                         rho[li]=rhoIce[li];
467                 }
468                 if(rho[li]>rhoIce[li])
469                 {
470                         rho[li]=rhoIce[li];
471                 }
472         }
473         else if(strcmp(RHO,"CONST")==0){
474                 rho[li]=921;
475         }
476     }
477 }
478
479 void setHeatVar(double *K,double *cp,double *told,int thickness, double *rho, double *rhoIce)
480 {
481     int li=0;
482     for(li=0; li<=thickness; li++)
483     {
484         if(strcmp(THERMAL,"FI")==0){
485             K[li]=9.828*exp(-0.0057*270.4);
486             cp[li]=152.5 + 7.122*270.4;
487         }
488         else{
489             K[li]=9.828*exp(-0.0057*told[li]);
490             if(strcmp(THERMAL,"SC")==0){
491                 K[li]=9.828*exp(-0.0057*270.4);
492             }
493             else if (strcmp(THERMAL,"CP")==0){
494                 K[li]=2.*K[li]*rho[li]/(3*rhoIce[li]-rho[li]);
495             }
496             cp[li]=152.5 + 7.122*told[li];
497         }
498     }
499 }
500
501 void computeMelt(double* m,double* tground,double* rho,double L,double K0,double cp0, double
         told1,double told0,double thick,double delz,double QG)
502 {
503     int li=0;
504     double tmelt=0;
505     double pressure=0;
506     //Computation of the pressure and the melting point
507     for(li=0; li<=(int)thick; li++)
508     {
509         pressure+=rho[li];
510     }
511     pressure+=(thick-(int)thick)*rho[(int)thick];
512     tmelt=273.16-8.7*pow(10,-4)*(pressure);
513
514     double diff=QG+K0*(told1-tmelt)/delz;
515
516     if(diff>0) //If enough energy is available to melt ice
517     {
518         *m= 1/(rho[0]*(L-cp0*(told0-tmelt))+cp0*(tmelt-told1)/2)* (-rho[0]*cp0*(tmelt-told0)/
                (2.*31556926.*100.) +diff);
519         *tground=tmelt;
520     }
521     else if(diff<=0) //If not enough energy is available, bottom temperature is decreased
522     {
523             *m= 0;
524             *tground=QG*delz/K0+told1;
525     }
526 }
527
```

```
528 double wDef (double z, double thickness,double mw)
529 {
530     if (strcmp(VERTICAL,"FI")==0){
531             return pow(((double)z/ thickness),(1+mw));
532     }
533     else if (strcmp(VERTICAL,"PA")==0){
534         double p=mw;
535         return ((z/ thickness)*0+(1.-0)*(1-(p+2)/(p+1)*(1-(z/ thickness))+1/(p+1)*pow(1-(z/
                thickness),p+2)));
536     }
537
538 }
539
540 //Compute the matrix element a and b used in explicit and CN scheme and the velocity profile
541 void setABW(double* a,double* b,double* w,double* cp,double* K,double* rho,double delt,double
        delz,double acc,double m,double dhdt,double* w_def,int thickness)
542 {
543     int li=0;
544     for(li=0; li<=thickness; li++)
545     {
546         b[li]=delt*K[li]/rho[li]/cp[li]/delz/delz;
547         w[li]=-(acc-m-dhdt)*w_def[li]-m;
548         a[li]=delt/delz/2*(1/rho[li]/cp[li]*(K[li+1]-K[li-1])/2/delz-w[li]);
549     }
550 }
551
552 void setSe(double *se,double *rho,double *w, double *cp, double *K, double delt,int thickness,
         double* told, double dH,double dhdt,double * tborder, int border,double len, double flat)
553 {
554     double P=0;
555     int li=0;
556     int deltaH=(int)dH;
557     //Internal energy production
558     for(li=thickness-1; li>=1; li--)
559     {
560         P+=rho[li-1]*9.81;
561         se[li]=0;
562         double cr=cbrt(getDwdz(w,li,thickness)+getDudz((double)li/thickness));
563         se[li]=2*cr*cr*getA(told[li])*delt/(rho[li]*cp[li])+(w[li]*P/rho[li]*(rho[li+1]-rho[li
                -1])/2)*delt/(rho[li]*cp[li]);
564     }
565     //Valley effect
566     if(deltaH>0 && border==0)
567     {
568         for(li=0; li<=thickness-deltaH; li++)
569         {
570             se[li+deltaH]+=4*K[li+deltaH]*2*(tborder[li]-told[li+deltaH])/len/len*delt/(rho[li
                    +deltaH]*cp[li+deltaH]);
571         }
572         for(li=1; li<deltaH; li++)
573         {
574             double l=((double)li/(double)deltaH)*((double)li/(double)deltaH);
575             se[li]+=K[li]*2*4*(told[0]+li*6.697E-4-told[li])/((flat+l*(len-flat))*(flat+l*(len
                    -flat)))*delt/(rho[li]*cp[li]);
576         }
577     }
578 }
579
580 //Linear piecewise approximation of the horizontal velocity vertical derivative profile
        squared
581 double getDudz(double zh)
582 {
583     double us=2.2594e-19;
584     double dudz=0;
585     if(zh>=0 && zh<=0.05)
586     {
587         dudz=1.942488E-06-1.952373E-05*zh;
588     }
589     else if(zh<=0.1)
590     {
591         dudz=1.357489E-06 -8.359790E-06*zh;
592     }
```

```
593        else if(zh<=0.2)
594        {
595            dudz=8.170050E-07 -2.934782E-06*zh;
596        }
597        else if(zh<=0.3)
598        {
599            dudz=4.579192E-07 -1.076580E-06 *zh;
600        }
601        else if(zh<=0.5)
602        {
603            dudz=2.656468E-07 -4.343890E-07*zh;
604        }
605        else if(zh<=0.75)
606        {
607            dudz=1.327851E-07 -1.664704E-07*zh;
608        }
609        else if(zh<=1)
610        {
611            dudz=4.236023E-08 -4.340220E-08*zh;
612        }
613        return (us*dudz);
614 }
615
616 //Square of the vertical derivative of the vertical velocity profile
617 double getDwdz(double*w,int z,int thickness)
618 {
619        double dwdz;
620        if(z==0)
621        {
622            dwdz=w[1]-w[0];
623        }
624        if(z==thickness)
625        {
626            dwdz=w[thickness]-w[thickness-1];
627        }
628        else
629        {
630            dwdz=(w[z+1]-w[z-1])/2;
631        }
632        return dwdz*dwdz;
633 }
634
635 //Linear piecewise approximation of A power -1/3 value profile
636 double getA(double t)
637 {
638        double A=0;
639        if(t<=210)
640        {
641            A=31519576971  -141986135 *t;
642        }
643        else if(t<=220)
644        {
645            A=19796924504   -86163980 *t;
646        }
647        else if(t<=230)
648        {
649            A=8301327112   -33868831*t;
650        }
651        else if(t<=240)
652        {
653            A=4956807495   -19262412*t;
654        }
655        else if(t<=255)
656        {
657            A=2755424785   -10096091*t;
658        }
659        else if(t<=275)
660        {
661            A=1802280733    -6324074*t;
662        }
663        return A;
664 }
```

```
665
666 //Explicit integrations scheme
667 void integrate_expl(double* told, double* a, double* b, double tground, double tsurf, double
        tsurf_old, int thickness, double* se)
668 {
669     int li,loop=0;
670     double c1[Z]= {0};
671     double c2[Z]= {0};
672     double c3[Z]= {0};
673     for(li=0; li <=thickness; li++)
674     {
675         c1[li]=b[li]/(365*100)-a[li]/(365*100);
676         c2[li]=-2*b[li]/(365*100)+1;
677         c3[li]=b[li]/(365*100)+a[li]/(365*100);
678     }
679     double tnew[Z]= {0};
680     //internal loop for a daily time step
681     for(loop=0; loop<100*365; loop++)
682     {
683         for(li=1; li<thickness; li++)
684         {
685             tnew[li]=told[li+1]*c3[li]+told[li]*c2[li]+told[li-1]*c1[li]+se[li]/(365.*100.);
686         }
687         //Set boundary conditions for the next loop
688         tnew[0]=tground;
689         tnew[thickness]=tsurf_old+(tsurf-tsurf_old)*(loop+1)/(365.0*100.0);
690         for(li=0; li <=thickness; li++)
691         {
692             told[li]=tnew[li];
693         }
694     }
695 }
696
697 //CN integrations scheme
698 void integrate_CN(double* tint, double* told,double* alpha,double* beta,double* alpha1,double*
         beta1,double tground,double tsurf,int thickness,int step,double* se)
699 {
700     double l[Z]= {0};
701     double d[Z]= {0};
702     double r[Z]= {0};
703     double b[Z]= {0};
704     int li,i=0;
705     double fact=0.7;
706     for(li=1; li <thickness; li++)
707     {
708         l[li]=fact*(-beta1[li]+alpha1[li]);
709         d[li]=fact*2*beta1[li]+1;
710         r[li]=fact*(-beta1[li]-alpha1[li]);
711         b[li]=told[li-1]*(1-fact)*(beta[li]-alpha[li])+told[li]*(1-(1-fact)*2*beta[li])+told[
                li+1]*(1-fact)*(beta[li]+alpha[li])+se[li];
712         se[li]=se[li];
713     }
714     b[1]=told[0]*(1-fact)*(beta[1]-alpha[1])+told[1]*(1-(1-fact)*2*beta[1])+told[2]*(1-fact)*(
            beta[1]+alpha[1])-tground*fact*(-beta1[1]+alpha1[1])+se[1];
715     b[thickness-1]=told[thickness-2]*(1-fact)*(beta[thickness-1]-alpha[thickness-1])+told[
            thickness-1]*(1-(1-fact)*2*beta[thickness-1])+told[thickness]*(1-fact)*(beta[thickness
            -1]+alpha[thickness-1])-tsurf*fact*(-beta1[thickness-1]-alpha1[thickness-1])+se[
            thickness-1];
716     double dp[Z],bp[Z],x[Z]= {0};
717     dp[1]=d[1];
718     bp[1]=b[1];
719     for(i=1; i<thickness; i++)
720     {
721         dp[i+1]=d[i+1]-l[i+1]/dp[i]*r[i];
722         bp[i+1]=b[i+1]-l[i+1]/dp[i]*bp[i];
723     }
724     x[thickness-1]=bp[thickness-1]/dp[thickness-1];
725     for (i=thickness-2; i>0; i--)
726     {
727         x[i]=(bp[i]-r[i]*x[i+1])/dp[i];
728     }
729     tint[0]=tground,
```

```
730              tint[thickness]=tsurf;
731      for (i=1; i<thickness; i++)
732      {
733          tint[i]=x[i];
734      }
735  }
736
737  //Scale the temperature profile to the next thickness value
738  void tempScale(double* told, double thick,double thickFuture,double tsurf)
739  {
740      double temperature[Z]= {0};
741      int thickness=(int)thick;
742      int thicknessFuture=(int) thickFuture;
743      int li=0;
744      double deltaThick=thicknessFuture-thickness;
745      if (deltaThick>0)//If next thickness is bigger, ass some layers at surface temperature
746      {
747          for(li=0; li <=thickness; li++)
748          {
749              temperature[li]=told[li];
750          }
751          for(li=1; li <=deltaThick; li++)
752          {
753              temperature[li+thickness]=tsurf;
754          }
755      }
756      else if (deltaThick<0)//If the next thickness is smaller, linearly scale the temperature
            profile
757      {
758          for(li=0; li <thicknessFuture; li++)
759          {
760              int oldLi=li*thickness/thicknessFuture;
761              int oldLiF=floor(oldLi);
762              temperature[li]= told[oldLiF]+(told[oldLiF+1]-told[oldLiF])*(oldLi-oldLiF);
763          }
764          temperature[thicknessFuture]=told[thickness];
765      }
766      else
767      {
768          for(li=0; li <=thickness; li++)
769          {
770              temperature[li]=told[li];
771          }
772      }
773      for(li=0; li <Z; li++)
774      {
775          told[li]=temperature[li];
776      }
777  }
```

code/main.h

Declaration

under Art. 28 Para. 2 RSL 05

Last, first name: Michel Adrien

Matriculation number: 07-319-833

Programme: M.Sc. in Climate Sciences

Bachelor ☐ Master ☒ Dissertation ☐

Thesis title: Transient modeling of borehole temperature and basal melting in an ice sheet

Thesis supervisor: Prof. Dr. Hubertus Fischer
Prof. Dr. Jakob Schwander

I hereby declare that this submission is my own work and that, to the best of my knowledge and belief, it contains no material previously published or written by another person, except where due acknowledgement has been made in the text. In accordance with academic rules and ethical conduct, I have fully cited and referenced all material and results that are not original to this work. I am well aware of the fact that, on the basis of Article 36 Paragraph 1 Letter o of the University Law of 5 September 1996, the Senate is entitled to deny the title awarded on the basis of this work if proven otherwise. I grant insprection of my thesis.

Geneva, 18 th of February 2016

Adrien Michel